SPACE SCIENCES LABORATORY

UNIVERSITY OF CALIFORNIA

BERKELEY, CALIFORNIA

Space Sciences Laboratory
University of California
Berkeley, California

A THEORETICAL AND EXPERIMENTAL STUDY
OF THE MECHANICAL BEHAVIOR OF THE CORNEA WITH
APPLICATION TO THE MEASUREMENT OF
INTRAOCULAR PRESSURE

by

Nathan Jay Schwartz

Series No. 6, Issue No. 31

July 28, 1965

SUMMARY

3446¹

A theoretical and experimental study was made of the mechanical behavior of the cornea. The theoretical analysis included an analytical solution for the symmetrical constraint of a thin, shallow, spherical shell by a rigid indenter. The experimental study investigated the rheology of the cornea with particular emphasis on its compliance with the requirements of the Boltzmann superposition principle. Representative results of tests on twenty enucleated hog eyes and two human eyes have been reported.

The corneas of the human and hog eyes behaved as linear viscoelastic solids; the human eyes differed from the hog eyes in having a long term creep component. Several eyes were tested at the site of procurement, six to seven minutes after the animal's death, and it was established that creep is not an artifact due to aging or enucleation.

The analytical and experimental results were combined to study some instruments used to detect the level of pressure in the eye. The theoretical analysis predicted that a type of elastic instability occurs during the process of flattening a small portion of the cornea; this is discussed with reference to the Goldmann and Mackay-Marg tonometers. The role of corneal creep was considered with reference to the response of the Schiøtz indentation tonometer during the time dependent process known as tonography.

author

PREFACE

The nature of this study of the measurement of intraocular pressure leads to a three-fold presentation. We first give an analytical solution for the symmetrical constraint of a thin elastic shell by a rigid indenter. In the next chapter we record our experimental investigation of the rheology of the cornea. And then, in chapter three, the analytical and experimental results are combined to study some problems of tonometry and tonography.

Consequently, chapter one begins with an introduction to the analytical work, and the introduction to the second chapter addresses itself to the experimental study. In the introduction to chapter three, we orient the previous results toward the glaucoma problem; therein we discuss the limitations of applying our results which are based on the linear theory of elasticity to the analysis of various instruments employed to measure intraocular pressure.

Although the basic analytical formulation is contained in chapter one, the problem of tonography requires an extension of these results. And in order to gain a slight insight into that problem, in Chapter 3 we extend the previous results to include the rising intraocular pressure (due to the applied load), the fluid outflow and some heuristic remarks based on the linear theory of visco-elasticity.

TABLE OF CONTENTS

CHAPTER ONE

"An Analytical Investigation of the Deformation of a Shallow Spherical Shell by a Rigid Indenter"

1.1. Introduction

The contact problem in elasticity is a boundary value problem of mixed type. Over a region, whose boundary is not a-priori known, displacements are specified; outside this region one specifies stresses. The solution must determine the stresses and displacements throughout the body as well as the boundary between the loaded and unloaded portions of the surface.

A classical example of this type problem is Hertz' [1] * solution for the contact of two solid, elastic spheres. In this investigation we are concerned with the symmetrical indentation of a shallow, spherical shell by a rigid constraint. The shell is assumed to have no edge restraint.

In 1962, Essenberg [2] considered the problem of a plate whose upper surface is partially constrained by a rigid, parabaloidal indenter. He found it necessary to employ the E. Reissner [3] plate theory (which extends the classical theory by considering the effect of transverse shear deformation) since the classical plate theory predicts the following unsatisfactory result: If a plate is loaded only from above by a rigid indenter whose contour is a bi-harmonic function, then the pressure between the plate and the constraint is zero; equilibrium is maintained by a discontinuous resultant shear stress.

Essenberg was able to obtain a physically consistent representation for the pressure; he also noted the divergence of the improved and classical

* Numbers in brackets refer to references given at the end.

theories * even for very thin plates. He showed that if the surface traction is a quantity of interest, it is necessary to employ the improved theory.

In 1946, E. Reissner [4] developed a theory to describe, from the standpoint of classical shell-theory, the stresses and small displacements in shallow spherical shells. In 1955 Naghdi [7] extended these results to include the effect of transverse shear deformation and normal stress in the stress-strain equations in the shell space.

For the problem that we are considering, the shallow spherical shell constrained by a rigid indenter, the result afforded by classical shell theory (under the Love-Kirchoff hypothesis [8]) and the shallow shell approximation is unsatisfactory. For constraint by any smoothly shaped indenter, classical theory predicts that the pressure between the shell and the constraining surface is negative, i.e., the shell does not contact the constraint. Equilibrium is maintained by the discontinuous resultant shear stress at the edge of the loaded region.

In view of Essenberg's success with the plate problem, we have solved the problem of a thin shallow shell, with no edge restraint and symmetrically loaded by a rigid indenter within the context of the improved theory due to Naghdi [7] . If the loaded region does not become too large, the pressure distribution between the shell and the constraint is always positive; the shell contacts the constraining surface. Beyond a certain contact radius, the solution predicts a negative pressure at the edge of the contact region.

* Throughout the text we shall refer to those developments that neglect the effect of transverse shear deformation and normal stress in the stress-strain equations as the "classical theories". The extensions, to include these effects, shall be referred to as the "improved theories".

There is some question of the consistency of an assumption inherent in shallow shell theory (the existence of a stress function from which the direct stress resultants are derived) and the simultaneous consideration of the effect of transverse shear deformation. This is discussed in the text for the particular contact problem under consideration.

Numerical results are presented for several values of the radius of curvature and shell thickness. And a physical interpretation is suggested for the prediction of an eventual loss of total contact between the indenter and the shell.

1.2. Reference Equations and Some Preliminary Results

A derivation (from the general bending theory of shells) of the equations of shallow shell theory is available in the text by Green and Zerna [9]. The extension to include the effect of transverse shear deformation was carried out by Naghdi [7]. Here we wish to recall the assumptions necessary to reduce the differential equations which govern the resultant stresses and couples in the shell space to the approximate equations known as shallow shell theory. Since we are only interested in shells loaded vertically at the apex we shall record the equations that result after the assumption of rotational symmetry.

We refer to the coordinate systems of figure 1; r is the distance from the apex measured in a plane parallel to the base plane. The resultant quantities are shown acting on a shell segment in figure 2.
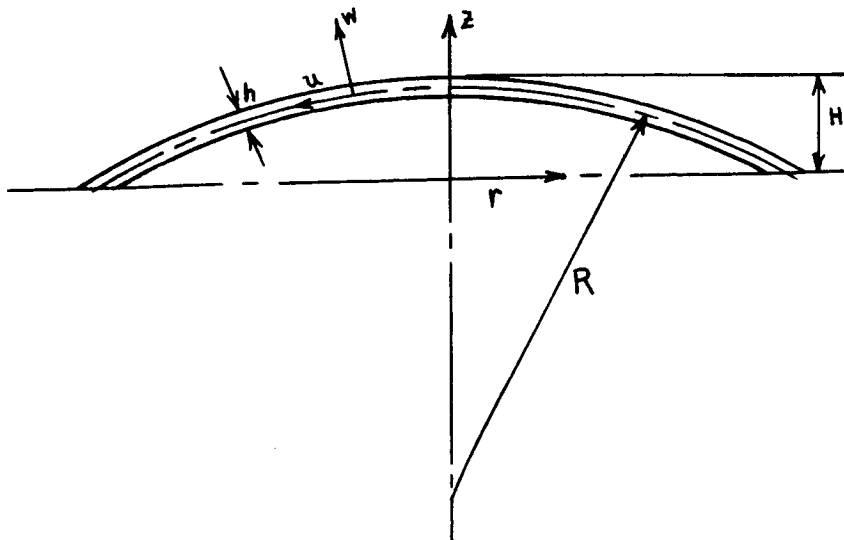
FIGURE 1
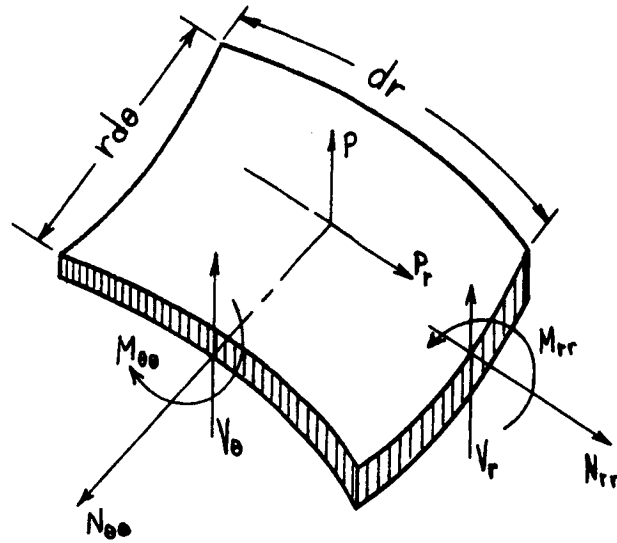
FIGURE 2

N_{rr} and $N_{\theta\theta}$ are the direct stress resultants, V_r and V_θ the transverse shear resultants and M_{rr} and $M_{\theta\theta}$ denote the stress couples. The displacement and load normal to the middle surface are w and p respectively. The middle surface strains are e_{rr} and $e_{\theta\theta}$. Primes denote differentiation with respect to r.

The middle surface of the shell is given by

$$Z = \sqrt{R^2 - r^2} - (R-H) \qquad (1)$$

and the assumption of shallowness is

$$\frac{dz}{dr} = -\frac{r}{\sqrt{R^2 - r^2}} \approx -\frac{r}{R} = o(1) \qquad (2)$$

or that for significant values of r, the quotient of $\frac{r}{R}$ is small compared to one. Reissner, who first obtained the shallow shell equations [4], considers a shell to be shallow if the ratio of its height to base diameter is less than say, $\frac{1}{8}$.

In their rotationally symmetric form, from [6] , the equilibrium equations are

$$\left(r \, N_{rr}\right)' - N_{\theta\theta} + \frac{r}{R} V_r + r \, P_r = 0 \tag{3a}$$

$$\left(r \, V_r\right)' - \frac{r}{R}\left(N_{rr} + N_{\theta\theta}\right) + r \, p = 0 \tag{3b}$$

$$\left(r \, M_{rr}\right)' - M_{\theta\theta} - r \, V_r = 0 \tag{3c}$$

Usually, in order to introduce a stress function, the term $\frac{r}{R} V_r$ is omitted in (3a). But in this section we wish to draw some conclusions that do not depend on the existence of a stress function.

If we denote Poisson's ratio by ν , Young's modulus by E, and the shell thickness by h, then the middle surface strains may be written alternatively in terms of displacements and stress resultants as

$$e_{rr} = u' + \frac{w}{R} = \frac{N_{rr} - \nu N_{\theta\theta}}{hE} \tag{4a}$$

$$e_{\theta\theta} = \frac{u}{r} + \frac{w}{R} = \frac{N_{\theta\theta} - \nu N_{rr}}{h \, E} \tag{4b}$$

and the stress strain equations are completed by

$$M_{rr} = -D\left(\beta' + \nu \beta/r\right) \tag{5a}$$

$$M_{\theta\theta} = -D\left(\beta/r + \nu\beta'\right) \tag{5b}$$

$$\beta = -w' + \frac{12(1+\nu)}{5 \, E \, h} V_r \tag{5c}$$

where $D = Eh^3/12 \, (1-\nu^2)$. We now obtain a relationship between the shear resultant V_r and the normal displacement w. We shall then see the singular perturbation nature (in the limit as $h \to 0$) of the contact problem.

If we substitute (5a,b) into (3c), and replace β by (5c), then

$$\frac{1}{k^2}\nabla^2 V_r - \left(1 + \frac{1}{k^2 r^2}\right)V_r = -D\left(\nabla^2 w\right)'$$ (6)

where $\quad k^2 = \frac{5(1-\nu)}{h^2}$, $\quad \nabla^2 \equiv \frac{d^2}{dr^2} + \frac{1}{r}\frac{d}{dr}$

Now let

$$\rho = \frac{r}{R}, \quad V_\rho = \frac{V_r R^3}{D}$$ (7)

Then (b) becomes

$$\left(\frac{1}{kR}\right)^2 \nabla_\rho^2(V_\rho) - \left(1 + \frac{1}{(kR\rho)^2}\right)V_\rho = -\frac{d}{d\rho}\left(\nabla_\rho^2 w\right)$$ (8)

where $\quad \nabla_\rho^2 \equiv \frac{1}{R^2}\nabla^2$.

And from (6), in the limit as $h \to o$, we have

$$V_\rho = -\frac{d}{d\rho}\left(\nabla_\rho^2 w\right)$$ (9)

Hence, if we obtain the non-dimensional shear resultant of classical theory [4], as the limit as the thickness approaches zero in the improved theory, we make a singular pertubation. (Alternatively, we can obtain the dimensional shear resultant of classical theory in the limit as $k^2 \to \infty$ in equation (6)). This is the root of the divergence of the classical prediction for the pressure from its improved value [2] even in the limit of a very thin plate. And from this singular pertubation relating the two theories we account for the improvement in the pressure distribution that is obtained by employing the improved theory in the contact problem for shells.

We shall now derive a representation for the normal displacement w that does not depend on the existence of a stress function. For convenience we neglect surface loading p_r.

From (4a,b) we obtain

$$\left(N_{\theta\theta} - \nu N_{rr}\right)' = \frac{N_{rr} - N_{\theta\theta}}{r}(1+\nu) + \frac{\lambda E}{R}w'$$

and with (3a)

$$N_{\theta\theta}' + \frac{N_{\theta\theta} - N_{rr}}{r} = \frac{\lambda E w'}{R} - \frac{\nu}{R}V_r \tag{10}$$

Upon adding (3a) and (10), and integrating their sum we have

$$N_{rr} + N_{\theta\theta} = \frac{E\lambda}{R}w - \frac{1+\nu}{R}\int^r V_r\, dr \tag{11}$$

Now to obtain a homogeneous representation for w substitute (5a,b) into (3b,c) and replace β by (4c). Then

$$D\nabla^4 w + \frac{1}{R}(N_{rr} + N_{\theta\theta}) - \frac{1}{k^2 R}\nabla^2(N_{rr} + N_{\theta\theta}) = 0 \tag{12}$$

and with (11) we have

$$D\nabla^4 w - \left(\frac{E\lambda}{k^2 R^2} + \frac{1+\nu}{R^2}D\right)\nabla^2 w + \frac{E\lambda}{R^2}w = \frac{1}{5}\left(\frac{\lambda}{R}\right)^2\frac{1+\nu}{1-\nu}\int^r \frac{V_r}{r^2}dr. \tag{13}$$

Before discussing (12) and (13) we record the differential equation for the slope β. If we substitute V_r from (3c) into (5c) and replace the couples by (5a,b), then

$$\beta'' + \frac{\beta'}{r} - \left(k^2 + \frac{1}{r^2}\right)\beta = k^2 w' \tag{14}$$

First we obtain the equation for w as given by classical theory [4]. In (12) let $k^2 \to \infty$. Then

$$D\nabla^4 w + \frac{1}{R}(N_{rr} + N_{\theta\theta}) = 0 \tag{12'}$$

From (6),

$$V_r = - D\left(\nabla^2 w\right)'$$

(6)'

so that (11) becomes

$$N_{rr} + N_{\theta\theta} = \frac{Eh}{R} w + \frac{1+\nu}{R} D\left(\nabla^2 w\right)$$

(11)'

And then (12)' yields

$$\nabla^4 w + \frac{1+\nu}{R^2} \nabla^2 w + \frac{Eh}{R^2 D} w = 0$$

(15)

If we further neglect the term $\frac{r}{R} V_r$ in (3a), then we obtain the equation for w given in [4] ,

$$\nabla^4 w + \frac{Eh}{R^2 D} w = 0$$

(15)'

We see that neglecting $\frac{r}{R} V_r$ in (3a) gives a more concise representation, for then a stress function F exists such that

$$N_{rr} = \frac{F'}{r}$$

(16a)

and

$$N_{\theta\theta} = F''$$

(16b)

From the compatability equation the entire problem is then posed in terms of two equations for w and F [4] , but actually (15) could have been solved in terms of Hankel functions and the direct resultant obtained from (4a,b). The solution of (15)' is given [5] in terms of Kelvin functions and for values of R such that $\frac{h}{R} \ll 1$, the solution of (15) in Hankel functions is nearly identical to the solution of (15)' in Kelvin functions. Hence introducing a stress function is just a convenience for the development within the framework of classical theory.

But if we include the effect of transverse shear deformation then the existence of a stress function is far more crucial if we are to obtain an analytical solution. For V_r is no longer determined by (6') and can only be given in terms of the solution of (14) and (5c). This solution involves the general solution of (14), i.e., a sum of modified Bessel functions and an integral involving the displacement w. So that if we represent Nrr + Nθθ by (11), equation (12) becomes an integro-differential equation for w involving constants of integration (from the complementary solution of (14)).

In view of this difficulty it is apparent that we shall introduce a great simplification if we adopt the formulation of reference [7] in which the effect of transverse shear deformation is accounted for while a stress function is simultaneously introduced. We present some arguments for the consistency of these operations for the case of the contact problem.

The derivation of (14) is independent of whether the term $\frac{r}{R} V_r$ in (3a) is retained or not. Hence, since w is specified in the contact problem, β is specified by the solution of (14). And from (5c) V_r is given and we obtain Mrr from (5a). Now consider the direct stress resultants. As we shall see below, the solution for V_r in the loaded region is given by

$$V_r = \frac{5E h}{12(1+\nu)} C I_1(kr) \qquad (17)$$

where C is a constant to be determined. Then from (11)

$$N_{rr} + N_{\theta\theta} = \frac{Eh}{R} w - \frac{5Eh}{12 kR} C I_0(kr) \qquad (18)$$

where I_n is a modified Bessel function.

Then from (3b), (17) and (18) we have

$$P(r) = \frac{Eh}{R^2} w + \frac{5E\sqrt{5(1-\nu)}}{12(1+\nu)} \left\{ 1 - \frac{1}{1-\nu} \left(\frac{h}{R}\right)^2 \right\} C I_0(kr) \qquad (19)$$

Hence introducing a stress function introduces an error of $O\left(\frac{h}{R}\right)^2$ in the pressure distribution (*). Now the vertical force R_v is given by [4]

$$R_v = \frac{r}{R} N_{rr} - V_r \qquad (19)'$$

and for the contact problem, if P is the total force exerted by the constraint, then outside the contact region

$$R_v = \frac{P}{2\pi r} \qquad (19)''$$

From (19) we know that introducing a stress function is consistant for the pressure and hence for the total force P. So from (19)', if we can argue the consistency for V_r, then we infer the consistency for Nrr and hence Noo.

Now whether the integro-differential equation (13) is solved for w, or if we solve[(†)] (21) , the boundary conditions do not change; they are specified in the contact problem. Moreover, the same number of boundary conditions are used in determining w, β, V_r, Mrr, Nrr, whether or not we introduce a stress function (see general boundary conditions in [6]). And we can assume that in solving (21) along with (14) we are not solving a system whose order is lower than that of (13) and (14).

So the fact that the boundary conditions for the problem are unchanged as well as the order of the system is a good indication that near the contact region the solution is not sensitive to the introduction of a stress function. And since we are also solving the problem for an unlimited shell, i.e., regularity conditions at infinity, we expect the solution to rapidly approach the membrane solution.

(*) Terms of the $O\left(\frac{h}{R}\right)^2$ are neglected in the shell theory from which the shallow shell equations are derived.

(†) Equation 21 is given at the end of this section (2.2). It is obtained by introducing a stress function in equation 12.

It is therefore reasonable to simultaneously introduce a stress function and the effect of transverse shear deformation for the contact problem. If the load instead of displacement were specified, then (13) or (21) would be solved with different boundary conditions and it would be difficult to argue the suitability of introducing a stress function. One would probably have to solve (13) by asymptotic integration.

In the contact problem, the continuity of Nrr yields the unknown contact radius. The expression for Nrr in the unloaded region, in order to satisfy equilibrium to $0\left(\frac{\ell}{R}\right)^2$, should be obtained from (19)'. Then, the continuity of Nrr as determined from the stress function F will yield a remaining constant of integration in the problem, (the constant A_9 in equation 41 below)

And so we close this section with the field equations as derived in $\begin{bmatrix} 7 \end{bmatrix}$. These equations will be employed in the solutions of the contact problem in the unloaded region.

$$\nabla^4 F - \frac{E\hbar}{R} \nabla^2 w = 0 \tag{20}$$

$$D\nabla^4 w + \left(1 - \frac{1}{k^2}\nabla^2\right)\frac{1}{R}\nabla^2 F = \left(1 - \frac{1}{k^2}\nabla^2\right)p \tag{21}$$

1.3. The Formulation of the Boundary Value Problem.

Let us consider the displacement boundary condition for the loaded portion of the shell. The result is the same as Hertz' contact problem and we find it useful to follow the development of the boundary condition in that problem as given by Timoshenko and Goodier[1].
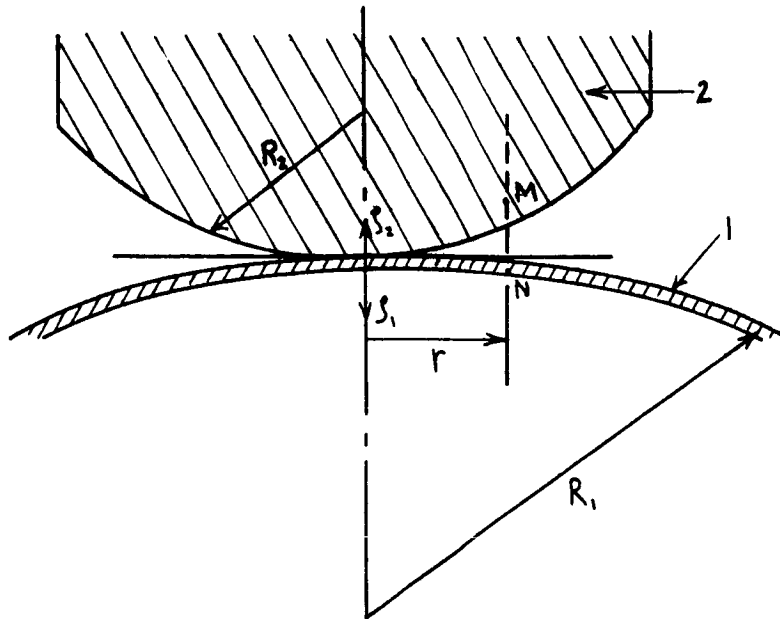

FIGURE 3

We refer to Figure 3. As long as $\frac{r}{R_1}$ and $\frac{r}{R_2}$ are small compared to one, the equations of the rigid body and the shell are respectively

$$\delta_1 = \frac{r^2}{2R_1} \qquad (22a)$$

and

$$\delta_2 = \frac{r^2}{2R_2} \qquad (22b)$$

Let T be a tangent plane at the point of contact, and w be the local deformation of the shell by the rigid constraint. Then, with respect to the tangent plane (assumed to move vertically such that as two points M and N move into the region of contact, they do so in a plane that remains perpendicular to that tangent plane) the displacement condition is $W + \delta_1 = -\delta_2$.

And if the center displacement of the tangent plane is δ, then with respect to the middle surface of the shell, the displacement boundary condition is

$$w = \delta - (S_1 + S_2)$$

If we let

$$\gamma = \frac{R_1 + R_2}{2 R_1 R_2}$$

then

$$w = \delta - \gamma r^2 \tag{23}$$

We designate by a subscript "i" the "inner" or (as simultaneously referred to,) the solution in the loaded region. Similarly we denote the solution in the "outer" or unloaded region by a subscript "o".

Then the boundary value problem for the shell with no edge restraint is posed as follows: Let r_0 be the boundary between the loaded and unloaded portions. Then we have the "inner" problem:

Solve

$$\beta'' + \frac{\beta'}{r} - \left(k^2 + \frac{1}{r^2}\right)\beta = k^2 w' \tag{24}$$

Subject to

$$\text{as } r \to 0, \ \beta \text{ is regular}$$

and

$$w = \delta - \gamma r^2$$

From the solution of the inner problem obtain V_r and Mrr from (5).

"Outer" Problem: $r \geq r_0$

Solve (see reference [6])

$$\nabla^4 F - \frac{E\hbar}{R} \nabla^2 w = 0 \qquad (25)$$

$$D\nabla^4 w - \frac{1}{\hbar^2 R^2} \nabla^4 F + \frac{1}{R} \nabla^2 F = 0 \qquad (26)$$

$$\beta'' + \frac{\beta'}{r} - \left(\hbar^2 + \frac{1}{r^2}\right)\beta = \hbar^2 w' \qquad (24)$$

Obtain V_r and Mrr from (5) and require that

as $r \to \infty$, β, V_r, Mrr, w are regular

Matching Problem

To obtain the constants of integration, match the inner and outer solutions at r_0 so that

at $r = r_0$, Mrr, β, V_r and w and Nrr are continuous

1.4. The Homogeneous Solution of the Equations Governing the Boundary Value Problem.

Equation (24) is a Bessel equation and its solution is

$$\beta = A_1 I_1(\hbar r) + A_2 K_1(\hbar r) + \beta_P \qquad (27)$$

where the particular integral, by variation of parameters, is given by

$$\beta_P = \hbar^2 \int^r \eta w'(\eta)\left\{I_1(\hbar r)K_1(\hbar \eta) - K_1(\hbar r)I_1(\hbar \eta)\right\} d\eta \qquad (28)$$

I_1 and K_1 are modified Bessel functions of the first and second kind respectively and A_1 and A_2 are constants.

By applying the operator ∇^2 to (26) and using (25) we have the following equation for w

$$\nabla^6 w - \frac{E\hbar}{\hbar^2 R^2 D} \nabla^4 w + \frac{E\hbar}{R^2 D} \nabla^2 w = 0 \qquad (29)$$

By linearity we factor (29) into a product of three operators as

$$\nabla^2 \left(\nabla^2 + C_1^2 \right)\left(\nabla^2 + C_2^2 \right) W = 0 \tag{30}$$

where C_1^2 and C_2^2 are the roots of

$$C^4 + \frac{E\hbar}{\hbar^2 R^2 D} C^2 + \frac{E\hbar}{R^2 D} = 0 \tag{31}$$

The solution of (29) is

$$W = \sum_{i=1}^{3} W_i \tag{32}$$

where W_i are the solutions of

$$\left(\nabla^2 + C_1^2 \right) W_1 = 0 \tag{33a}$$

$$\left(\nabla^2 + C_2^2 \right) W_2 = 0 \tag{33b}$$

$$\nabla^2 W_3 = 0 \tag{33c}$$

if [12, Chapter 5] the factored operators commute and $C_1^2 \neq C_2^2 \neq 0$.

The solution of (31) is

$$C_1^2 = \frac{1}{\ell^2} e^{i\Theta} \tag{34a}$$

$$C_2^2 = \frac{1}{\ell^2} e^{-i\Theta} \tag{34b}$$

where the bar $(\overline{})$ denotes the complex conjugate and

$$\ell = \sqrt{R\hbar} \Big/ \sqrt[4]{12(1-\nu^2)} \quad , \quad \Theta = \tan^{-1} \sqrt{\frac{25}{3} \frac{(1+\nu)}{(1-\nu)}\left(\frac{R}{\hbar}\right)^2 - 1} \tag{35}$$

Since the requirement of commutivity of operators and distinctness of the roots C_i is met, the solution of (29) is the sum of the solutions of (33).

We require a solution that is regular as $r \to \infty$ and therefore we take the solutions of (33) in terms of Hankel functions.

$$W = D_1 H_o^{(1)}(C_1 r) + D_2 H_o^{(2)}(C_1 r) + D_3 H_o^{(1)}(\overline{C}_1 r) \tag{36}$$

$$+ D_4 H_o^{(2)}(\overline{C}_1 r) + D_5 + D_6 \ln\frac{r}{\ell}$$

where $H_n^{(1,2)}$ are Hankel function of order n and of the first and second kind, respectively. But (36) must be real and therefore we set

$$D_1 + D_4 = D_1' \quad , \quad D_3 + D_2 = D_3'$$

$$(D_3 - D_2)i = D_2' \quad , \quad (D_4 - D_1)i = D_4'$$

(37)

Then if we employ the identities

$$H_0^{(1)}(\bar{z}) = \overline{H_0^{(2)}(z)}$$

$$H_0^{(2)}(\bar{z}) = \overline{H_0^{(1)}(z)}$$

(38)

and solve (37) for D_i and substitute into (36)

we have

$$W = D_1' \, Re \, H_0^{(1)}(c_1 r) + D_3' \, Re \, H_0^{(2)}(c_1 r) + D_5$$

$$+ D_6 \ln \frac{r}{\ell} - D_4' \, Im \, H_0^{(1)}(c_1 r) - D_2' \, Im \, H_0^{(2)}(c_1 r)$$

(39)

Where Re ($\times$) and Im ($\times$) designate the real and imaginary parts respectively. Now if we further note that

$$H_0^{(2)}(x) = 2 J_0(x) - H_0^{(1)}(x)$$

Where J_n is a Bessel function of order n, then with (35) and for convenience new real constants A_i, the solution (39) becomes,

$$W = A_3 \, Re \, H_0^{(1)}(z) + A_4 \, Im \, H_0^{(1)}(z) + A_5 \, Re \, J_0(z)$$

$$+ A_6 \, Im \, J_0(z) + A_7 + A_8 \ln \frac{r}{\ell} \quad ,$$

(40)

where $z = \frac{r}{\ell} e^{i\theta/2}$.

From (25) the solution for F is then given by

$$F = -\frac{E\hbar}{R} \ell^2 \left\{ A_3 \, Re \left[e^{-i\theta} H_0^{(1)}(z) \right] + A_4 \, Im \left[e^{-i\theta} H_0^{(1)}(z) \right] \right.$$

$$+ A_5 \, Re \left[e^{-i\theta} J_0(z) \right] + A_6 \, Im \left[e^{-i\theta} J_0(z) \right]$$

$$\left. - A_9 \ln \frac{r}{\ell} + A_{10} \right\} .$$

(41)

We note that if we neglect transverse shear deformation ($k^2 \to \infty$), then $\theta \to 3\pi/2$ and $z \to \frac{r}{\ell} i^{3/2}$. And if we recall that

$$\operatorname{Re}\left[H_o^{(1)}\left(\frac{r}{\ell} i^{3/2}\right)\right] = \frac{2}{\pi} \operatorname{kei} \frac{r}{\ell} \tag{42a}$$

$$\operatorname{Im}\left[H_o^{(1)}\left(\frac{r}{\ell} i^{3/2}\right)\right] = -\frac{2}{\pi} \operatorname{ker} \frac{r}{\ell} \tag{42b}$$

$$\operatorname{Re} J_o\left[\left(\frac{r}{\ell} i^{3/2}\right)\right] = \operatorname{ber} \frac{r}{\ell} \tag{42c}$$

$$\operatorname{Im}\left[J_o\left(\frac{r}{\ell} i^{3/2}\right)\right] = \operatorname{bei} \frac{r}{\ell} \tag{42d}$$

where kei, ker, ber, and bei are Kelvin functions, then as $k^2 \to \infty$, (40, 41) reduce to Reissner's solution [5] .

1.5. The Solution for a Point Load at the Apex,

To derive the solution to the problem of a point load at the apex of a shallow spherical shell having no edge restraint we shall employ the technique used by Koiter (Ref. [16]) in his solution for a complete spherical shell under point loads at its poles. Accordingly, we require the following representation of the divergence theorem: If S is the surface area enclosed by a smooth countour C, and $\vec{n}$ is the unit normal vector to the contour C in the tangent plane to the surface, then for a twice continuously differentiable function ϕ on S,

$$\iint_S \nabla^2 \phi \, d\sigma = \oint_C \vec{n} \cdot \nabla \phi \, d\Delta \tag{43}$$

Let us consider the solution for the normal displacement w, and required that

$$\text{as } r \rightarrow o \, , \, N_{rr} \, , \, N_{\theta\theta} \quad \text{are finite} \tag{44a}$$

$$\text{as } r \rightarrow o \, , \, W, W' \quad \text{are finite} \tag{44b}$$

$$\text{as } r \rightarrow \infty \, , \, \beta, W \rightarrow O \tag{44c}$$

where w is the solution of equation (22) in the absence of surface loads except for a concentrated force -P at the apex.

Our result (40) is the solution of the homogeneous form of (21), and the only component that is bounded at r=o and approaches zero at infinity is

$$W = A_3 \, \text{Re} \, H_o^{(1)} \left(\frac{r}{\ell} e^{i\theta/2} \right) \tag{45}$$

And so in order to complete the solution we must determine the constant A_3. But we first record some formulas for the behavior of the value of Bessel functions for small values of their argument.

If z is a complex variable, then by definition

$$J_m(z) = \sum_{r=o}^{\infty} \frac{(-1)^r \left(\frac{1}{2} z \right)^{m+2r}}{r! (n+r)!} \tag{46a}$$

We denote the real and imaginary parts of $J_n(\bar{z})$ with $\bar{z}$ in polar representation as $\bar{z} = \rho e^{i\varphi}$ by u_n and v_n so that

$$J_n(\bar{z}) = u_n(\rho, \varphi) + i\, v_n(\rho, \varphi) \tag{46b}$$

If the Bessel functions $Y_m(\bar{z})$ have their real parts denoted by U_m and their imaginary parts by V_m, then

$$Y_n(\bar{z}) = U_n(\rho, \varphi) + i\, V_n(\rho, \varphi) \tag{46c}$$

We require the representations for $n=0, n=1$; from the introduction to reference (17) we have

$$U_0(\rho,\varphi) = \frac{2}{\pi}\left\{ u_0(\rho,\varphi)(\gamma + \log \rho/2) - \varphi\, v_0(\rho,\varphi)\right\} + S_0(\rho,\varphi) \tag{46d}$$

$$V_0(\rho,\varphi) = \frac{2}{\pi}\left\{ v_0(\rho,\varphi)(\gamma + \log \rho/2) + \varphi\, u_0(\rho,\varphi)\right\} + T_0(\rho,\varphi) \tag{46e}$$

$$U_1(\rho,\varphi) = \frac{2}{\pi}\left\{ u_1(\rho,\varphi)(\gamma + \log \rho/2) - \varphi\, v_1(\rho,\varphi)\right\} - \frac{2}{\pi\rho}\cos\varphi - S_1(\rho,\varphi) \tag{46f}$$

$$V_1(\rho,\varphi) = \frac{2}{\pi}\left\{ v_1(\rho,\varphi)(\gamma + \log \rho/2) + \varphi\, u_1(\rho,\varphi)\right\} + \frac{2}{\pi\rho}\sin\varphi - T_1(\rho,\varphi) \tag{46g}$$

where S_0, T_0, S_1, T_1 are regular near $\rho = 0$ and γ is Euler's constant.

We now proceed with the solution. Integrate equation (21) over a portion of the surface of the shell, with p a concentrated load.

$$D\iint_S \nabla^4 W\, d\sigma + \iint_S \left(1 - \frac{1}{k^2}\nabla^2\right)\frac{1}{R}\nabla^2 F\, d\sigma = \iint_S p\, d\sigma$$

Then with (43)

$$\oint_C \vec{n}\cdot\nabla(\nabla^2 W)\, dA + \frac{1}{DR}\iint_S \nabla^2 F\, d\sigma - \frac{1}{Dk^2 R}\oint_C \vec{n}\cdot\nabla(\nabla^2 F)\, dA \tag{47}$$

$$= \frac{12(1-\nu^2)}{E\hbar^3}\iint_S p\, d\sigma$$

Now let c be a circular path symmetrical about the apex and given parametrically by polar coordinates r_0, ω. We take the limit of (47) as $r_0 \to 0$.

$$\lim_{r_0 \to 0} \left\{ \int_0^{2\pi} \frac{\partial}{\partial r}(\nabla^2 W) r \, d\omega - \frac{1}{D k^2 R} \int_0^{2\pi} \frac{\partial}{\partial r}(\nabla^2 F) r \, d\omega \right\} \Bigg|_{r=r_0} = -\frac{12(1-\nu^2)}{E h^3} P \quad (48)$$

where P is the point load and we have dropped the terms that obviously will not contribute (see the conditions 44a) in the limit as $r_0 \to 0$.

But from equation (20),

$$\nabla^2 F = \frac{E h}{R} W + a_1 + a_2 \ln r$$

where a_1 and a_2 are constants and $a_2 = 0$ by (44a). Hence from (44b) we see that as $r_0 \to 0$ the second term in (48) gives no contribution and we are left with

$$\lim_{r_0 \to 0} \left\{ \int_0^{2\pi} \frac{\partial}{\partial r}(\nabla^2 W) r \, d\omega \right\} \Bigg|_{r=r_0} = -\frac{12(1-\nu^2)}{E h^3} P \quad (49)$$

Now since

$$H_n^{(1)}(z) = J_n(z) + i Y_n(z)$$

from (46 f,g) we see that

$$H_1^{(1)}\left(\frac{r}{\ell} e^{i\theta/2}\right) = -\frac{2\ell}{\pi r}\left(\sin\frac{\theta}{2} + i\cos\frac{\theta}{2}\right) + \mathcal{S}(r) \quad (50)$$

Where $\mathcal{S}(r)$ represents terms containing singularities $0 (\ln r)$ and the remaining regular terms in the series expansion for $H_1^{(1)}(z)$. And since

$$\frac{\partial}{\partial r}\left(\nabla^2 H_0^{(1)}\left(\frac{r}{\ell} e^{i\theta/2}\right)\right) = \frac{e^{i3\theta/2}}{\ell^3} H_1^{(1)}\left(\frac{r}{\ell} e^{i\theta/2}\right)$$

we have

$$\frac{\partial}{\partial r}\left(\nabla^2 H_0^{(1)}\left(\frac{r}{\ell} e^{i\theta/2}\right)\right) = \frac{2}{\pi \ell^2 r}\left(\sin\theta - i\cos\theta\right) + \mathcal{S}(r) \quad (51)$$

Then (45), (49), and (51) yield

$$A_3 \cdot 2\pi \left(\frac{2}{\pi \ell^2}\right) \sin\theta = -\frac{12(1-\nu^2)}{E h^3} P$$

or

$$A_3 = -\frac{P}{2\pi} \frac{12(1-\nu^2)\ell^2}{E h^3} \frac{\pi}{2} \sin\theta \quad (52)$$

Hence the solution w_δ for the point load is

$$W_\delta = -\frac{\sqrt{12(1-\nu^2)}}{2\pi} \frac{PR}{E\lambda^2} \frac{\pi}{2} \sin\Theta \; Re\left[H_0^{'''}\left(\frac{r}{\ell} e^{i\Theta/2}\right)\right] \qquad (53)$$

From (42a) we see that as $k^2 \to \infty$, $(\Theta \to 3\pi/2)$,

$$Re \; H_0^{'''}\left(\frac{r}{\ell} e^{i\Theta/2}\right) \to \frac{2}{\pi} kei \frac{r}{\ell}$$

and

$$W_\delta \to \frac{\sqrt{12(1-\nu^2)}}{2\pi} \frac{PR}{E\lambda^2} kei \frac{r}{\ell}$$

the solution given by Reissner[5].

We now determine the stress function F given by equation (41). From the determination of constants in the solution for w, we see that,

$$F = -\frac{E\lambda}{R}\ell^2\left\{A_3 Re\left[e^{-i\Theta}H_0^{'''}\left(\frac{r}{\ell}e^{i\Theta/2}\right)\right] - A_9 \ln\frac{r}{\ell}\right\} \qquad (54)$$

and we must determine A_9. But this follows immediately from requiring Nrr to be finite at $r = 0$. From equation (10), $Nrr = \frac{F'}{r}$, so from (54) and (50) we see that Nrr is given by

$$N_{rr} = \frac{E\lambda}{R}\ell^2\left\{A_3 Re\left[\frac{2}{\pi r^2}e^{-i\Theta/2}\left(\sin\frac{\Theta}{2}+i\cos\frac{\Theta}{2}\right)+f(r)\right] + \frac{A_9}{r^2}\right\} \qquad (55)$$

And then the requirement (44a) is met if

$$A_9 = -\frac{2}{\pi}\left\{2\sin\frac{\Theta}{2}\cos\frac{\Theta}{2}\right\}A_3 . \qquad (56)$$

And with A_3 given by (52) we have

$$A_9 = \frac{\sqrt{12(1-\nu^2)}}{2\pi} \frac{PR}{E\lambda^2} 2\sin\Theta\left(\sin\frac{\Theta}{2}\cos\frac{\Theta}{2}\right) \qquad (57)$$

Hence, the stress function F_δ is

$$F_\delta = -\frac{PR}{2\pi}\sin\Theta\left\{\frac{\pi}{2} Re\left[e^{-i\Theta}H_0^{'''}\left(\frac{r}{\ell}e^{i\Theta/2}\right)\right]-2\sin\frac{\Theta}{2}\cos\frac{\Theta}{2}\ln\frac{r}{\ell}\right\} \qquad (58)$$

If we make use of (42b), we see that as $k^2 \to \infty$, $\Theta \to 3\pi/2$

$$F_\delta \longrightarrow -\frac{PR}{2\pi}\left\{ \ell_{en}\frac{r}{\ell} + \ell_n\frac{r}{\ell}\right\}$$

the result derived by Reissner [5].

To complete the solution we require β. From (27), with $A_1 = 0$ by (44c) we have

$$\beta = A_2 K_1(kr) + \beta_p \tag{59}$$

and β_p is given in appendix I, equation (h) so that

$$\beta = A_2 K_1(kr) + Re\left[\frac{e^{i\Theta/2}}{k^2 + e^{i\Theta}/\ell^2}H_1^{(1)}\left(\frac{r}{\ell}e^{i\Theta/2}\right)\right]\frac{k^2}{\ell}A_3 \tag{60}$$

Now, from equilibrium, the total resultant normal force V_v acting on a vanishingly small circular region with center $r = 0$ is

$$V_v = -\frac{P}{2\pi r} = \lim_{r\to 0}\int_0^{2\pi}\left(V_r - \frac{r}{R}N_{rr}\right)d\omega \tag{61}$$

With V_r given by (5c), Nrr from (55) and recalling [11, page 115] that

$$K_1(kr) = \frac{1}{kr} + \log_e\left(\frac{kr}{2}\right)I_1(kr) + \gamma(r)$$

where $\gamma(r)$ represents terms bounded near $r = 0$, equation (61) becomes

$$-\frac{P}{2\pi} = \lim_{r\to 0}\frac{5E\lambda}{12(1+\nu)}\left\{\frac{A_2}{k} + \frac{k^2}{\ell}A_3 Re\left[\frac{e^{i\Theta/2}}{\gamma_0}H_1^{(1)}\left(\frac{r}{\ell}e^{i\Theta/2}\right)\right]\right\} \tag{61'}$$

where $\gamma_0 = k^2 + e^{i\Theta}/\ell^2$

And with the behavior of $H_1^{(1)}$ (z) given by (50), and A_3 from (52), (61') yields

$$A_2 = -\frac{P}{2\pi}\frac{12(1+\nu)k}{5E\lambda}\left\{1 + \frac{k^4 \sin\Theta}{12\,\gamma_0\bar\gamma_0(1+\nu)(1-\nu)}\right\} \tag{62}$$

We note that it is further necessary to verify that the solution obtained is the same solution as an appropriate limit applied to a sequence of problems involving continuous external loads which in the limit approach the concentrated load. We have not carried out this procedure but rely on Koiter's [16] conjecture that there is no difficulty as long as the strain energy is bounded; this is the case in the solution given,

$$W_\delta = -\frac{PR}{\pi E h^2}\left[\frac{\sqrt{12(1-\nu^2)}}{4}\sin\theta\,\mathrm{Re}\,H_0^{(1)\prime}\!\left(\frac{r}{\ell}e^{i\theta/2}\right)\right] \tag{53}$$

$$F_\delta = -\frac{PR}{\pi}\sin\theta\left[\frac{1}{4}\mathrm{Re}\left\{e^{-i\theta}H_0^{(1)}\!\left(\frac{r}{\ell}e^{i\theta/2}\right)\right\} - \sin\frac{\theta}{2}\cos\frac{\theta}{2}\ln\frac{r}{\ell}\right] \tag{58}$$

$$\beta = -\frac{P}{\pi E h^2}\left[\frac{6(1+\nu)}{5}k h\left\{1 + \frac{k^4\sin\theta}{12\,\gamma_o\,\bar{\gamma}_o(1+\nu)(1-\nu)}\right\}K_1(kr)\right.$$

$$\left.+\left\{12(1-\nu^2)\right\}^{3/4}k^2\sqrt{\frac{R}{h}}\frac{\pi}{4}\sin\theta\,\mathrm{Re}\left\{\frac{e^{i\theta/2}}{\gamma_o}H_1^{(1)}\!\left(\frac{r}{\ell}e^{i\theta/2}\right)\right\}\right] \tag{63}$$

1.6. The Symmetrical Constraint of a Shallow Spherical Shell with No Edge Restraint.

In Section 1.3 we have formulated this boundary value problem. For convenience we recall it as follows: Let r_o denote the boundary between the loaded and unloaded portions of the shell. Then for

$$0 \leq r < r_o \ , \quad W, \beta, V_r, M_{rr}, N_{rr} \ \text{are finite} \tag{64a}$$

$$r > r_o \ , \quad \text{as } r \to \infty, W, \beta, V_r, M_{rr}, N_{rr} \to 0 \tag{64b}$$

and at $r = r_o$, W, β, V_r, Mrr, Nrr are continuous $\tag{64c}$

If $p(r)$ is the load on the upper surface, the equilibrum condition is

$$2\pi \int_0^{r_o} r \, p(r) \, dr = P(r_o) \tag{65}$$

Once again we denote the solution in the loaded region by a subscript i and in the unloaded region by a subscript o. We shall denote the resultants (64a) by V_i; M_i and N_i and those of (64b) by V_o, M_o, N_o. Then, from (23, 27, 28) the requirement (64a) is satisfied by taking

$$W_i = \delta - \gamma r^2 \tag{66a}$$

$$\beta_i = A_1 I_1(kr) + 2\gamma r \tag{66b}$$

From (5c)

$$V_i = \frac{5E\lambda}{12(1+\nu)} A_1 I_1(kr) \tag{66c}$$

and from (5a)

$$\frac{M_i}{D} = A_1 \left[k I_0(kr) - (1-\nu) \frac{I_1(kr)}{r} \right] + 2\gamma(1+\nu) \tag{66d}$$

From equation (40), we satisfy (64c) with

$$W_o = A_3 \, Re \, H_o^{(1)''}(z) + A_4 \, Im \, H_o^{(1)''}(z) \ . \tag{67a}$$

And then from appendix I, equation (i) we have

$$\beta_o = A_2 K_1(kr) + A_3 \, Re\left[\lambda H_1^{(1)''}(z)\right] + A_4 \, Im\left[\lambda H_1^{(1)''}(z)\right] \tag{67b}$$

from (m)

$$V_o = \frac{5E\lambda}{12(1+\nu)} \left[A_2 K_1(kr) + A_3 \, Re\left\{ (\lambda - \frac{e^{i\theta/2}}{\ell}) H_1^{(1)''}(z) \right\} \right.$$
$$\left. + A_4 \, Im\left\{ (\lambda - \frac{e^{i\theta/2}}{\ell}) H_1^{(1)''}(z) \right\} \right] \tag{67c}$$

and from (1)

$$\frac{M_o}{D} = A_2 \left[-k\, K_0(kr) - \frac{(1-\nu)\, K_1(kr)}{r} \right]$$

$$+ A_3\, \text{Re}\left[\left(\frac{\lambda e^{i\theta/2}}{\ell}\right)\left(H_0^{(1)}(z) - (1-\nu)\frac{H_1^{(1)}(z)}{z}\right) \right]$$

$$+ A_4\, \text{Im}\left[\left(\frac{\lambda e^{i\theta/2}}{\ell}\right)\left(H_0^{(1)}(z) - (1-\nu)\frac{H_1^{(1)}(z)}{z}\right) \right] \qquad (67d)$$

After some algebra, the continuity conditions (64c) determining A_1, A_2, A_3 and A_4, are $\left(z_0 \equiv \frac{r_0}{\ell}e^{i\theta/2} \right)$

$$A_3\, \text{Re}\left[H_0^{(1)}(z_0) \right] \quad + A_4\, \text{Im}\left[H_0^{(1)}(z_0) \right] \qquad\qquad = \delta - \gamma r_0^2 \quad (68a)$$

$$A_3\, \text{Re}\left[\frac{e^{i\theta/2}}{\ell} H_1^{(1)}(z_0) \right] + A_4\, \text{Im}\left[\frac{e^{i\theta/2}}{\ell} H_1^{(1)}(z_0) \right] \qquad = 2\gamma r_0 \quad (68b)$$

$$A_3\, \text{Re}\left[\lambda H_1^{(1)}(z_0) \right] \quad + A_4\, \text{Im}\left[\lambda H_1^{(1)}(z_0) \right] + A_2\, K_1(kr_0) - A_1 I_1(kr_0) = 2\gamma r_0 \quad (68c)$$

$$A_3\, \text{Re}\left[\frac{\lambda e^{i\theta/2}}{\ell} H_0^{(1)}(z_0) \right] + A_4\, \text{Im}\left[\frac{\lambda e^{i\theta/2}}{\ell} H_0^{(1)}(z_0) \right] - A_2\, k\, K_0(kr_0) - A_1 k\, I_0(kr_0) = 4\gamma \quad (68d)$$

The solutions for A_3 and A_4 follow from (66a,b) alone and therefore the algebra is not too tedious. Once again a bar denotes the complex conjugate

$$A_3(r_0;\delta) = \frac{\text{Im}\left\{ (\gamma r_0^2 - \delta)(e^{i\theta/2} H_1^{(1)}(z_0)) + 2\gamma r_0 \ell\, H_0^{(1)}(z_0) \right\}}{\text{Im}\left\{ e^{-i\theta/2} H_0^{(1)}(z_0)\, \overline{H_1^{(1)}(z_0)} \right\}} \qquad (69a)$$

$$A_4(r_0;\delta) = \frac{-\text{Re}\left\{ 2\gamma r_0 \ell\, H_0^{(1)}(z_0) + (\gamma r_0^2 - \delta)e^{-i\theta/2} H_1^{(1)}(z_0) \right\}}{\text{Im}\left\{ e^{-i\theta/2} H_0^{(1)}(z_0)\, \overline{H_1^{(1)}(z_0)} \right\}} \qquad (69b)$$

$$A_2(r_0;\delta) = \frac{S(r_0)}{K_1(kr_0)} - \delta(r_0)\mu(r_0) - \frac{\frac{\eta(r_0)}{k} - \frac{K_0(kr_0)}{K_1(kr_0)} S(r_0)}{K_0(kr_0) + \frac{I_0(kr_0)}{I_1(kr_0)} K_1(kr_0)} \qquad (69c)$$

$$A_1(r_0; \delta) = \delta(r_0)\mu(r_0) - \frac{\frac{\eta(r_0)}{k} - \frac{K_0(kr_0)}{K_1(kr_0)}\mathcal{S}(r_0)}{I_0(kr_0) + \frac{K_0(kr_0)}{K_1(kr_0)}I_1(kr_0)} \tag{69d}$$

$$\eta(r_0) = \frac{4\gamma}{k} + \frac{\mathcal{I}m\left\{\frac{2\gamma\lambda e^{i\theta/2}}{R}r_0 H_0^{(1)}(z_0)\overline{H_0^{(1)}(z_0)} + \gamma r_0^2\frac{\lambda}{kl}H_0^{(1)}(z_0)\overline{H_1^{(1)}(z_0)}\right\}}{\mathcal{I}m\left\{e^{-i\theta/2}H_0^{(1)}(z_0)\overline{H_1^{(1)}(z_0)}\right\}} \tag{70a}$$

$$\mathcal{S}(r_0) = 2\gamma r_0 + \frac{\mathcal{I}m\left\{2\gamma r_0\lambda l\, H_1^{(1)}(z_0)\overline{H_0^{(1)}(z_0)} + \gamma r_0^2\lambda e^{-i\theta/2}H_1^{(1)}(z_0)\overline{H_1^{(1)}(z_0)}\right\}}{\mathcal{I}m\left\{e^{-i\theta/2}H_0^{(1)}(z_0)\overline{H_1^{(1)}(z_0)}\right\}} \tag{70b}$$

$$\mu(r_0) = \frac{\mathcal{I}m\left\{\frac{\lambda}{kl}H_0^{(1)}(z_0)\overline{H_1^{(1)}(z_0)} + \frac{K_0(kr_0)}{K_1(kr_0)}\lambda e^{-i\theta/2}H_1^{(1)}(z_0)\overline{H_1^{(1)}(z_0)}\right\}}{I_0(kr_0) + \frac{K_0(kr_0)}{K_1(kr_0)}I_1(kr_0)} \tag{70c}$$

And for convenience we recall the following definitions:

$$\lambda = \frac{k^2}{l}\frac{e^{i\theta/2}}{k^2 + e^{i\theta}/l^2} \qquad\qquad \text{(Appendix I, equation (h'))}$$

$$\theta = \tan^{-1} - \sqrt{\left(\frac{R}{h}\right)^2\frac{16}{3}\frac{1-\nu}{1+\nu} - 1} \qquad\qquad \text{(equation 35)}$$

$$k^2 = \frac{5(1-\nu)}{h^2} \qquad\qquad \text{(equation 6')}$$

$$l = \sqrt{Rh}\Big/\sqrt[4]{12(1-\nu^2)} \qquad\qquad \text{(equation 35)}$$

$$\gamma = \frac{R_1 + R_2}{2R_1R_2} \qquad\qquad \text{(equation 23)}$$

We now recover the center displacement $\delta(r_o)$ which follows from the Greens function for the problem, W_δ, derived in section 1.5. For as in Hertz' problem $[1]$, the center displacement $\delta(r_o)$ satisfies

$$2\pi \int_0^{r_o} p(r)\, \frac{W_\delta}{P}\, r\, dr = \delta(r_o) \tag{71}$$

and $p(r)$ is now given by (3b, 11)

$$r\, p(r) = -\frac{E\lambda}{R}\cdot\frac{r}{R}\left(\delta - r r^2\right) - \frac{SE\lambda}{12(1+\nu)} A_1(r_o;\delta))\, k r\, I_o(kr) \tag{72}$$

And from (53)

$$W_\delta = A_3\, \text{Re}\left[H_o^{(1)}\left(\frac{r}{\ell} e^{i\theta/2}\right)\right] \tag{73a}$$

Where

$$A_3 = -\frac{\sqrt{12(1-\nu^2)}}{2\pi}\, \frac{PR}{E\lambda^2}\, \frac{\pi}{2}\, \sin\theta \tag{73b}$$

From (71,72,73) it is evident that we require the following integrals: (for details of the evaluation see appendix 1, section C)

$$\Lambda_1(r_o) = \int_0^{r_o} H_o^{(1)}\left(\frac{r}{\ell} e^{i\theta/2}\right) r^3\, dr$$

$$= \ell^4 e^{-2i\theta}\left\{ (z_o^3 - 4 z_o) H_1^{(1)}(z_o) + 2 z_o^2 H_o^{(1)}(z_o) - \frac{8}{\pi} i\right\} \tag{74a}$$

$$\Lambda_2(r_o) = \int_0^{r_o} H_o^{(1)}\left(\frac{r_o}{\ell} e^{i\theta/2}\right) r\, dr = \ell^2 e^{-i\theta}\left\{ z_o H_1^{(1)}(z_o) + \frac{2i}{\pi}\right\} \tag{74b}$$

$$\Lambda_3(r_o) = \int_0^{r_o} H_o^{(1)}\!\left(\frac{r}{\ell}e^{i\theta/2}\right) I_o(kr)\, r\, dr$$

$$= \frac{1}{\frac{e^{i\theta}}{\ell^2}+k^2}\left\{ z_o H_1^{(1)}(z_o) I_o(kr_o) + kr_o H_o^{(1)}(z_o) I_1(kr_o) + \frac{2i}{\pi}\right\} \tag{74c}$$

Then substituting (72) into (71), making use of (73) and letting

$$\lambda_i = Re\left[\Lambda_i\right] \tag{75}$$

results in

$$\delta(r_o) = \frac{-\frac{\alpha R}{h}\left\{\frac{\gamma}{R^2}\lambda_1(r_o) + \frac{5k}{12(1+\nu)} C(r_o)\lambda_3(r_o)\right\}}{1 + \frac{\alpha}{R\lambda}\lambda_2(r_o) - \frac{\alpha R}{h}\frac{5k}{12(1+\nu)}\lambda_3(r_o)\mu(r_o)} \tag{76a}$$

where

$$\mu = \frac{\pi}{2}\sqrt{12(1-\nu^2)}\,\sin\theta \tag{76b}$$

and

$$C(r_o) = \frac{\mathcal{H}(r_o) - \frac{K_o(kr_o)}{K_1(kr_o)}\varsigma(r_o)}{I_o(kr_o) + \frac{K_o(kr_o)}{K_1(kr_o)}I_1(kr_o)} \tag{77}$$

To obtain a relationship for P and r_o we employ (65) (or the continuity of N_{rr}, with N_{rr} consistant with (65)), and with P and δ as given by (72) and (76a) respectively.

$$\frac{P(r_o)}{\pi E h^2} = -\frac{\gamma r_o^2}{2R^2\lambda} + \frac{\delta r_o^2}{\lambda R^2} + \frac{5}{6}\frac{A_1(r_o;\delta) I_1(kr_o) r_o}{1+\nu}\frac{}{\lambda} \tag{78}$$

With $A_1(r_o;\delta)$ and $\delta(r_o)$ given by (69d) and (76) respectively.

1.7. Discussion of the Results for a Flat Indenter

Figure 4 shows the pressure distribution $p(r)$ between a shell and a plane rigid Indenter for a series of areas of applanation.* On the same figure, the resultant force $P(r_o)$ (equation 78) Is shown as a function of r_o, the radius of the flattened area. Figure 5 shows the resultant force for a shell radius of 30, thickness 1.0 and Poisson's ratios of 0.5 and 0.3. Figure 6 is the same presentation for a thickness of 0.5.

The pressure distributions predicted by the theory are seen to be physically consistent up to $r_o = 1.27$ for the dimensions of fig. 4. The classical theory predicts that the pressure distribution is immediately negative.

We may regard the point at which the pressure becomes negative as the end of the validity of solution since we have assumed that the Indenter contacts the shell everywhere in the applaned region. But, the fact that after a certain radius of flattening the pressure distribution becomes negative, may be indicative of the initiation of some kind of instability. In the examples shown the pressure becomes negative while the deformations are less than 1/3 the shell thickness and conform to Donnell's criteria [13] for the validity of shallow shell theory.

Although the accurate prediction of instability would probably require a more elaborate (at least geometrically non-linear) theory, these results do predict a physically reasonable situation. That is, if a shell is symmetrically deformed by a rigid surface, than beyond a certain contact area the shell's resistance to deformation is no longer monotone; the portion of the deformed shell near the edge of that contact region is unable to further resist deformation.

---

* The calculations were carried out on the IBM 7090 computer at the University of California at Berkeley.

Appendix I

A. The Evaluation of β_p

We evaluate the particular integral β_p, equation (28) with w given by

$$W = A_3 Re\left[H_0^{(1)}(z)\right] + A_4 \mathfrak{Im}\left[H_0^{(1)}(z)\right] + A_5 Re\left[J_0(z)\right] + A_6 \mathfrak{Im}\left[J_0(z)\right] \quad \text{(a)}$$

If $\omega_\nu(z)$ and $W_\mu(z)$ are two cylinder functions, then [15, pg. 90]

$$\int^x \omega_\nu(\alpha x) W_\nu(\gamma x) x \, dx = \frac{x}{\gamma^2 - \alpha^2}\left\{\gamma W_{\nu+1}(\gamma x)\omega_\nu(\alpha x) \right. \quad \text{(b)}$$
$$\left. - \alpha W_\nu(\gamma x)\omega_{\nu+1}(\alpha x)\right\}$$

In (b) let

$$\alpha = \frac{e^{i\theta/2}}{\ell}, \quad \gamma = ik \quad \text{(c)}$$

and recall that

$$I_1(k\eta) = -i J_1(ik\eta)$$
$$K_1(k\eta) = -\frac{\pi}{2} H_1^{(1)}(ik\eta)$$
$$I_2(k\eta) = J_2(ik\eta) \quad \text{(d)}$$
$$K_2(k\eta) = -i\frac{\pi}{2} H_2^{(1)}(ik\eta)$$

Then from (b,d) we have

$$\int^r \eta \,\omega_\nu\left(\eta \frac{e^{i\theta/2}}{\ell}\right) K_1(k\eta) \, d\eta =$$

$$-\frac{r}{k^2 + \frac{e^{i\theta}}{\ell^2}}\left\{k K_2(kr)\omega_\nu\left(r\frac{e^{i\theta/2}}{\ell}\right) - \frac{e^{i\theta/2}}{\ell} K_1(kr)\omega_{\nu+1}\left(r\frac{e^{i\theta/2}}{\ell}\right)\right\} \quad \text{(e)}$$

and $\displaystyle\int^{r}\eta\,\omega_{\flat}\!\left(\frac{\eta}{\ell}e^{i\theta/2}\right)I_{1}(k\eta)\,d\eta =$

$$\frac{r}{k^{2}+\frac{e^{i\theta}}{\ell^{2}}}\left\{kI_{2}(kr)\,\omega_{\flat}\!\left(\frac{r}{\ell}e^{i\theta/2}\right)+\frac{e^{i\theta/2}}{\ell}I_{1}(kr)\,\omega_{\flat+1}\!\left(\frac{r}{\ell}e^{i\theta/2}\right)\right\} \tag{f}$$

From (e,f) it follows that

$$\int^{r}\eta\,\omega_{\flat}\!\left(\frac{e^{i\theta/2}}{\ell}\eta\right)\left\{K_{1}(k\eta)I_{1}(kr)-I_{1}(k\eta)K_{1}(kr)\right\}d\eta \tag{g}$$

$$= -\frac{1}{k^{2}+\frac{e^{i\theta}}{\ell^{2}}}\,\omega_{\flat}\!\left(\frac{r}{\ell}e^{i\theta/2}\right)$$

And hence, from (28), (a) and (g) we have

$$\beta_{p}= A_{3}\,\mathrm{Re}\;\lambda H_{1}^{(1)}(z)+A_{4}\,\mathrm{Im}\;\lambda H_{1}^{(1)}(z)+A_{5}\,\mathrm{Re}\;\lambda J_{1}(z) \tag{h}$$

$$+\,A_{6}\,\mathrm{Im}\;\lambda J_{1}(z)$$

where

$$\lambda = \frac{k^{2}}{\ell}\frac{e^{i\theta/2}}{k^{2}+e^{i\theta}/\ell^{2}}\;,\quad z=\frac{r}{\ell}e^{i\theta/2}\;. \tag{h'}$$

B. Evaluation of the Resultant Stresses and Couples

We first evaluate M_{rr}, $M_{\theta\theta}$, V_{r} as given by equation 5, N_{rr} and $N_{\theta\theta}$ as given by equation (b), for the normal displacement w from equation (a). The slope β is (27,h)

$$\beta = A_{1}I_{1}(kr)+A_{2}K_{1}(kr)+A_{3}\,\mathrm{Re}\;\lambda H_{1}^{(1)}(z)$$

$$+\,A_{4}\,\mathrm{Im}\;\lambda H_{1}^{(1)}(z)+A_{5}\,\mathrm{Re}\;\lambda J_{1}(z)+A_{6}\,\mathrm{Im}\;\lambda J_{1}(z) \tag{i}$$

From equation (a)

$$-w' = A_3 \, Re\left[\frac{e^{i\theta/2}}{\ell} H_1^{(1)}(z)\right] + A_4 \, \Im m\left[\frac{e^{i\theta/2}}{\ell} H_1^{(1)}(z)\right]$$

$$+ A_5 \, Re\left[\frac{e^{i\theta/2}}{\ell} J_1(z)\right] + A_6 \, \Im m\left[\frac{e^{i\theta/2}}{\ell} J_1(z)\right]$$

and we denote this and similar expressions below as

$$-w' = \begin{Bmatrix} A_3 \, Re \\ A_4 \, \Im m \end{Bmatrix}\left\{\frac{e^{i\theta/2}}{\ell} H_1^{(1)}(z)\right\} + \begin{Bmatrix} A_5 \, Re \\ A_6 \, \Im m \end{Bmatrix}\left\{\frac{e^{i\theta/2}}{\ell} J_1(z)\right\} \qquad (j)$$

Differentiating (i) yields

$$\beta = A_1\left\{k I_0(kr) - \frac{I_1(kr)}{r}\right\} - A_2\left\{k K_0(kr) + \frac{K_1(kr)}{r}\right\}$$

$$+ \begin{Bmatrix} A_3 \, Re \\ A_4 \, \Im m \end{Bmatrix}\left\{\frac{\lambda e^{i\theta/2}}{\ell}\left(H_0^{(1)}(z) - \frac{H_1^{(1)}(z)}{z}\right)\right\}$$

$$+ \begin{Bmatrix} A_5 \, Re \\ A_6 \, \Im m \end{Bmatrix}\left\{\frac{\lambda e^{i\theta/2}}{\ell}\left(J_0(z) - \frac{J_1(z)}{z}\right)\right\}. \qquad (k)$$

Hence

$$-\frac{M_{rr}}{D} = \beta' + \frac{\nu\beta}{r} = A_1\left\{k I_0(kr) - (1-\nu)\frac{I_1(kr)}{r}\right\}$$

$$+ A_2\left\{-k K_0(kr) - (1-\nu)\frac{K_1(kr)}{r}\right\}$$

$$+ \begin{Bmatrix} A_3 \, Re \\ A_4 \, \Im m \end{Bmatrix}\left\{\left(\frac{\lambda e^{i\theta/2}}{\ell}\right)\left(H_0^{(1)}(z) - (1-\nu)\frac{H_1^{(1)}(z)}{z}\right)\right\}$$

$$+ \begin{Bmatrix} A_5 \, Re \\ A_6 \, \Im m \end{Bmatrix}\left\{\left(\frac{\lambda e^{i\theta/2}}{\ell}\right)\left(J_0(z) - (1-\nu)\frac{J_1(z)}{z}\right)\right\} \qquad (l)$$

$$-\frac{M_{\theta\theta}}{D} = \frac{\beta}{r} + \nu\beta' = A_1\left\{\nu k I_0(kr) + (1-\nu)\frac{I_1(kr)}{r}\right\}$$

$$+ A_2\left\{-\nu k K_0(kr) + (1-\nu)\frac{K_1(kr)}{r}\right\}$$

$$+ \begin{Bmatrix} A_3 \, Re \\ A_4 \, \Im m \end{Bmatrix}\left\{\left(\frac{\lambda e^{i\theta/2}}{\ell}\right)\left(\nu H_0^{(1)}(z) + (1-\nu)\frac{H_1^{(1)}(z)}{z}\right)\right\} \qquad (m)$$

$$+ \begin{Bmatrix} A_5 \, Re \\ A_6 \, \Im m \end{Bmatrix}\left\{\left(\frac{\lambda e^{i\theta/2}}{\ell}\right)\left(\nu J_0(z) + (1-\nu)\frac{J_1(z)}{z}\right)\right\}$$

and

$$\frac{12(1+\nu)}{5E\lambda} V_r = A_1 I_1(kr) + A_2 K_1(kr)$$

$$+ \left\{\begin{matrix} A_3 \, Re \\ A_4 \, Im \end{matrix}\right\} \left\{\left(\lambda - \frac{e^{i\theta/2}}{\ell}\right) H_1^{(1)}(\hat{z})\right\}$$

$$+ \left\{\begin{matrix} A_5 \, Re \\ A_6 \, Im \end{matrix}\right\} \left\{\left(\lambda - \frac{e^{i\theta/2}}{\ell}\right) J_1(\hat{z})\right\} \tag{n}$$

The direct resultants are obtained from equation (16) as

$$N_{rr} = \frac{F'}{r} = \frac{E\lambda}{R}\left[\left\{\begin{matrix} A_3 Re \\ A_4 Im \end{matrix}\right\}\left\{\frac{H_1^{(1)}(\hat{z})}{\hat{z}}\right\} + \left\{\begin{matrix} A_5 Re \\ A_6 Im \end{matrix}\right\}\left\{\frac{J_1(\hat{z})}{\hat{z}}\right\} + \frac{A_9 \ell^2}{r^2}\right] \tag{o}$$

$$N_{\theta\theta} = F'' = \frac{E\lambda}{R}\left[\left\{\begin{matrix} A_3 Re \\ A_4 Im \end{matrix}\right\}\left\{\ell e^{i\theta/2}\left(H_0^{(1)}(\hat{z}) - \frac{H_1^{(1)}(\hat{z})}{\hat{z}}\right)\right\}\right.$$

$$\left. + \left\{\begin{matrix} A_5 Re \\ A_6 Im \end{matrix}\right\}\left\{\ell e^{i\theta/2}\left(J_0(\hat{z}) - \frac{J_1(\hat{z})}{\hat{z}}\right) - \frac{A_9 \ell^2}{r^2}\right\}\right] \tag{p}$$

C. The Evaluation of the Integrals $\Lambda_1, \Lambda_2, \Lambda_3,$ of section 1.

These integrals are evaluated with the aid of equation (b) of Appendix I, the result [18, pg. 133] that for W_ν a cylinder function,

$$\int^X x^{\mu+1} W_\nu(x)dx = -(\mu^2-\nu^2)\int^X x^{\mu-1} W_\nu(x)dx$$

$$+ \left[x^{\mu+1} W_{\nu+1}(x) - (\mu-\nu)W_\nu(x)\right] \tag{q}$$

and the following limits (which result from the formulas [11, pg. 54])

$$\lim_{r\to 0} r\, H_1^{(1)}\left(\frac{r}{\ell}e^{i\theta/2}\right) = -\frac{2}{\pi}i\ell e^{-i\theta/2} \tag{r}$$

$$\lim_{r \to 0} r \, H_0^{(1)}\left(\frac{r}{\ell} e^{i\theta/2}\right) I_1(kr) = 0 \tag{s}$$

From (q) we have

$$\Lambda_1(r_0) = \int_0^{r_0} H_0^{(1)}\left(\frac{r}{\ell} e^{i\theta/2}\right) r^3 \, dr = \left[-4\left(\frac{e^{i\theta/2}}{\ell}\right)^{-3} r \, H_1^{(1)}\left(\frac{r}{\ell} e^{i\theta/2}\right) \right.$$

$$\left. + \left(\frac{e^{i\theta/2}}{\ell}\right)^{-1} r^3 H_1^{(1)}\left(\frac{r}{\ell} e^{i\theta/2}\right) + \left(\frac{2 e^{i\theta/2}}{\ell}\right)^{-2} r^2 H_0^{(1)}(z) \right]_0^{r_0}$$

The lower limit is evaluated using (r) above; setting $z_0 = \dfrac{r_0}{\ell} e^{i\theta/2}$, we have

$$\Lambda_1(r_0) = \ell^4 e^{-2i\theta} \left\{ \left(z_0^3 - 4 z_0\right) H_1^{(1)}(z_0) + 2 z_0^2 \, H_0^{(1)}(z_0) - \frac{8}{\pi} i \right\} \tag{t}$$

The evaluation of $\Lambda_2(r_0)$ follows similarly from (q and r) as

$$\Lambda_2(r_0) = \int_0^{r_0} H_0^{(1)}(z) r \, dr = \ell^2 e^{-i\theta} \left\{ z \, H_1^{(1)}(z_0) + \frac{2i}{\pi} \right\} \tag{u}$$

and $\Lambda_3(r_0)$ follows from (b), (r) and (s)

$$\Lambda_3(r_0) = \int_0^{r_0} H_0^{(1)}(z) I_0(kr) r \, dr$$

$$= \frac{1}{\frac{e^{i\theta}}{\ell^2} + k^2} \left\{ \frac{e^{i\theta/2}}{\ell} H_1^{(1)}(z) I_0(kr) r + kr \, H_0^{(1)}(z) I_1(kr) \right\} \Bigg|_0^{r_0}$$

$$= \frac{1}{\frac{e^{i\theta}}{\ell^2} + k^2} \left\{ z_0 \, H_1^{(1)}(z_0) I_0(kr_0) + k r_0 \, H_0^{(1)}(z_0) I_1(kr_0) + \frac{2i}{\pi} \right\} \tag{v}$$

CHAPTER 2

An Experimental Study of the Rheology of the Cornea in Vitro

2.1. Introduction

The purpose of this study is to understand under what conditions of magnitude and duration of loading the cornea behaves as a linear viscoelastic solid. Accordingly, our experiment has been designed to ascertain under what circumstances the cornea conforms to the requirements of the Boltzmann Super-position principle. Basically we have relied on hogs eyes, but several human eyes have also been tested.

An attempt was made to assess any changes in the mechanical properties of the cornea due to physiological change after death. Hence, we performed some experiments at the site of procurement of the enucleated eyes, approximately six minutes after the animal's death. Although the results show some consistency, the temperature was not controlled and due to the simultaneous action of the variables age and temperature the results on the aging dependency of the mechanical properties of the _in vitro_ cornea must be regarded strictly as preliminary. However, it was definitely established that the creep response shown by the cornea is not an artifactual result of enucleation.

The experiments may be grouped as follows:

A. Creep Tests at an Intraocular pressure of 40 mm.Hg. (Figures 9-15).

These experiments represent the most complete element of the rheological study. An internal pressure of 40 mm.hg was choosen to simulate the state of the cornea under Schiøtz tonometry or tonography. The plunger diameter in these tests was 3 mm. This diameter and the loading range (4 g. to 12 g.) are appropriate to the conditions during the application of the Schiøtz tonometer.

B. Creep Tests at a Fixed Load and Different Intraocular Pressures. (Figures 16-20).

These experiments were designed to investigate the dependence of the rheological behavior of the cornea on the level of intraocular pressure. The creep response of the cornea was measured for a given load and an intraocular pressure _fixed_ at the consecutive values of 20, 30, 40, 50, and 60 mm.Hg.

To obtain a description of the corneal response at a loading range pertinent to applanation tonometry, a larger plunger (4mm. diameter) was employed with a loading range of 2-12 grams. Hence we have an applied pressure (due to plunger loading) that is at one degree considerably lower than class A and its upper range overlaps the lower loading range of the experiments in class A.

C. <u>Corneal Compression Tests. (Figure 21)</u>.

Since the cornea is capable of compression, this deformation mode was investigated as follows. A portion of the cornea was removed and placed on a steel ball whose radius was approximately equal to the corneal radius at an internal pressure of 20 mm.Hg. The experiments were then performed as though the cornea was supported by an intraocular hydrostatic pressure. Since we are basically interested in the instantaneous (elastic) compression response, the steel ball was thought to present a negligible source of error from the viewpoint of obstructing the diffusion of fluid across the inner surface of the cornea.

D. <u>Volume Expansion Tests (Figure 22). (Eye Loaded Only by the Intraocular Pressure)</u>.

When the intraocular pressure is raised, the upper surface of the cornea (and sclera) symmetrically deforms. If the material behaves linearly, and a pressure increase from P_o to $P_o + \delta p$ yields an increased displacement δw, then $P_o + \alpha \delta p$ should induce a displacement change of $\alpha \delta w$. These tests were

designed to check the material linearity of the eye in this deformation mode. A pressure range of 20 - 60mm.Hg. was covered in 10mm.Hg. increments.

In section 2.2 we record some ideas from the theory of linear visco-elasticity. Section 2.3 contains a description of the experimental equipment, and in section 2.4 we describe the experimental procedure.

The results of the creep tests are discussed in this chapter (section 2.5). The corneal compression tests and volume expansion tests respectively provide an estimate of the foundation constant (see chapter 3) of the corneal stroma and the Young's modulus of the combined layer of Descemet's membrane and the pavement epithelium (see Figure 23). These tests are pertinent to the measurement of intraocular pressure and are discussed in chapter three.

2.2 Results from the Linear Theory of Viscoelasticity

The results stated here are from the foundations of linear viscoelasticity. These have been rigorously given by Gurtin and Sternberg [ref.24] . Discussions oriented toward engineering application are numerous; here we refer to the discussion by Lee [ref.26] . The distinction of a semi-relaxing viscoelastic solid is due to Hunter [ref.25] .

If P and Q are linear operators in time, and $\sigma(t)$ is the stress variation with $e(t)$ its corresponding strain variation, then a material is linear viscoelastic if it obeys the law:

$$P(\sigma) = Q(e) \tag{79}$$

The relationship (79) may also be given as a hereditary integral. The existence of this representation stems from the postulate of linearity which is equivalent to the Boltzmann Superposition principle:

Let a particular load variation be given by

$$L(t) = L_1(t) \tag{79a}$$

and the deformation response by

$$\delta(t) = \delta_1(t)$$

<div align="right">(79b)</div>

Then if the load is changed to

$$L(t) = \alpha_r L_1(t)$$

<div align="right">(79c)</div>

where α_r are a series of constants covering the domain of loading, then the superposition principle requires that the resulting deformations

$$\delta(t) = \delta_r(t)$$

<div align="right">(79d)</div>

satisfy

$$\delta_r(t) = \alpha_r \delta_1(t)$$

<div align="right">(79e)</div>

If the requirement outlined in (79) is met, then the stress and strain in the body are related by a Duhamel integral as

$$e(t) = \int_{-\infty}^{t} \psi(t-\tau) \frac{d\sigma(\tau)}{d\tau} d\tau$$

<div align="right">(80)</div>

where $\psi(t)$ is known as the creep function. Alternatively

$$\sigma(t) = \int_{-\infty}^{t} G(t-\tau) \frac{de(\tau)}{d\tau} d\tau$$

<div align="right">(81)</div>

where $G(t)$ is known as the relaxtion function.

A material is called semi-relaxing if the extension response due to an applied constant load approaches a finite limit as time increases. It is possible to show that for such materials, the force required to maintain a constant deformation does not fall to zero in time but appraoches a constant value.

In order to check the applicability of the superposition principle (79) we plot

$$\frac{\delta_r(t)}{\alpha_r}$$

as a function of time and see if these curves (for successive α_r) coincide with the curve $\delta_1(t)$. A viscoelastic material will have a response curve $\delta(t)$ that differs in shape from the load curve L (t). The special case of an elastic solid is included in (79); in that case the load and deformation response curves will have the same shape.

If a material can be represented by the laws (80) or (81), (i.e. 79 holds) and is of a semi-relaxing nature, then in the quasi-static case, assuming the boundary conditions for the elastic and viscoelastic problems are the same, the viscoelastic result follows by a correspondence principle applied to the solution of the elastic problem. (see section 3.6).

2.3 The Description of the Experimental Equipment

To facilitate the discussion we first give a review of the equipment employed. Each item is designated by a numeral and shall be referred to by name (e.g., motion transducer) and numeral. The detailed description of any particular apparatus will now be given and this list is referred to in the text.

1. Motion Transducer

The mechanical transducer employed was a Taft-Peirce Versacheck Electronic Gage. The basic equipment consists of 1) a pick-up head which operates on the linear differential transformer principle and is capable of detecting motion changes of the order of 1×10^{-6} inches. 2) A phase-sensitive, extremely linear, carrier amplifier to magnify the transducer signal, and a DC meter which reads in fractions of an inch. The Versacheck unit has an internal calibriation circuit for determining the gain of the entire circuit. The unit may be selected to operate any one of four meter graduations: In inches these are

5×10^{-4}, 1×10^{-4}, 5×10^{-5}, 1×10^{-5}.

The meter is of the dead beat type, accuracy to within 1% and a response time of $\frac{1}{4}$ second with no over shoot. After a 30 minute warm up time, the stability is 2×10^{-6} inches per hour assuming good temperature control.

II. Brush Recorder Mark II

This recorder was used to continuously record the motion transducer's output.

III. Pressure Transducer

The intraocular pressure was monitored by a Statham Model P23 pressure transducer.

IV. Visicorder Oscillograph

The output of the pressure transducer was recorded by a Honeywell Model 906 C Visicorder Oscillograph. The Heiland galvanometer type chosen was No. M200-120.

V. Statham Control Unit

The Model CB-19 Control Unit was employed for calibrating the pressure transducer and for providing its DC input voltage.

VI. Silastic

The eyes were set in Dow Corning Silastic RTV 502 with a Stannous octoate catalyst. The setting process is not exothermic.

The motion transducer (I) was supported on two parallel rails to facilitate placement over the eye. The rails were attached to a heavy steel plate which was the support for all the equipment directly involved in measurement (see Figure 7). The plate rested on a felt pad; the measuring equipment was sufficiently isolated from vibration.

The motion transducer was fitted with a rigid extension arm capable

of extending from 5 to 12 inches. It was found that a lever arm   seven

inches along with the 1 x 10^{-4} and 5 x 10^{-4} inch scales of the DC meter of

the motion transducer (1) was capable of measuring the imposed corneal defor-

mations. The variable extension arm was required to allow operation in the

vicinity of the eye and to accommodate the transducer choosen since a-priori

we could not be sure of the deformation range. A weighting platform (covered

with foam rubber to damp any impulse due to the application of the load) was

attached at the end of the supporting arm. The underside of the platform

accepted the plunger that contacted the cornea.

The experimental results below are appended with the pertinent data of

eye age, internal pressure, outer corneal radius of curvature and room tem-

perature. Two classes of experiments were carried out:

a) After procurement of the enucleated eyes, each eye
was set in its own covered container with the eye
resting on saline saturated cotton and allowed to
equilibrate with room temperature.

b) At the site of procurement three eyes were tested six
to seven minutes after death. The mated eye was
chilled and tested one to two hours later (see
figures 8, 14, 15)

The class a includes the two human eyes and over twenty hogs eyes.

2.4 Experimental Procedure

1. The eye was removed from the moist saline atmosphere (see section 2.3b) and set in silastic (VI). Approximately three-fourths of the posterior globe was immersed in the silastic. Prior to placement an 18 gage needle was inserted in the anterior chamber and attached to a water column.

2. The eye was covered with 4-5 c.c. of saline during each creep test.

3. The 3 mm. diameter, concave plunger attached to the motion transducer (I) via a seven inch extension arm was placed over the eye. The eye was raised on a cam-adjusted platform so as to pre-load the cornea with a 0.5 gram pre-load.

4. The plunger was loaded and the deformation response recorded until it was no longer possible to discern changes in deformation.

5. The eye was unloaded and allowed to rest for a time period equal to the loading time. The saline was removed during the rest time.

6. The eye was reimmersed in saline, loaded with a larger weight, and the measurement process repeated.

7. After the complete run the corneal curvature was measured.

2.4 A. Discussion of the Experimental Procedure

1.a The silastic receptor was pliable and did not interfere (due to its distance from the loaded region), with the measurement.

2.a The plunger head and stem were wetted, hence maintaining a constant surface tension throughout the run. The entire unit was balanced with the surface tension acting on the plunger, hence the surface tension was controlled and eliminated as an operative force and as a source of experimental error. (If the plunger was not immersed in saline, then the surface tension could change during the run and the corneal load could not accurately be known).

3.a The pre-load was necessary to smooth out any surface defects and to make certain that the plunger contacted the cornea at the time it was loaded. The pre-load can always be calculated and it is too small to be subject to an error due to corneal creep. Hence, it may be found from the elastic calibration of the instrument. It does not interfere with the calculation involved in superimposing the creep curves.

4.a It was possible to visually discern meter motions of one-tenth unit, or .0087 mm. This is better accuracy than can normally be obtained with electronically recording indentation tonometers.

2.4 B Corneal Compression

A central portion of the cornea was dissected and placed on a rigid ball of radius 7.5 mm. The cornea was then loaded as in the creep tests above except it was not immersed in saline. The surface tension was eliminated by covering the corneal segment with a piece of 0.00025 inch thick teflon.

Since this test is a compression test, the teflon does not introduce any conceptual problem, whereas in the creep tests a similar procedure might have introduced extraneous membrane forces. Young's modulus for teflon is several

orders of magnitude greater than for the cornea, so in the compression tests the teflon sheet introduces no experimental error.

2.4 C. Volume Expansion Experiments

These experiments closely followed the procedure in 2.4 A, except the only loading on the cornea (or sclera) was a preload less than 0.1 grams. The deformation response was obtained by raising the intraocular pressure through 10 mm.Hg.increments. (The eye was set in the silastic in such a way that there was no motion of the limbus during the corneal expansion test).

2.5 Discussions of the Creep Tests

The cornea conforms to the requirements of the Boltzmann superposition principle.

1. Figures 9, 10 show the results of creep tests for two excised human eyes. The creep curves superimpose to within 10 percent for the 3.2 and 7.2 gram loads. The tendency toward deviation from linearity in the 11 - 12 gram loading range occurs outside the clinical range of interest for the Schiøtz tonometer. Figures 11, 12, 13 show representative results for three of the twenty enucleated hog eyes tested. It is important to note that whereas the human eyes showed a long term creep component, the hogs eyes demonstrated no creep after two - three minutes. (*)

   The elastic response for all the eyes superimposed linearly, and the initial response for the 3.2 and 7.2 gram loads indicate that in that loading range it is reasonable to consider the initial response of the cornea as that of a linear elastic solid undergoing small strains.

(*) Our experiments indicate a maximum of seven to eight minutes for the 7.2 gram load. St. Helen & McEwen [22] report a measureable creep up to thirty minutes for the sclera.

2. Figures, 14,15 show results for two (of three) hog eyes tested
   at the slaughter house. The solid lines show the creep response
   of two eyes tested six - seven minutes after the animals death.(**)
   It is clear that the creep response is not an artifact due to
   ageing of the _in vitro_ specimen.

3. Figures 16 - 19 show that the response of an enucleated hog eye to
   a sequence of loads at a given pressure; the figures in sequence in-
   dicate the results for internal pressures of 20, 30, 40, 50 and
   60 mm.Hg. Figure 20 shows the results replotted to show the corneal
   response for a fixed load with the internal pressure as the para-
   meter. At a fixed level of pressure the cornea behaves linearly for
   the applied load sequence.

(**) The mated eyes were refrigerated after enucleation. When they were
tested, approximately $1\frac{1}{2}$ hours later, they all showed geometrically similar
responses but the magnitude of the instantaneous response was diminished in
one case by 20 percent and by less than ten percent for the others. Although
this result is of some interest, it is inconclusive due to the simultaneously
acting variables of temperature and aging.

CHAPTER 3

Tonometry and Tonography

3.1 Introduction

In this chapter we shall employ the previous results to analyze some instruments that are used in the detection of glaucoma. Two of the devices that we discuss are the Goldmann [21] and the Mackay-Marg [23] tonometers,[*] and in particular, their sensitivity to the magnitude of:

a) The radius of curvature of the coronea

b) The thickness of the various corneal layers

c) The Young's moduli of the corneal layers

From an estimate of the magnitude of the surface tension force operative during Goldmann applanation tonometry, and from our volume expansion tests (figure 22) from which we deduce Young's modulus for the outer layer of the hog's cornea, we are able to infer the order of magnitude of Young's modulus for the central corneal layer. Hence we are able to extend Goldmann's analysis of his applanation tonometer to a quantitative description of the forces involved during applanation tonometry. Our results indicate that a certain kind of elastic instability might appear during the applanation procedure.

After discussing the applanation tonometers, we consider the indentation tonometers; in particular the Schiøtz tonometer (see, e.g., [19]). The linear viscoelastic behavior of the cornea allows us to analyze some aspects of the time dependent process known as tonography.

For completeness we include, in section 3.2, a brief description of both the anatomy of the eye and the glaucoma problem. Section 3.3 is devoted to the development of a structural model of the eye. In section 3.4 we discuss the Goldmann tonometer and in section 3.5, the Mackay-Marg tonometer.

---

[*]Mackay-Marg tonometry differs from the use of previous applaning tonometers in distinct ways set forth on page 60.

Section 3.6 is devoted to some aspects of Schiøtz tonometry and tonography.

3.2 The Anatomy of the Human eye. The Glaucoma Problem

Figure 24 is a drawing of the internal structure of the human eye. The eye is formed by two layered, spherical shell segments. The segments are flexible and (see section 3.3) they may have considerably different mechanical properties. Fluid is continuously transferred into and out of the anterior chamber. Hence we have the typical physiological process of fluid transfer in a flexible vessel. Figure 25 shows the range of dimensions of the shell segments.

As far as the fluid mechanical situation is concerned it is sufficient to consider that at any instant the anterior chamber of the eye contains fluid, reasonably treated as Newtonian, (see article by Goldmann [20], p. 105 - 125), at some pressure P_0 above atmospheric. In normal eyes P_0 is 15 - 17 mm.Hg.

The mechanism by which fluid enters the anterior chamber is not completely understood but it is known (see article by Kinsey ref. 20, p. 62 - 88), that at least the simultaneously acting processes of secretion and diffusion are of importance. Whatever the actual chemical potentials and their sources may be, for our purpose it is sufficient to consider that there is a flow of aqueous out of the posterior chamber, along the lens-iris passage way, and into the anterior chamber. Fluid leaves the anterior chamber by flowing through the trabecular meshwork, which can be considered as a porous media, and into the canal of Schlemm. In normal eyes the rate of fluid out-flow, from the anterior chamber (volume 250 micro-liters) is approximately 1.4 micro-liters/minute.

Figure 26 illustrates the flow pattern in a normal eye. Figures 27-29 illustrate various pathological situations which can cause an increased intraocular pressure. It is this increase in intraocular pressure, whether constant or periodic, (as in the majority of cases), that is a most frequent sign of glaucoma.

Tonometry and tonography are processes which attempt to detect abnormal (say above 20 mmHg.) pressure levels or the response capability of the eye to an increase in pressure. A person can be said to have glaucoma only after there is damage to the optic nerve, but it is generally held such damage can be caused by abnormally high or periodically high intraocular pressure.

3.3 A Structural Model of the Eye

Goldmann [21] has suggested that the cornea behaves structurally as a three layered sandwich shell. The outer layer, composed of the pavement epithilium and Bowman's membrane, the center layer made-up of the corneal stroma, and the lower layer being Descemet's membrane. (See figure 23).

We shall also adopt this conceptualization while describing the mechanical properties of the cornea. Since the outer layer is by far the most rigid, the volume expansion tests (figure 22) for the cornea are essentially governed by the properties of that layer. In these tests we measured the motion of the upper surface, and this motion is less than or equal to the motion of the lower surface. The lower surface is so thin, and the central layer has such a low rigidity under the compressive strain during the expansion test, that the pressure rise is transmitted across the shell and decreases to zero across the upper surface. We see that the cornea demonstrates a linear behavior, and we can obtain Young's modulus (of the outer layer) from membrane theory.

If ΔW is an incremental displacement for a pressure rise ΔP, then

$$\Delta W = \frac{\Delta P \cdot R^2}{E \, h} \qquad (82)$$

where R = shell radius, E = Young's modulus, and h = the shell thickness. From figure 22, $\frac{\Delta W}{\Delta P} = 4 \times 10^{-3}$ mm./mmHg. The radius of the outer layer was 7.5 mm., and its thickness was between 0.1 and 0.2 mm. Then from (82), Young's

modulus for the outer layer E_1 is bounded as follows:

$$14.0 \times 10^4 \text{ mm.Hg.} > E_1 > 7.0 \times 10^4 \text{ mm.Hg.}$$

A thickness of .2 mm. was a generous upper bound and E_1 is probably close to 14×10^4 mmHg.

The volume expansion test for the sclera, figure 22, indicates the non-linear material behavior of the sclera. Opthalmologists have introduced the concept of the coefficient of "scleral rigidity"; this coefficient is a constant of proportionality in the logarithmic relationship found between a pressure change δP and an induced scleral volume change ΔV. If δP is the rise above a pressure level P_o, then the coefficient of scleral rigidity F, is defined by

$$\Delta V = F \log_{10} \frac{P_o + \delta P}{P_o} \qquad (83)$$

The non-linear relationship (83) closely fits our data for the sclera. Since the expansion is symmetrical, equation (83) is the same if ΔW replaces ΔV. For the hog eye shown, $F \doteq 0.02$. Hence the cornea is supported on a shell segment (the sclera) that demonstrates a non-linear material behavior while undergoing small strains. Elastically, the sclera has a constitutive law in which (in a direction parallel to its surface) an increment of stress d , is related to an increment of strain de by

$$de = F \log_{10} d\sigma \qquad (84)$$

The cornea itself is not free from a non-linear behavior as demonstrated by the corneal compression tests (fig. 21). We infer from these tests that the central layer, the stroma, behaves as a non-linear foundation for the upper layer.   But since the entire cornea conforms to the requirement of the Boltzmann superposition principle (Chapter 2),

we expect the nonlinearity to manifest in a direction in a plane perpendicular to the outer corneal layers. Moreover, if we define a foundation constant E_n by

$$\sigma_n = e_n E_n \qquad (85)$$

where σ_n is the normal stress, and e_n the compressive strain $=$ displacement/ thickness, then from figure 21 we see that for the loads pertinent to applanation tonometry (about 2 grams on a 3.0 mm. diameter plunger) $E_n \doteq 200$ mmHg.

Therefore, for applanation tonometry the non-linearity of the central layer manifests in a material whose rigidity in a plane normal to the outer layers is negligible compared to the rigidity of the outer layer. We can separately estimate its effect during applanation tonometry. During indentation tonometry, the stroma are "compressed out" and we can ignore the compression mode.

In view of the apparent non-isotropy of the inner layer, (this also is indicated by the anatomy of that layer) we must estimate the modulus of elasticity in a direction along the middle surface of the layer. Denote this modulus by E_t.

Since we cannot separate the individual layers of the cornea, we can only infer E_t indirectly. Our estimate follows from the magnitude of the surface tension force operative during Goldmann applanation tonometry and the analytical results of chapter one.

During the application of the Goldmann tonometer the surface tension balances the structural resistance of the cornea. In section 3.4 we will estimate the surface tension force (equation 87). Suppose that the cornea is applaned to an area whose radius is .75 mm., and suppose that the tears spread out to cover a 1.5 mm. radius. Then the surface tension (for a corneal

radius of 8.0 mm.) force is about .35 grams.

Now if the outer layer of the cornea is .1 mm. thick, and we assume $E_1 = 7.0 \times 10^4$ mm.Hg. then the structural resistive force P_1 from that layer is at least (figure 31 , and see the discussion in 1.7)

$$\frac{P_1}{E h^2} \geq 0.03$$

or

$$P_1 \geq 0.285 \; grams$$

Hence the corneal stroma can at most contribute .06 grams to the resistance, (since, [21] , surface tension over balances the corneal resistance at an applanation radius of 1.0 mm.).

If we assume the central layer to be 0.6 mm. thick, then (figure 36)

$$\frac{P_2}{E h^2} = 0.05$$

and if $P_2 = 0.1$ gram, then

$$E_t \leq 2.7 \times 10^2 \, mm \cdot Hg. \approx 3.85 \times 10^{-3} \, E_1$$

Since we have employed a lower bound for E_1, a lower bound for the thickness of the upper layer, and have neglected the factor of corneal compression, all of which contribute to a high estimate of P_2, we see that E_t is at least 2 and probably 3 orders of magnitude lower than E_1.

Since we have measured the displacement of the upper layer, and since the actual thickness of the lower layer was unknown (for the eye pertinent to figure 22,)we cannot estimate the modulus of elasticity of this layer. (It may be possible to "peel off" Descemet's membrane and separately obtain its modulus of elasticity.)

However, during applanation tonometry wrinkles can be seen in this layer [21] and we can assume that its contribution to the rigidity of the applaned

cornea is negligible. For indentation tonometers, the magnitude of the modulus of elasticity for Descemet's membrane is of importance for any quantitative analysis. In section 3.6, we concern ourselves with the qualitative behavior of the Schiøtz tonometer.

So we propose the following structural model of the eye.

The eye is composed of two different mechanical structures, the cornea, and the sclera. The cornea is a shallow shell segment and is attached to the sclera, a spherical shell whose volume is about 15 - 20 times the volume contained by the cornea.

The cornea is a three layered sandwich shell. The modulus of rigidity of the upper layer is several order of magnitude greater than the modulus of the other layers. The center layer is an anisotropic material demonstrating a non-linear material behavior in a direction normal to its surface. The other layers behave as linear materials. In the loading range (2-7.5 grams over a $(1.5)^2 mm.^2$ area) of interest for indentation tonometers, the entire cornea behaves as a linear viscoelastic solid.

The sclera is a non-linear material. In a direction along its surface, an increment of stress $d\sigma$, is related to a strain increment de by $de = F \log_{10} d\sigma$, where F is a constant.

3.4 Applanation tonometry

An applanation tonometer flattens a central portion of the cornea and measures the reaction to this deformation; it is a force measuring device. Two tonometers that deform the cornea in this way are the Goldmann and the Mackay-Marg tonometers.

The Goldmann tonometer measures the force required to flatten a 3.06 mm. diameter area. (The perimeter of the circle of applanation is detected optically and the somewhat curious 3.06 mm. dimension corresponds to an area over which 1 gram applied load is equivalent to an average pressure of 10 mm.Hg). The argument, given by Goldmann [21] , for why this instrument measures the intraocular pressure may be outlined briefly.

1. The forces acting on the rigid applaning surface are the structural resistance of the cornea, the intra-ocular pressure and the surface tension of tears.

2. The basic resistance to applanation comes from Bowman's membrane and the remainder of the cornea offers a resistance that is a higher order effect.

3. During the applanation process, Descemet's membrane relaxes, the pressure inside the cornea becomes equal to the intraocular pressure, and when the flattened portion of the cornea is 7.35 mm^2 in area, the applied pressure equals the intraocular pressure. The force induced by the surface tension of tears, at that flattened area, balances the structural resistance of the cornea. During the process, the load is sufficiently small to neglect any induced pressure rise due to loading.

The Mackay-Marg tonometer flattens a small central portion of the cornea but records only the force operative on a plunger situated concentrically within the overall applaning surface. As the tonometer contacts the cornea

the force on the plunger is continuously recorded on an electronic recorder. The following sequence of events are the rationale given for the instrument measuring the intraocular pressure [23].

1. As the cornea is flattened beyond the pressure sensitive region, the structural resistance of the cornea is largely distributed over the applaned area outside the force sensitive region and the response curve gradually begins to decrease.

2. As the flattening process continues, the loading will become of a sufficient magnitude (which corresponds to a flattened perimeter of approximately 1.5 mm. radius) to cause the intraocular pressure to begin to rise; at this time the force curve begins to rise.

3. The magnitude atthis trough (see diagram below) is a measure of the intraocular pressure, and the actual value is deduced through a reference calibration curve simply obtained by turning the tonometer through 180 degrees so as to measure the gravity load on the total, force sensitive unit.
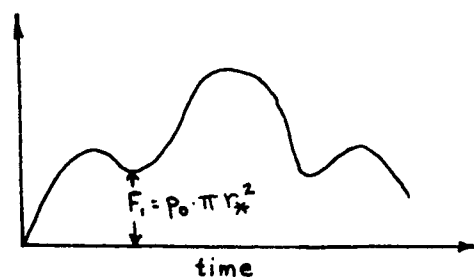
Po = intraocular pressure

πr_*^2 = force sensitive area

$F_1 = P_0 \cdot \pi r_*^2$

time

4. The surface tension of tears is not a factor since the applaning end of instrument is covered by a thin membrane which offers a negligible error in the measuring process.

In this section we shall analyze these two tonometers. The analytical results of chapter 1 are combined to the experimental results of chapter 2, to offer a theoretical basis for both of these instruments.

3.4 A. The Goldmann tonometer

The resistance that the Goldmann tonometer measures is composed of:

a) The pressure distribution $p(r)$ between the rigid indenter

and the upper surface of the cornea; designate the associated force

resultant as P_a. If r_o is the edge of the applaned area, then

$$P_a = 2\pi \int_0^{r_o} p(r)\, r\, dr$$

b) The cornea's resistance in compression to the work done to

initiate the deformation of the bottom surface; designate this

resultant force as P_b.

c) The surface tension of tears imposing a force P_c.

d) The intraocular pressure whose integrated reaction is P_d.

The component P_a which is the representative of the deviation of the

corneal behavior from that of an infinitely thin membrane, is given by equa-

tion (78). And the component P_d is simply the intraocular pressure p_o

multiplied by the area of applanation. Before discussing P_a we consider P_b

and P_c.

The force P_b may be estimated from the following considerations. Gold-

mann's experiments([21], figure 51) show that after the outer surface of the

cornea is flattened to circular area whose radius is about 0.2 mm., the

inner surface also begins to deform. The radius of that surface then is nearly

in a 1-1 proportion to that of the applaned area.

We estimate the compressive strain for a total thickness $h = 0.6$, an applanation

radius $r_o = 0.2$, and corneal radius of 8.0 as

$$e_n \doteq \frac{1}{2}\frac{r_o^2}{Rh} = 4\times 10^{-3}$$

And from the corneal compression test we have estimated (see Section 3.3) the

foundation modulus as 200 mmHg. Therefore the force P_b is derived from a

resultant pressure in the neighborhood of about 0.8 mmHg.

The force P_c is very difficult to estimate since we must know the contact radius for the tear-cornea-tonometer interface. However, the following calculation indicates the order of magnitude of the force. With respect to figure 30, let R_t be the radius of the fluid surface, in a plane parallel to the tonometer, which has spread along the surface of the tonometer. Let r_t be the tear radius at the edge of the wetted area. Then the pressure drop across the tear surface is [27]

$$\Delta p = \gamma \left(-\frac{1}{R_t} + \frac{1}{r_t} \right) \qquad (86)$$

where γ is the surface tension constant of tears. The contact angle, and hence the radius r_t depends, in part, on the spreading distance R_t. Hence the tonometer surface and anesthetic are factors in the size of r_t.

As the tonometer contacts the layer of tears on the cornea, a fluid layer spreads over part of the tonometer surface. If the radius of curvature of the cornea is R_c, then if $R_t^2 \ll R_c^2$, it follows that

$$r_t \doteq \frac{1}{4} \frac{R_t^2}{R_c}$$

and hence

$$P_c \doteq \pi \gamma \left(-\frac{R_c^2}{R_T} + \frac{4R_c^3}{R_T^2} \right) \qquad (87)$$

The surface tension constant γ is known to be about [ref. 14] 59 dynes/cm. So if $R_t = 1.7$ mm (a reasonable choice for an applanation radius of 1.5 mm) and $R_c = 8.0$ mm., then

$$\Delta p = 5.55 \times 10^3 \frac{dynes}{cm^2} = 4.15 \text{ mm.Hg.}$$

Hence the force P_c, at the contact area for Goldmann tonometry ($\pi(1.53)^2 mm^2$), is approximately .415 grams. This resultant is directed along a normal into the cornea and pulls the tonometer into the eye. Hence it tends to balance the forces P_a and P_b.

Our analytical results indicate that beyond a certain radius, the force P_a ceases to increase, i.e., a form of elastic instability manifests (see section 1.7). Now it is important to recall that our analytical solution assumes no edge restraint, and we expect the solution to break down for some flattened radius. (Probably beyond 1.5 mm. for a 12 mm. scleral radius, i.e. the edge of shell about 8 diameters away from the loaded region). Also, since we specify displacements in the loaded region, the solution applies for any layer that flattens.

From figures 31,32 we see that after the outer layer is flattened beyond about 0.5 mm. (if its thickness is 0.1 or 0.2 mm.), the force P_a no longer increases. For that radius, the center layer has only flattened to about a radius of 0.3 mm., and the force P_b corresponds to a pressure less than 0.8 mm.Hg.

Experimentally, [21] , we know that for an applanation radius of 0.5 mm., the surface tension force often over balances the structural resistance. And this is consistent with our analytical results even if the center layer is 0.6 mm. thick (see figure 36 and the estimates for Young's modulus in section 3.3).

Therefore, our explanation of the process of Goldmann applanation tono-metry is as follows:

1. Up to a flattened radius of 0.5 mm. the structural resis-
    tance of the cornea is due to its outer layer.

2. Beyond this radius, the resistance in compression and the
    structural resistance of the central layer increase to balance
    the surface tension force.

3. As flattening increases, end effects come into play and the
    resistance continues to rise.

This explanation is consistent with Goldmann's observation [21] that the instrument's accuracy does not depend on the level of intraocular pressure. If the instrument were calibrated at, say, a 20 mm.Hg. intraocular pressure, and the pressure were raised to 60 mm.Hg., the cornea would be in a different state of tension. And if there was no elastic instability in the rigid outer layer, it is difficult to see how surface tension could balance the structural resistance independent of the level of intraocular pressure.

Also, it is known [21] that wrinkles can be seen in Descemet's membrane during the applanation process; hence we have the experimental observation that at least Descemet's membrane goes into an elastically unstable configuration.

If the outer layer's structural resistance was monotone with an increasing applanation radius, then our results indicate that for a 1.5 mm. applanation radius, its structural resistance would be much higher than could be balanced by surface tension. Moreover, in view of its rigidity, it is difficult to see how the convenient 1.53 mm. applanation radius could be found, and how this number could be the same for all eyes unless the corneal resistance was very low beyond a certain applaned region.

Our analysis shows that the Goldmann tonometer has a very weak dependence on the radius of curvature of the cornea. If the thickness of the outer layer is nearly the same (say to within 15 percent) for all eyes, then in view of the low modulus of elasticity of the central layer, the tonometer is insensitive* to variations in the overall corneal thickness of different human eyes.

3.4 B The Mackay-Marg tonometer

The corneal resistance that the Mackay-Marg tonometer detects is the same as that of the Goldmann tonometer until the flattened area exceeds

* By "insensitive" we mean that the instrument's response is changed by less than ten per cent.

that of the force sensitive region. Let r_0 be the radius of the flattened area and r_* the radius of the central, force sensitive plunger. Then the force measured by the Mackay-Marg tonometer is composed of the following factors:

a) The pressure distribution $p(r)$ (between the rigid, applaning surface and the upper surface of the cornea) integrated over the area $\pi \, r_*^2$. Let this component of the resultant force be $P_1 (r_0; r_*)$.

b) The cornea's resistance in compression until the bottom surface begins to deform; designate the force as $P_2 (r_0)$

c) The intraocular pressure P_0 yielding a resultant force
$P_3 (r_*) = P_0 \pi r_*^2$.

d) The degree of co-planarity of the central plunger and the remainder of the tonometer's surface. Let the plunger's extension or insertion relative to a point on its surface, outside the force sensitive area be e. And let $P_e (r_0; r_*)$ be the measured force arising from the deviation from co-planarity.

The force $P_1 (r_0; r_*)$ is given by $^{(*)}$

$$ P_1(r_0; r_*) = 2\pi \int_0^{r_0} r \, p(r) \, dr \, , \qquad r \le r_0 < r_* \qquad (88) $$

$$ P_1(r_0; r_*) = 2\pi \int_0^{r_*} r \, p(r) \, dr \, , \qquad r \le r_0 \ge r_* \qquad (89) $$

The pressure distribution $p(r)$ is given by equation (72) of Chapter I, and if we perform the above integration we have -

(*) The expressions assume pressure sensitivity over a central area. If this area is disjoint from the outer applaning surface, then the membrane forces in (72) are not measured for $r_0 > r_*$.

$$\frac{P_1(r_0;r_*)}{E h^2} = \pi \left\{ -\frac{r_0^4}{4R^3 h} + \frac{\delta(r_0) r_0^2}{h R^2} + \frac{5}{6} \frac{A_1(r_0;\delta)}{1+\nu} r_0 \frac{I_1(kr_0)}{h} \right\}, \quad r_0 < r_* \quad (90)$$

$$\frac{P_1(r_0;r_*)}{E h^2} = \pi \left\{ \frac{5}{6} \frac{A_1(r_0;\delta)}{1+\nu} \frac{I_1(kr_*)r_*}{h} \right\}, \quad r_0 \geq r_* \quad (91)$$

where $A_1(r_0,\delta)$ and $\delta(r_0)$ are given by (69d) and (76) respectively. The resultant force P_2 is identical to P_b for the Goldmann tonometer, and the factor P_e can be estimated. Analytically it would be very difficult to include the effect of a non-zero e, for if the plunger and surrounding tonometric surface are not in plane, than we cannot continuously specify the cornea's displacement in the region of contact. However, from our corneal compression experiments we may arrive at an upper bound for the case of an extended plunger, while it is obvious that if the plunger is recessed the observed reading may (if the cornea did not completely conform to the plunger) be low.

If the plunger is extended, then as r_0 increases beyond r_*, the pressure distribution p (r) depends on the extension e. But we assume that beyond some r_0 greater than r_*, say $\tilde{r}_0$, the cornea once again conforms to the tonometer surface. Then if e is much smaller than the center deflection in the co-planar case, we estimate the deviation of p (r) from equation (72) as an additional pressure due to corneal compression. The center deflection $\delta(r_0)$ is greater than that of a membrane of the same radius and hence $\delta(r_0) \geq \frac{1}{2} r_0^2/R$. For $r_0 = 1$, and R = 8 mm., $\delta(r_0) \geq 6.25 \times 10^{-2}$ mm.

The actual pre-set plunger extensions that may be operative in the clinical use of the Mackay-Marg tonometer[*] are about 5×10^{-3} mm. and the

_____
(*) If e were initially set, then during applanation of the tonometer e would decrease, and the compressive strain would be induced by a deformation less than e. The actual amount depends on the limpness of the plunger suspension.

force P_e may reasonably be estimated as outlined above for e up to, say

10×10^{-3} mm. From the corneal compression experiment (figure 21) we have

estimated the foundation Young's modulus as about 200mm.Hg. And the local

compressive strain in a 0.5 mm. thick cornea deformed 10×10^{-3} mm. is approximately

$$e_n \doteq 2 \times 10^{-2}$$

so that for $e = 10^{-2}$ mm.

$$\sigma_{22} \doteq 4 \, mm.Hg.$$

If $e = 2 \times 10^{-3}$ mm.,

$$\sigma_{22} \doteq 0.8 \, mm.Hg.$$

These values are upper bounds and are very reasonable bounds for the

experimental values obtained on rabbit eyes by Mackay, Marg and Oechsli [31].

If the tonometer was constructed with a very stiff suspension, and

a very small protrusion, say $e = 5 \times 10^{-4}$ mm., then the factor P_e would always

cause a high reading in excess of the intraocular pressure by no more than one

or two percent.

Now consider the force P_1 $(r_0; r_*)$. It is known that the effect of

transverse shear deformation is important for thick shells. If this effect

were negligible for the eye, then from the classical theory of thin, shallow

spherical shells, [4], the pressure distribution is

$$P(r) = D\nabla^4 W + \frac{1}{R}(N_{rr} + N_{\theta\theta}) \tag{92}$$

where w is the normal displacement and Nrr, Nθθ are the membrane resultants.

But for small flattening $w = \delta - \frac{1}{2} r_0^2/R$, where δ is the center displacement,

and $\nabla^4 W = 0$. Hence

$$P_1(r_0; r_*) = \frac{2\pi}{R} \int_0^{r_0} (N_{rr} + N_{\theta\theta}) r \, dr \quad , \qquad r_0 < r_* .$$

And for $r_0 > r_*$, the membrane resultants are held out by the ring (the

central plunger and the guard ring are separate mechanical parts) so that

$P_1 (r_0 \geq r_*, r_*) = 0$, as indicated in the sketch below.
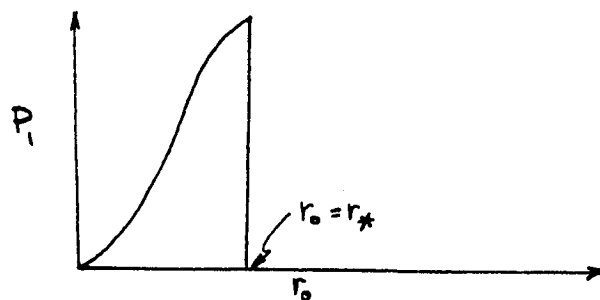
The prediction of classical shell theory

In figure 37 we have plotted $P_1(r_0; r_* = .75)$ for corneal thicknesses of 0.4 and 0.5 mm. and several values of the corneal radius. $P_1(r_0; r_*) = 0$ before $r_0 = 2r_*$. Hence the Mackay-Marg tonometer fulfills the requirement that $P_1(r_0 = 2r_*; r_*) = 0$ for $r_* = .75$.

During the applaining procedure, the pressure distribution between the surface of the tonometer and the cornea is continuously altered, and we note that our theoretical prediction of instability does not necessarily imply the occurrence of any sudden structural changes. (The experiments of Mackay, et.al.[23] indicate that snap through buckling does not occur).

We do predict that as flattening increases beyond some value of r_0, say $\overline{r_0}$, the integrated pressure distribution is no longer monotone. And unless $r_0 \geq \overline{r_0}$, then whatever the value of r_*, $P_1(r_0; r_*) \neq 0$. For the above example, while $P_1 (r_0 = 2r_*, r_* = .75) = 0$, $P_1 (r_0 = 2r_*, r_* = .5) \neq 0$. And it is by a sufficiently large choice of r_* (if the degree of flattening r_0 is to be approximately $2r_*$ at the time that the instrument indicates the pressure) that the Mackay-Marg tonometer takes advantage of the elastic instability occurring during the applanation procedure.

The magnitude of the force P_e depends on the stiffness of the plunger suspension and the initial deflection e. The error due to P_e is dependent on the technical quality of the instrument and does not enter in a fundamental way. $P_2(r_0)$ overestimates the pressure by less than 0.8 mm.Hg. (The second dip, during unloading in Mackay-Marg tonometry is often lower than the initial dip which

indicates the intraocular pressure. One reason for this is that during

loading there is some stress relaxation of the force $P_2(r_o)$; outflow is another.

The only theoretical limitation of the Mackay-Marg tonometer is the force

$P_2(r_o)$ which causes an overestimate of the intraocular pressure. If the plunger

extension was less than 2×10^{-3} mm., then the instrument's response is always

an upper bound for the pressure, and for a normal pressure of 16.0 mm.Hg. it

yields an error of less than 10%. As the intraocular pressure increases, the

relative error decreases.

3.4C Summary of the Goldmann and Mackay-Marg tonometers

The practical limitations of the Goldmann tonometer appear to be more

severe than for the Mackay-Marg tonometer. A 10 percent error in estimating

the radius of the applanation area yields nearly a 20% error for the measured

pressure. Hence the skill of the opthalmologist during Goldmann applanation

tonometry is an important factor. Also, the surface tension force has a strong

dependence on factors such as the condition of the surface of the tonometer

and the amount of fluid on the cornea before it is applaned. Either of the

factors: accuracy in judging the applanation area or a variability in the

surface tension could cause a high or a low reading.

The Mackay-Marg tonometer's accuracy basically depends on the stiffness

and protrusion of the central plunger. If this factor is controlled (e.g.

employing a small, (e $< 2 \times 10^{-3}$ mm.) positive protrusion and a stiff suspension,

then the instrument will always yield an upper bound for the actual pressure,

measuring accurately to within 10 percent of the pressure. We note that due

to its weak dependence on Young's modulus, the Mackay-Marg tonometer should

yield good accuracy when applied on the sclera, which has a higher rigidity

than the cornea.

3.5 Indentation Tonometers

In this section we shall discuss the Schiøtz tonometer as representative of instruments that indent the cornea under a constant force (*). The instantaneous, elastic response is measured in tonometry and during tonography the time dependent response is measured for about four minutes. In contrast to applanation tonometers, indentation tonometers, weighing 16.5 grams in a typical clinical application, induce a rise in the intraocular pressure , and the magnitude of this induced pressure rise plays an important role in the theory of the Schiøtz tonometer. During tonography, the fluid outflow is altered and the induced pressure rise depends on the loading, geometry, material properties and the change in the rate of fluid outflow. Figure (38) illustrates a portion of the cornea under a Schiøtz tonometer.

The deformation of the cornea probably exceeds 1/3 its thickness and hence the elastic solution is beyond the scope of the geometrically linear theory (small displacements as well as infinitesimal strains) of thin elastic shells. But we are not so concerned with predicting the magnitude of the elastic response as we are with its functional dependence on the intraocular pressure and the material properties of the cornea. And we have shown that for a fixed intraocular pressure the cornea conforms to the requirements of the Boltzmann superposition principle. Thus a correct elastic solution in conjunction with the correspondence principle of linear viscoelasticity would yield the time dependent solution (The level of strain in the cornea during the application of a Schiøtz tonometer with a 5.5 gram plunger load is probably less than 5 per cent.)

(*) The cornea is loaded by two concentric cylinders. The curvature and load of the central cylinder, the plunger, is such that its total surface contacts the cornea; the total surface of the outer cylinder, the foot-plate, does not contact the cornea. The applied pressure of the plunger is greater than that of the foot-plate and the plunger deformation relative to the foot-plate is measured. The problem is a combined fixed (the plunger contact radius) and free (footplate contact radius) boundary value problem. (see p.71,72,below)

We shall regard the elastic result obtained from the equations governing the linear theory of thin, shallow, elastic shells as a first approximation for the functional dependence of the center displacement on the intraocular pressure P_t, corneal geometry, and material properties. And we consider the corresponding viscoelastic result as a first approximation for the time dependent change in the deformation relative to the initial, elastic response.

Consider a homogeneous, linear viscoelastic shell, symmetrically loaded over a small circular area whose center is the apex and simultaneously under an inplane tensile force $T = P_t R$. We assume no edge restraint; it is known that the center displacement of a shallow shell segment loaded over a small area at its apex with this edge condition closely approximates the center displacement of a complete spherical shell under the same loading.

The shape of the cornea under the internal pressure P_0 is changed by a constant factor under the load $P_0 + \hat{\delta} p$. Hence the initial shape, [ref. 10] is not a factor and the governing equations are related to (20,21) by adding an inplane tensile force as in plate theory.

$$\nabla^4 F - \frac{E\lambda}{R} \nabla^2 W = 0 \tag{20'}$$

$$D \nabla^4 W + \frac{1}{R}\left(1 - \frac{1}{k^2}\nabla^2\right)\nabla^2 F = \left(1 - \frac{1}{k^2}\nabla^2\right)p(r) + T\nabla^2 W \tag{21'}$$

We only require the center displacement which is easily obtained from the Greens function for the problem. Equations $(20', 21')$ are solved with the procedure and boundary conditions of section 1.5.

The solution for the point load w_δ is

$$W_\delta(r) = -\frac{PR}{4\pi Eh}\sqrt{12(1-\gamma^2)}\, \sin\Theta\, \operatorname{Re} H_0^{(1)}(z) \tag{93}$$

r = distance from the apex measured in a horizontal reference plane

$$\bar{z} = \frac{r}{\ell} \, e^{i\Theta/2}$$

h = shell thickness

R = shell radius

γ = Poisson's ratio

E = Young's modulus

$$\ell = \sqrt[4]{12(1-\gamma^2)} \Big/ \sqrt{Rh}$$

P = magnitude of the point load

But now

$$\Theta = \tan^{-1} - \sqrt{\frac{\frac{25}{3} \frac{1-\gamma}{1+\gamma} \left(\frac{R}{h}\right)^2}{\left(1 + \mathcal{E}_p\right)^2} - 1} \qquad (94)$$

where

$$\mathcal{E}_p = \frac{P_t}{E} \left(\frac{R}{h}\right)^3 5(1-\gamma) \qquad (95)$$

The displacement at the apex is

$$W_\delta(0) = -\frac{PR}{4\pi E h^2} \sin\Theta \sqrt{3(1-\gamma^2)} \qquad (96)$$

The center displacement for the shell loaded by a uniformly distributed pressure Π over a small central area πr_p^2 is

$$W(0) = 2\pi \int_0^{r_p} \Pi \, \frac{W_\delta}{P} \, r \, dr \qquad (97)$$

where $\quad -P = \Pi \pi r_p^2$.

Integrating (97) with w_δ from (93) yields

$$W(0) = -\frac{PR}{E h^2} \frac{\sin\Theta}{Z} \sqrt{12(1-\gamma^2)} \, \text{Re}\left\{ \frac{H_1^{(1)}(\bar{z}_p)}{\bar{z}_p} - \frac{\bar{z}}{\pi} \frac{1}{\bar{z}_p^2} \right\} \qquad (98)$$

where $\quad z_p = \dfrac{r_p}{\ell}\, e^{\,i\theta/2}$.

Since r_p is a constant, the center displacement in the time dependent problem is given by the correspondence principle of quasi-static linear viscoelasticity. Let Poisson's ratio $\gamma = 0.5 \equiv \gamma_0$ in the quasi-static problem. We designate the solution (98) by

$$W(o) = P\, H(t)\; f\left(E, \gamma_0, P_t, h, R\right) \tag{98'}$$

where H is the unit step function.

Let the Laplace transform of some function $\psi(t)$ be denoted by

$$\overline{\psi}(s) = \int_0^\infty e^{-st}\, \psi(t)\, dt \tag{99}$$

Then from the correspondence theorem, the Laplace transform of w (t) is

$$\overline{W}(s) = \frac{P}{S}\, \overline{f}\left(\overline{E}(s), \gamma_0, \overline{P_t(s)}, h, R\right) \tag{100}$$

where $\overline{E}(s) = \left[s\,\overline{\psi}(s)\right]^{-1}$, with the creep function $\psi(t)$ defined by equation 80 and $\overline{P_t(s)}$ is the transform of the time varying intraocular pressure. The solution W (t) is the inverse Laplace transform of $\overline{W}$ (s), but E (s) occurs in the argument of the Hankel function $H_0^{(1)}$ and the inversion of W (s) would be extremely difficult. (If there were no in-plane tension the inversion would be trivial).

But there is a technique known as the "reduced modulus method" that is very simple to employ and is exact for the instantaneous response and for the assymptotic solutions as $t \to \infty$ $\left[\,28\,\right]$. And since the cornea behaves as a semi-relaxing solid, well over ninety percent of the creep response occuring in the first

two minutes, the method should be nearly exact at the end of four minutes, the normal time elapsed during Schiøtz tonography.

Suppose that we were to perform a uniaxial tension test on a strip of cornea. Let the tensile stress be some constant value F, and the strain response be e(t).
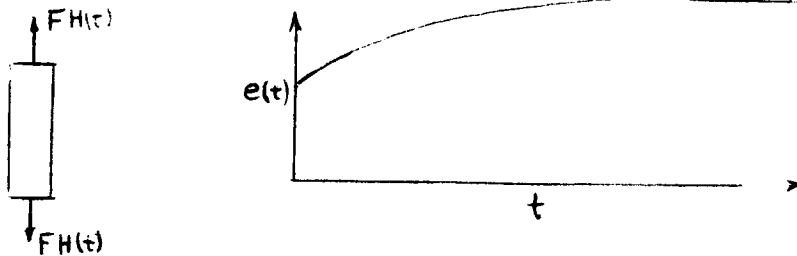
Then the creep function $\Psi(t) = \dfrac{e(t)}{F}$, and w(t) is derived from w(0), equation 98':

$$W(t) = P\,H(t)\,f\!\left(\frac{1}{\Psi(t)}, \nu_0, \; P_0 + \delta p(t), \hbar, R\right) \tag{101}$$

Or, explicitly from equation 98

$$W(t) = -\frac{P\,H(t)\,R}{\hbar^2}\,\Psi(t)\,\frac{\sin\Theta(t)}{2}\sqrt{12(1-\nu^2)}\,\mathcal{R}e\left\{\frac{H_1^{(1)''}(z_p)}{z_p} - \left(\frac{2}{\pi z_p}\right)^2\right\} \tag{102}$$

where

$$\Theta(t) = \tan^{-1}\sqrt{\frac{\frac{25}{3}\frac{(1-\nu_0)}{(1+\nu_0)}\left(\frac{R}{\hbar}\right)^2}{\left(1+\mathcal{E}_p(t)\right)^2} - 1} \tag{103}$$

$$\mathcal{E}_p(t) = \frac{P_0 + \delta p(t)}{1/\Psi(t)}\left(\frac{R}{\hbar}\right)^3 5(1-\nu_0) \tag{104}$$

For the two human eyes (same person) tested (figures 9,10), $\frac{w(4 \text{ minutes})}{w(0)} = .33$

and 0.33 respectively, and for the hog eyes (figures 11,12, 13) $\frac{w(4)}{w(0)} = .53$,

.44, and .39 respectively. Creep, for the human eyes, would account for a

30 percent increase in the measured Schiøtz deformation at constant internal

pressure.

Before discussing the solution we relate the pressure $p_0 + \delta p(t)$

to the fluid flow out of the anterior chamber and into the canal   of Schlemm.

The flow problem is very complex and it serves no useful purpose to attempt to

characterize it more accurately than the present approach taken by opthalmolo-

gists, [29]. It is basically a low Reynold's number porous media flow, and

often (see article by Scheidegger, [30]) a linear relationship exists between

the pressure drop and the flow rate. Since the porosity of the media (the

trabecular meshwork) has not been measured, to say nothing of its possible

dependence on the level of the intraocular pressure at any instant, it is best

to characterize the flow problem in terms of pressure gradiants across certain

"resistances".

Let the flow rate out of the anterior chamber be Q_a and the in-flow rate

be Q_p. Let the pressure drop out of the anterior chamber be $\Delta P_{A.c.}$ and

the pressure gradiant allowing the fluid to flow from the posterior chamber be

$\Delta P_{p.c.}$. Define resistance coefficients α and β by

$$Q_a = \frac{1}{\alpha} \Delta P_{a.c} \qquad\qquad (105)$$

$$Q_p = \frac{1}{\beta} \Delta P_{p.c.} \qquad\qquad (106)$$

Then in steady flow, $Q_a = Q_p$ so that

$$\Delta P_{A.C} = \frac{\alpha}{\beta} \Delta P_{P.C.} \tag{107}$$

And we can distinguish several cases relative to normal values α_N, β_N.

a) $\beta = \beta_N$, $\alpha \gg \alpha_N$ ... open angle glaucoma

b) $\beta \ll \beta_N$, $\alpha = \alpha_N$ ... perhaps a form of hypersecretion glaucoma

The pressure drop $\Delta P_{A.C.}$ is the difference between the venous pressure P_v and the anterior chamber pressure P_t. Therefore

$$P_t = P_v + \alpha\, Q_a$$

and equation (104) becomes

$$\mathcal{E}_p(t) = \frac{P_v(t) + \alpha\, Q_a}{1/\psi(t)} \left(\frac{R}{h}\right)^3 5(1-\gamma_0) \tag{108}$$

The initial measured response of the Schiøtz tonometer is the relative deformation of the plunger and the guard ring. Therefore the initial reading has a more complex parametric representation than (98) including the weight of the foot plate, and the radius ρ_f with which the foot plate contacts the cornea. The radius ρ_f itself depends on the load, internal pressure and the material behavior. So the elastic solution (98) basically shows us the least complex way that the level of intraocular pressure affects the measured response. We see that the level of pressure, creep and geometry enter non-linearly, and a small change in these variables would not yield a proportional change in deformation. Hence it is not difficult to understand how the Schiøtz tonometer can be quite sensitive to intraocular pressure changes.

The sensitivity is illustrated by the behavior of the Greens function (93) at the apex. There is a strong dependence on the magnitude of P/E, the

72

sensitivity to pressure changes being greater for smaller Young's modulus. (See the experimental results, figures 16-20). In a certain range of the value P/E, the instrument may be quite sensitive to the value of R/h.

Now the correspondence principle of linear viscoelasticity only applies if the boundary conditions in the elastic and viscoelastic problems are the same. But during tonography, the area of contact between the footplate and the cornea changes and our solution indicates an over simplification of the relative change in time between the footplate and the plunger.

The solution (102) shows that the change in the measured response of the Schiøtz tonometer may have a basic dependence on two quantities: the creep function $\psi(t)$ and an expression that we denote by $\mu(t)$.

$$\mu(t) = \frac{P_0 + \delta p(t)}{{}^{1/}\psi(t)} = \frac{P_. + \alpha \,(\cdot)_-}{{}^{1/}\psi(t)} \tag{109}$$

Moreover, we see that the material properties, (represented by the creep function ψ) and the level of intraocular pressure (or the fluid outflow) are linked by the parameter μ (t). And a possible inference from this parametric dependence is illustrated by the following situation. Suppose Schiøtz tonography were performed on the eyes of two people, and the resulting tonograms were different. Then the difference could be due to not only their respective outflow resistances, but to a difference in their creep functions.

ACKNOWLEDGEMENT

REFERENCES

1. Timoshenko, S. and Goodier, J.N., <u>Theory of Elasticity</u> , Ch. 13; McGraw-Hill Book Co., 1954.

2. Essenburg, F., " On Surface Constraints in Plate Problems, " <u>J. Appl. Mech.</u>, p.340, pp.340-44, June 1962.

3. Reissner, E., " The Effect of Transverse Shear Deformation on the Bending of Elastic Plates," <u>J. Appl. Mech.</u>, v.12, pp.69-77, 1945.

4. Reissner, E., " Stresses and Small Displacements of Shallow Spherical Shells, " I, <u>J.Math. Phys.</u>, pp.80-85, v.25,1946.

5. Reissner, E., "Stresses and Small Displacements of Shallow Spherical Shells, " II, <u>J. Math. Phys.</u>, pp.279-300, v.25, 1946.

6. Naghdi, P.M., " On the Theory of Thin Elastic Shells, "<u>Quart. Appl. Math.</u>, vol. xiv, no. 4, pp. 369-80, 1957.

7. Naghdi, P.M., " Note on the Equations of Shallow Elastic Shells, " <u>Quart. Appl. Math.</u>, vol. xiv, no.3 , pp. 331-33, 1956.

8. Love, A.E.H., <u>A Treatise on the Mathematical Theory of Elasticity</u> , Ch. xxiv, Dover Publications, fourth ed., 1927.

9. Green, A.E. and Zerna, W., <u>Theoretical Elasticity</u> , Ch. xi, Oxford Press, 1954.

10. Fung,Y.C. and Sechler, E.E., " Instability of Thin Elastic Shells, " <u>Proc. First Symp. Naval Structural Mech.</u>, Pergamon Press, pp.115-68, 1960.

11. Mc Lachlan,N.W., <u>Bessel Functions for Engineers,</u> second ed., Oxford Press, 1955.

12. Ince,E.L., <u>Ordinary Differential Equations,</u> Dover Publications, first ed., 1926.

13. Donnell, L.H., " Shell Theory, " 4th <u>Midwestern Conference on Solid Mechanics,</u> Univ. of Texas, 1959.

14. Cerrano,E., " Ricerche Fisico- Chimiche sulle Lacrime in Relazione alla dei Collirii, "<u>Archivio di Farmacologia Sperimentalle e Scienze Affine,</u> v.8, 1909.

15. Erdelyi,A., et. al., <u>Higher Transcendental Functions</u>, vol.2, Mc Graw Hill Book Co., 1953.

16. Koiter, W.T., " A Spherical Shell Under Point Loads at its Poles, " <u>Progress in Solid Mechanics, The Prager Anniversary Volume</u>, New York, Macmillan, 1963.

17. Natl. Bureau of Standards, " Tables of Bessel Functions $Y_0(z)$ and $Y_1(z)$ for Complex Arguments, " Columbia Univ. Press, New York, N.Y., 1950.

18. Watson, G.N., <u>A Treatise on the Theory of Bessel Functions,</u> Second ed. Cambridge Univ. Press, 1962.

19. Friedenwald, J.S. et. al., <u>Standardization of Tonometers,</u> Decennial Report of the American Academy of Opthalmology and Otolaryngology, Rochester, Minn., 1954, The Academy.

20. Duke-Elder, S., (editor) <u>Glaucoma</u>, Charles Thomas, Publisher, 1955.

21. Newell, F.W.,(editor) <u>Glaucoma</u>, Josiah Macey, Jr. Foundation, 1957, p.167-220.

22. St. Helen, R. and Mc Ewen, W.K., " Rheology of the Human Sclera, " <u>Amer. J. Opthalmology</u>, v.52, no.4, pp. 540-48, 1961.

23. Mackay, R.S., Marg, E. and Oechsli, R., " Automatic Tonometer with Exact Theory: Various Biological Applications, " <u>Science,</u> v.131, 1668-69, 1960.

24. Gurtin,M.E., and Sternberg,E., " On the Linear Theory of Viscoelasticity, " <u>Arch. Rational Mech. Analysis,</u> v.11, pp.291-355, 1962.

25. Hunter, S.C., <u>Progress in Solid Mechanics,</u> vol.1, North- Holland Publishing co., Amstedam, 1960.

26. Lee,E.H., " Viscoelastic Stress Analysis, " <u>Proc. First Symp. Naval Structural Mechanics, Pergamon Press</u>, pp.456-82, 1960.

27. Prandtl, L., <u>Essentials of Fluid Dynamics</u>, Ch.1, Hafner Publishing Co., 1955.

28. Distefano, J.N., " Sul Comportamento Asintorico dei Corpi Viscoelastici Nella Coazioni, " <u>Atti della Accademia delli Scienzedi Torino,</u> v.95, 1960-61.

29. Becker, B., and Shaffer, R.N., Diagnosis and Therapy of the Glaucomas, Ch.6, The C.V. Mosby Co., 1961.

30. Scheidegger, A.E., " Hydrodynamics in Porous Media, " Handbuch der Physik, Bd.viii/2, pp.625-62.

31. Mackay, R. S., Marg, E., and Oechsli, R.,"Arterial and Tonometric Pressure Measurements in the Eye", Nature 194:687 (1962).
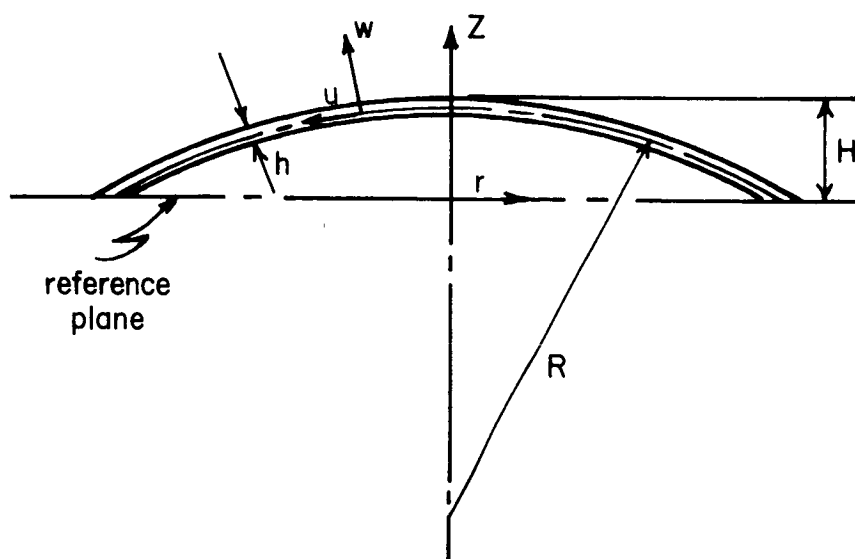
FIGURE I
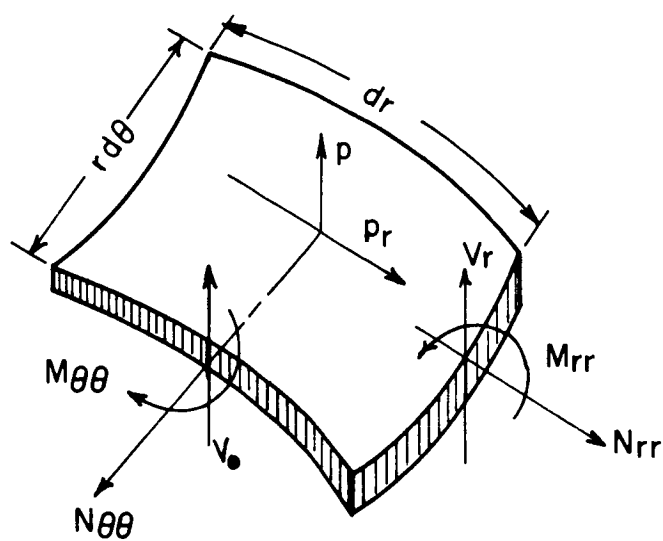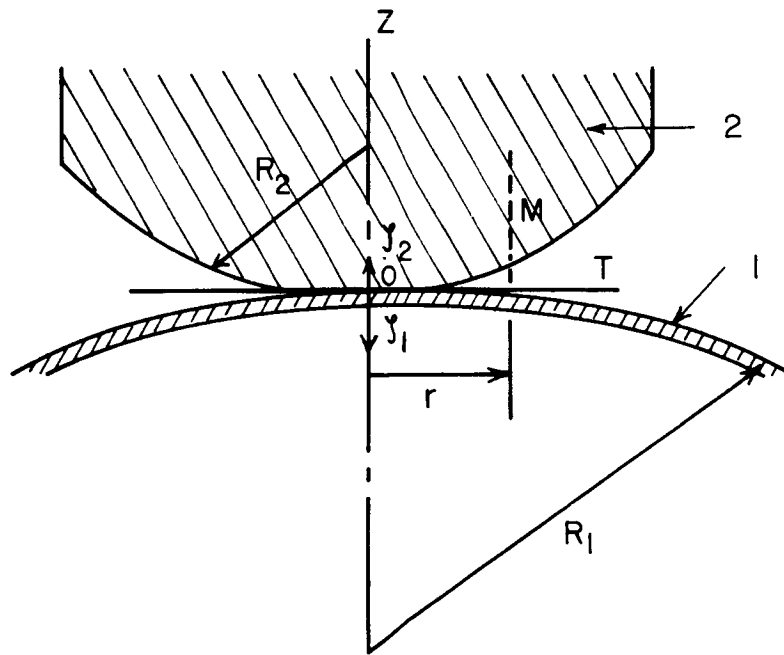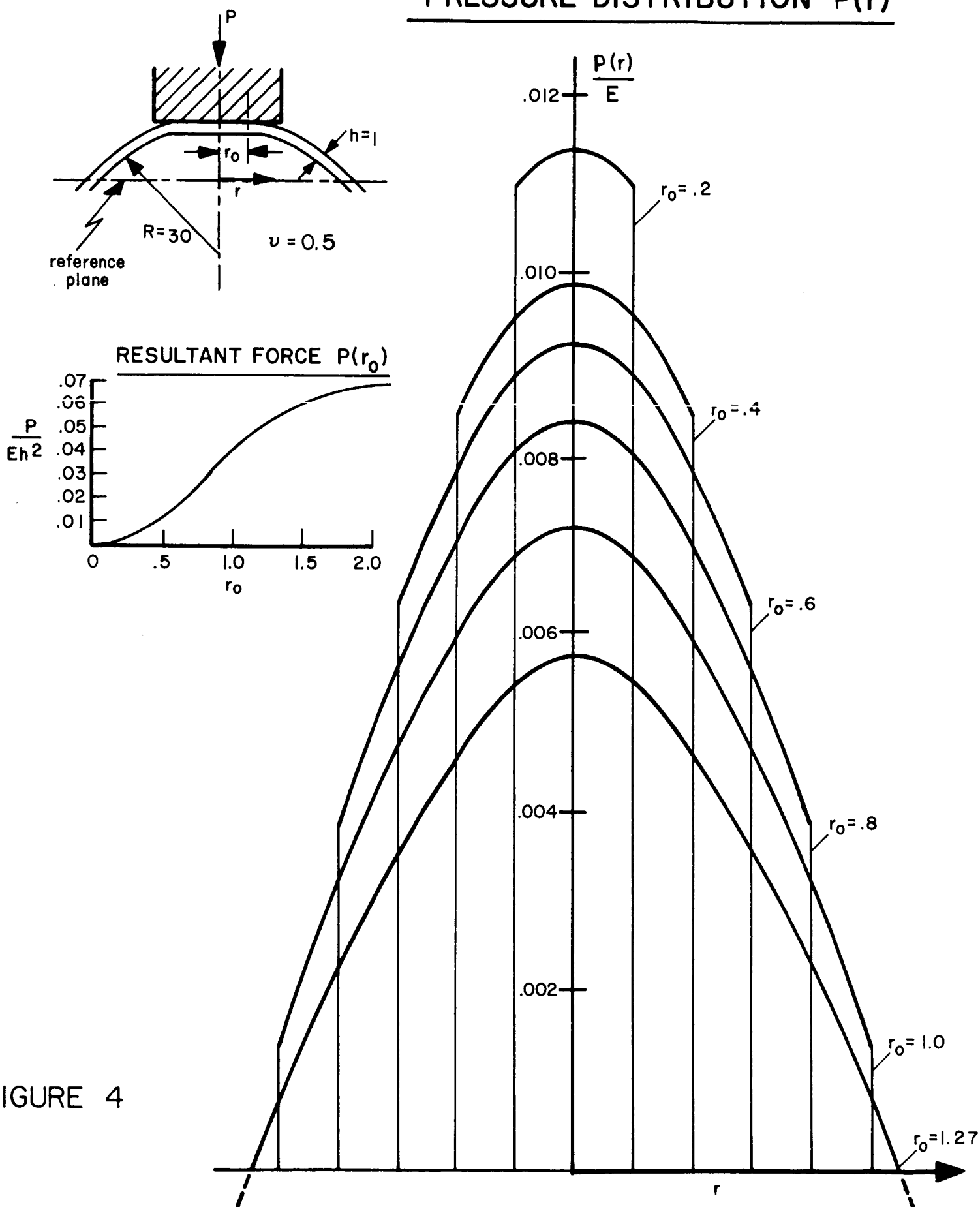
FIGURE 2

FIGURE 3

FIGURE 4

RESULTANT FORCE P(r₀)
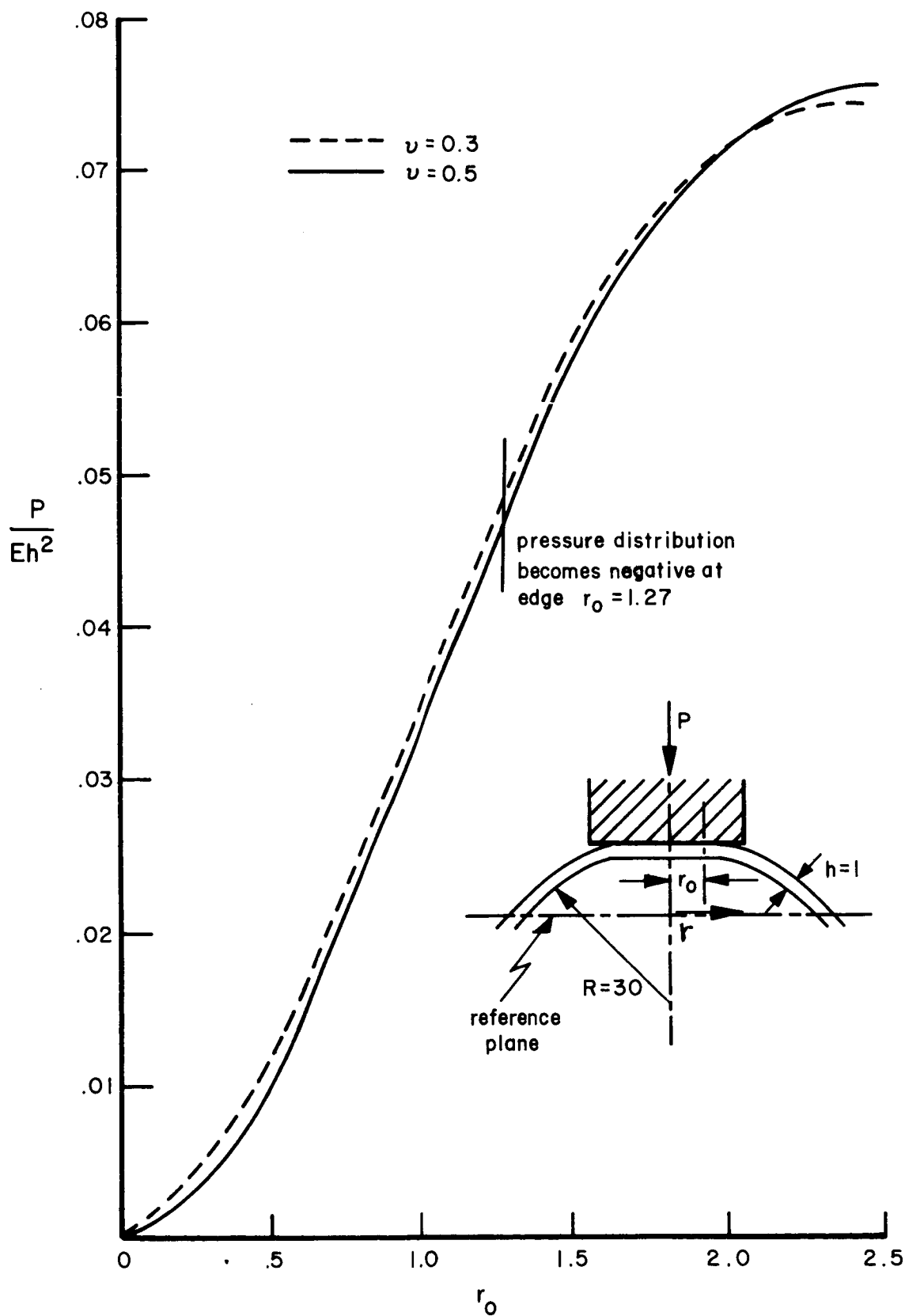
FIGURE 5

RESULTANT FORCE P(r$_0$)
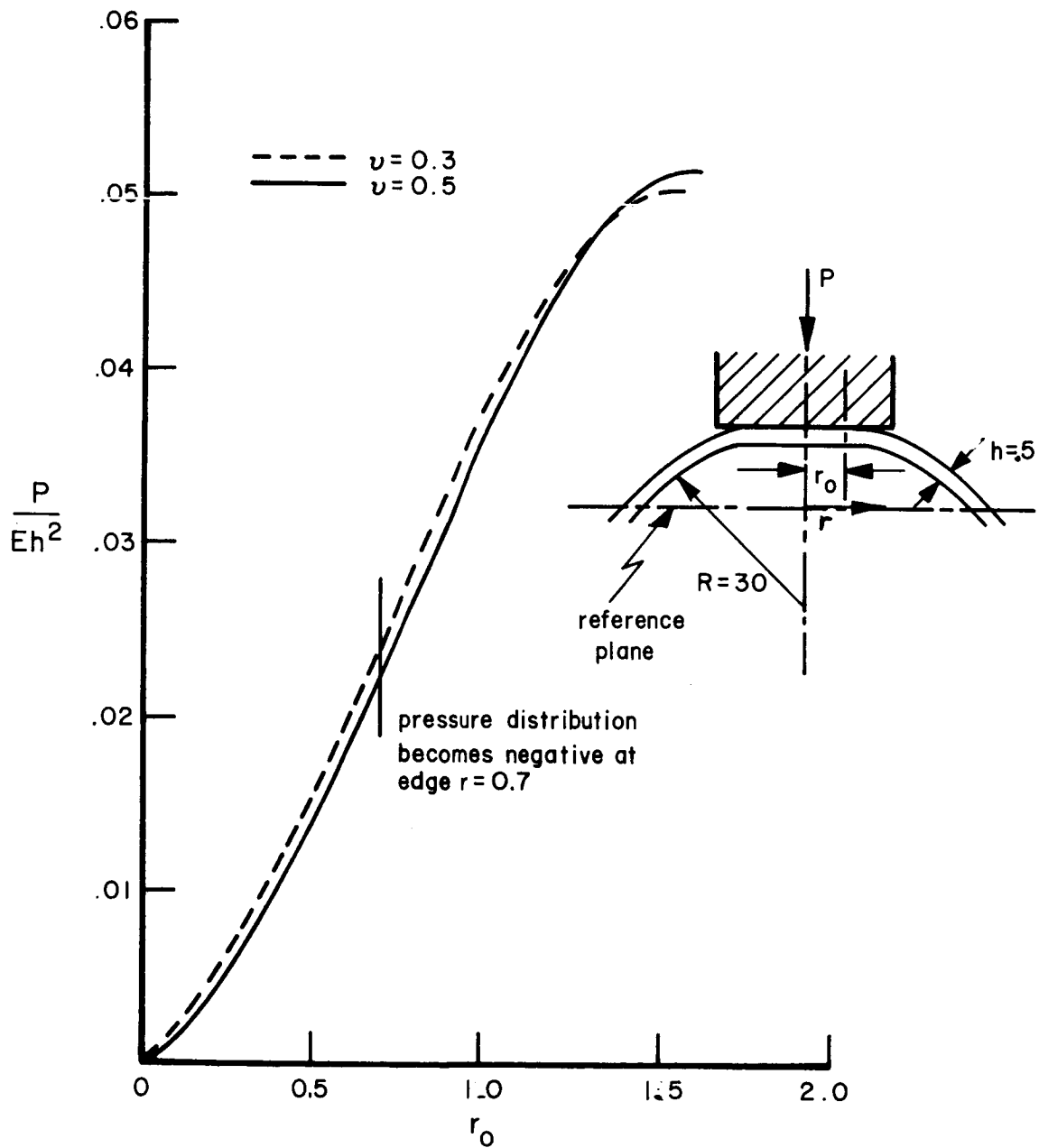
FIGURE 6
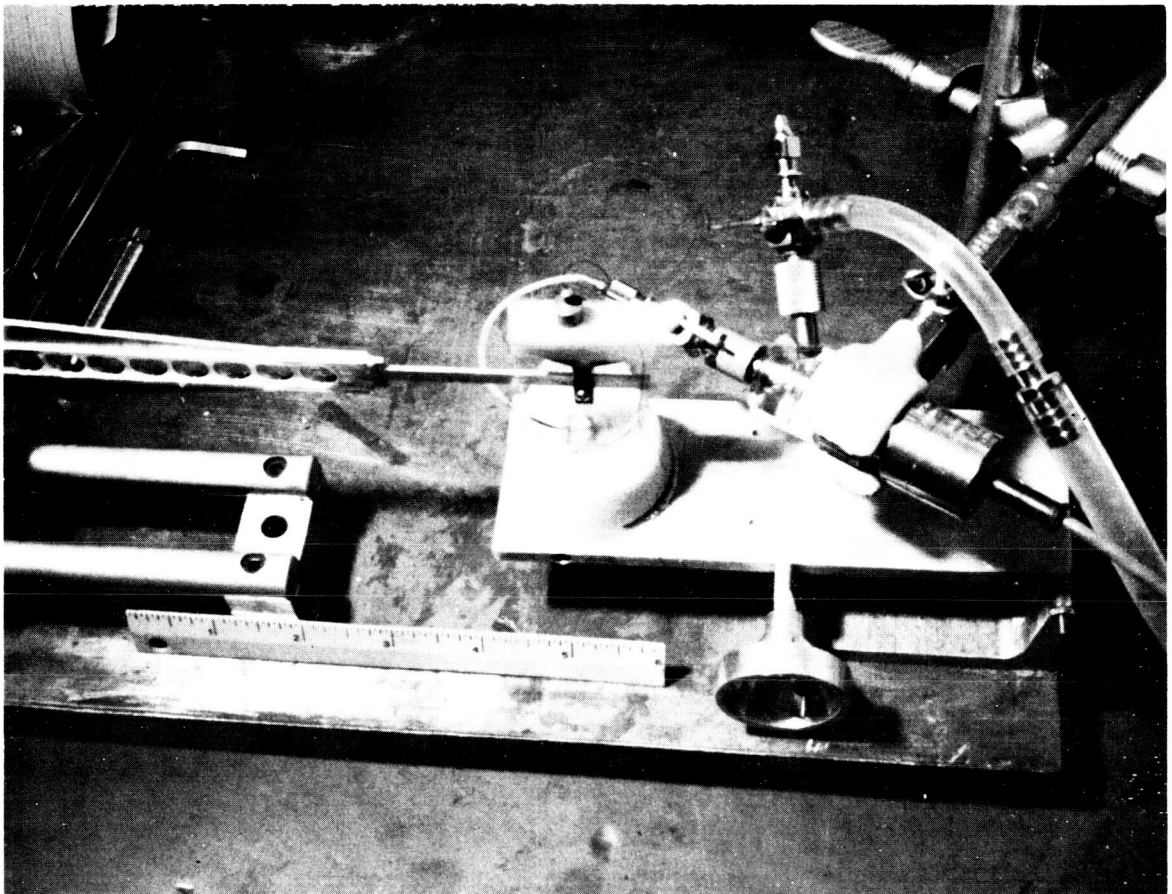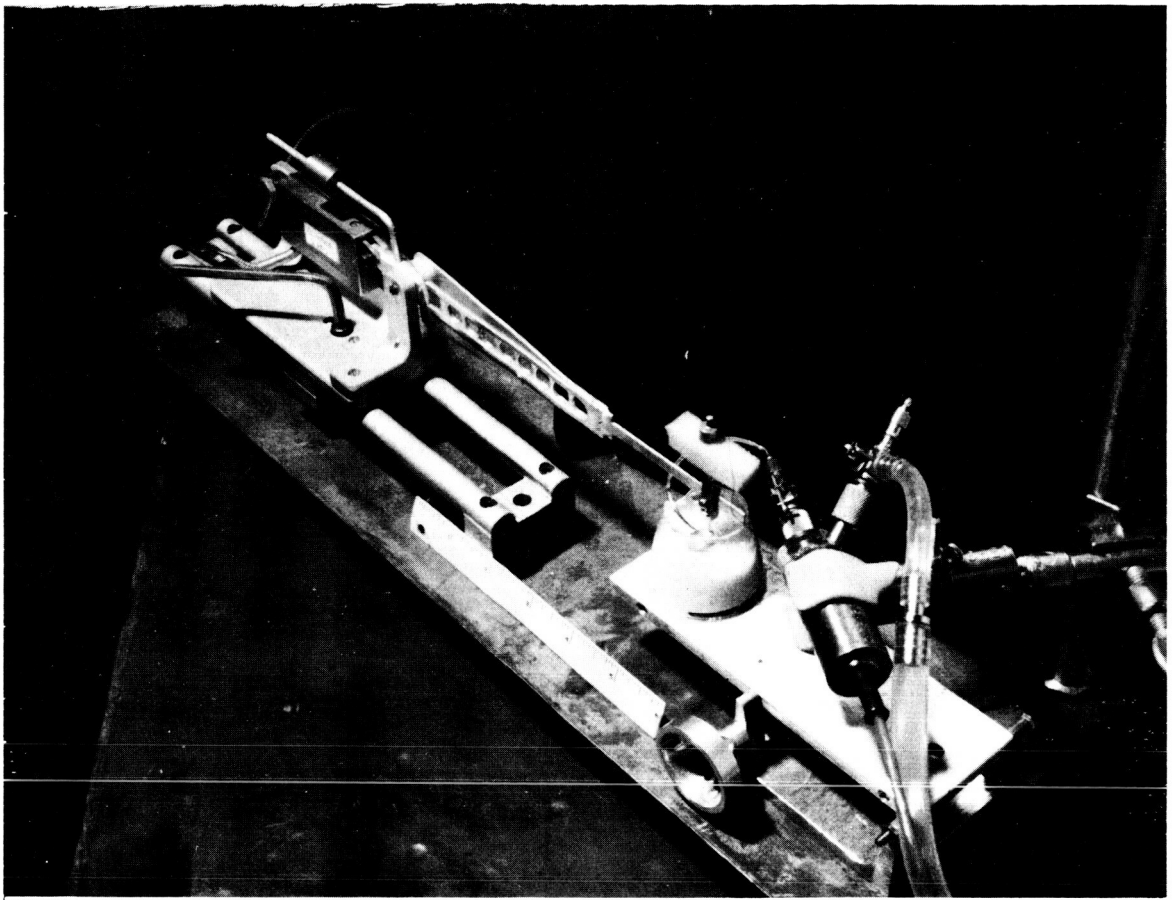
FIGURE 7

FIGURE 8

HUMAN EYE no. 1

AGE	70 years
DEATH	2:00 a.m.
ENUCLEATED	7:30 a.m.
TESTED	11:30 a.m.
PRESSURE	40 mm. Hg
RADIUS	7.5 mm
ROOM TEMP	70° F

SUPERPOSITION

CREEP TEST

TIME IN MINUTES
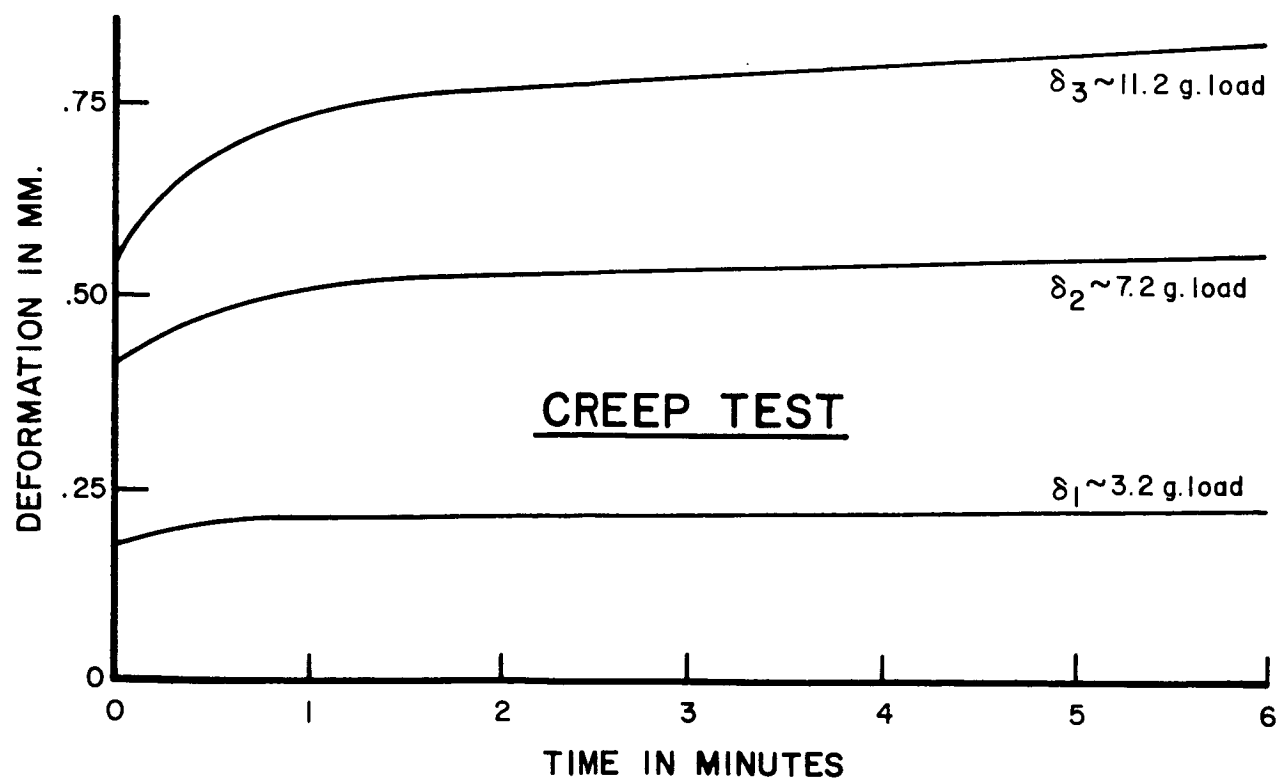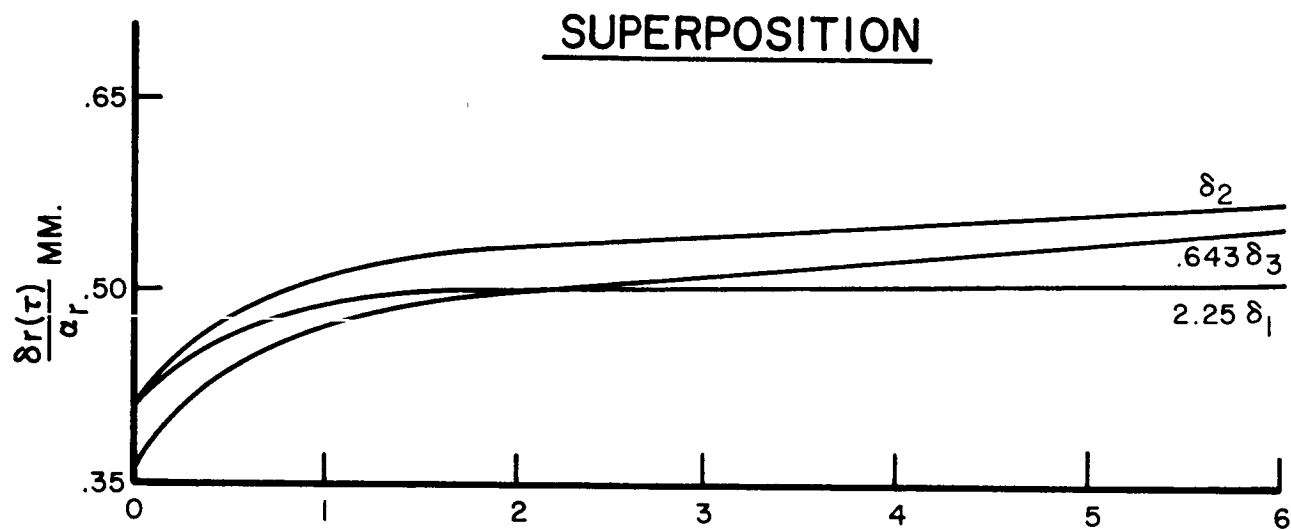
FIGURE 9

HUMAN EYE no. 2

AGE	70 years
DEATH	2:00 a.m.
ENUCLEATED	7:30 a.m.
TESTED	1:00 p.m.
PRESSURE	35 mm.Hg
RADIUS	7.5 mm
ROOM TEMP	70° F

SUPERPOSITION

$.643\delta_3$

δ_2

$2.25\delta_1$

$\frac{\delta r(\tau)}{a_r}$ MM.

CREEP TEST

$\delta_3 \sim 11.2$ g. load

$\delta_2 \sim 7.2$ g. load

$\delta_1 \sim 3.2$ g. load

DEFORMATION IN MM.

TIME IN MINUTES
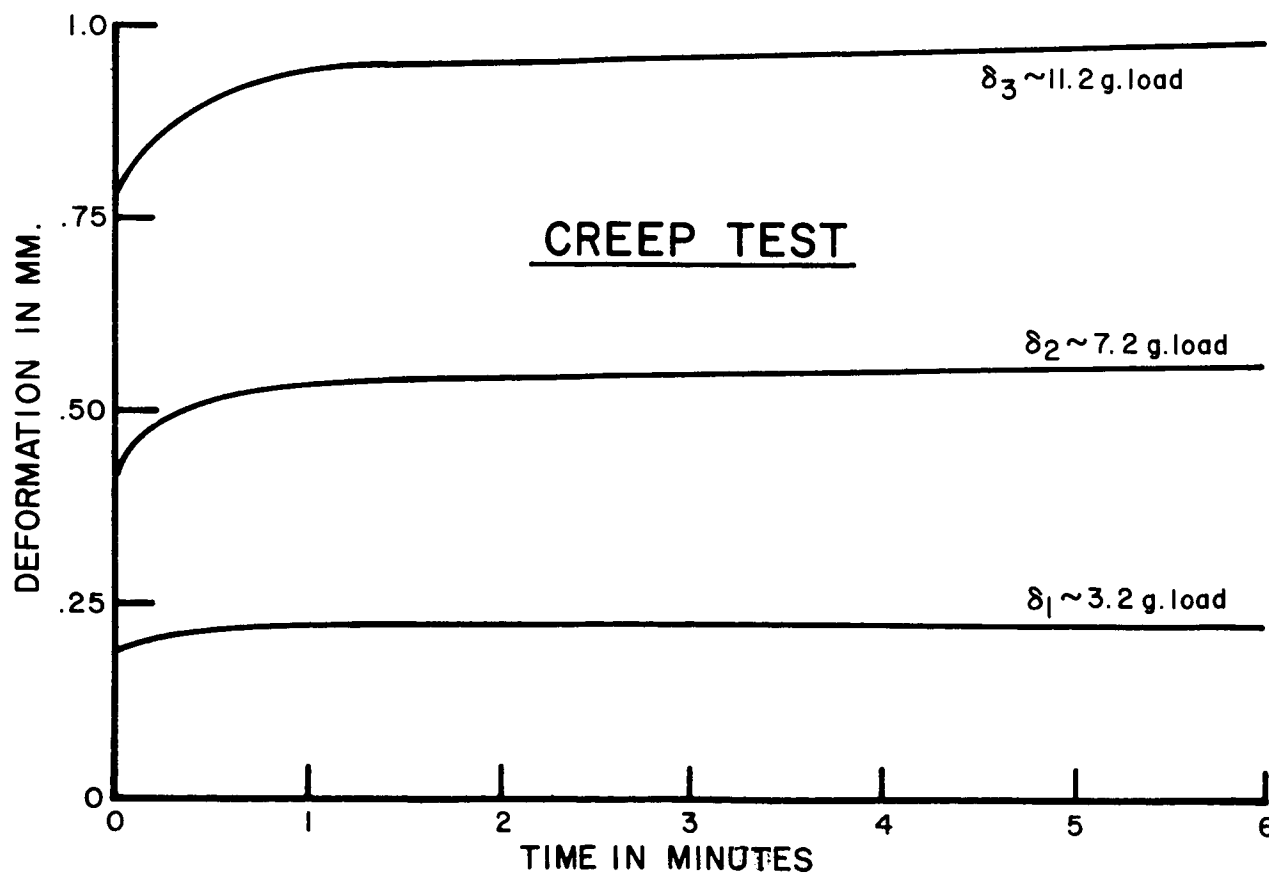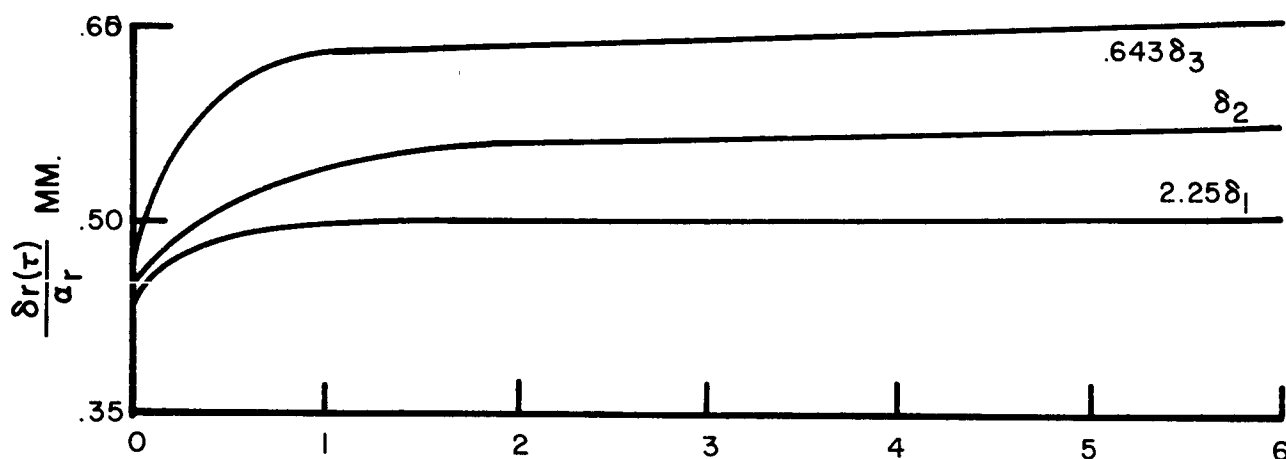
FIGURE 10

ENUCLEATED HOG EYE no. I

TESTED	50 min POST
	MORTEM
RADIUS	8.0 mm
PRESSURE	40 mm.Hg.

SUPERPOSITION

.643 δ_3

δ_2

2.25 δ_1

CREEP TEST

$\delta_3 \sim 11.2$ g.load

$\delta_2 \sim 7.2$ g.load

$\delta_1 \sim 3.2$ g.load

TIME IN MINUTES
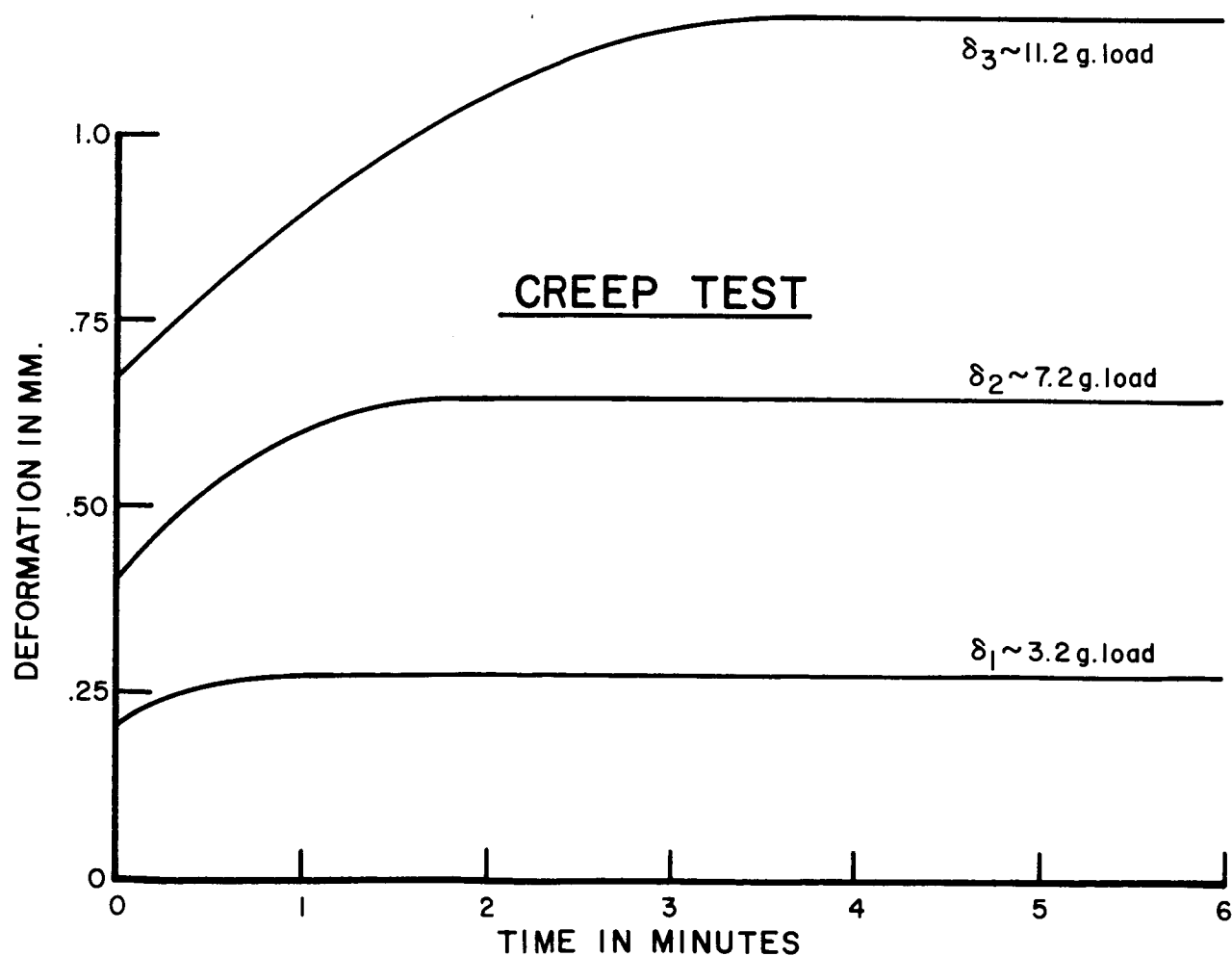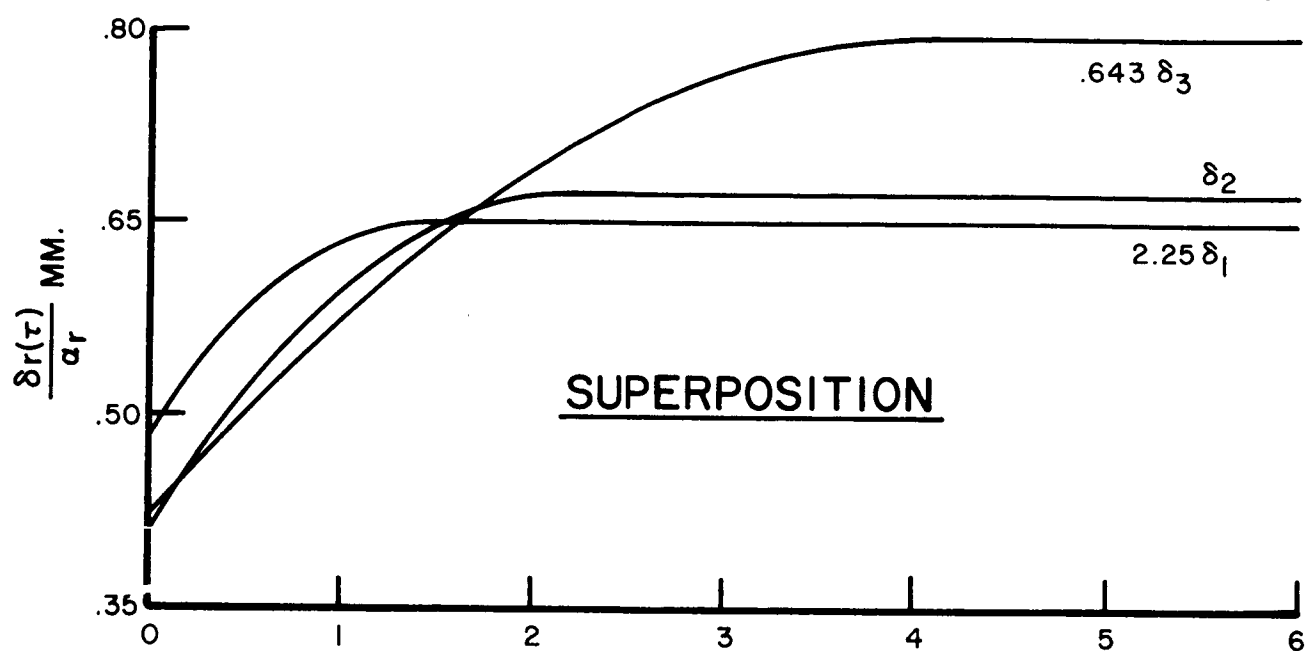
FIGURE II

ENUCLEATED HOG EYE no. 2

TESTED	2 hrs. POST MORTEM
RADIUS	10.5 mm
PRESSURE	40 mm. Hg.

SUPERPOSITION

.643 δ_3

δ_2

2.25 δ_1

$\frac{\delta r(\tau)}{\alpha_r}$ MM.

CREEP TEST

$\delta_3 \sim 11.2$ g. load

$\delta_2 \sim 7.2$ g. load

$\delta_1 \sim 3.2$ g. load

DEFORMATION IN MM.

TIME IN MINUTES
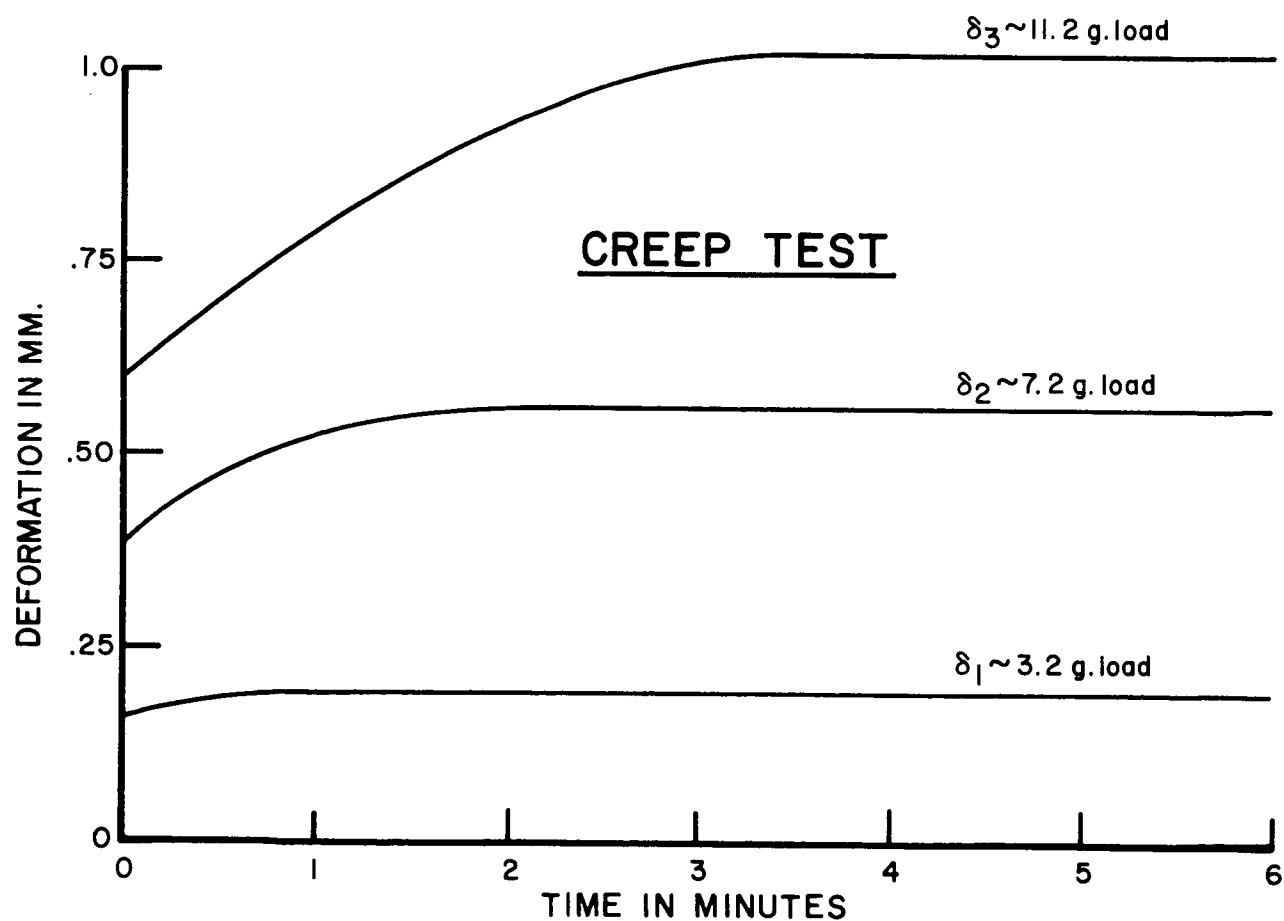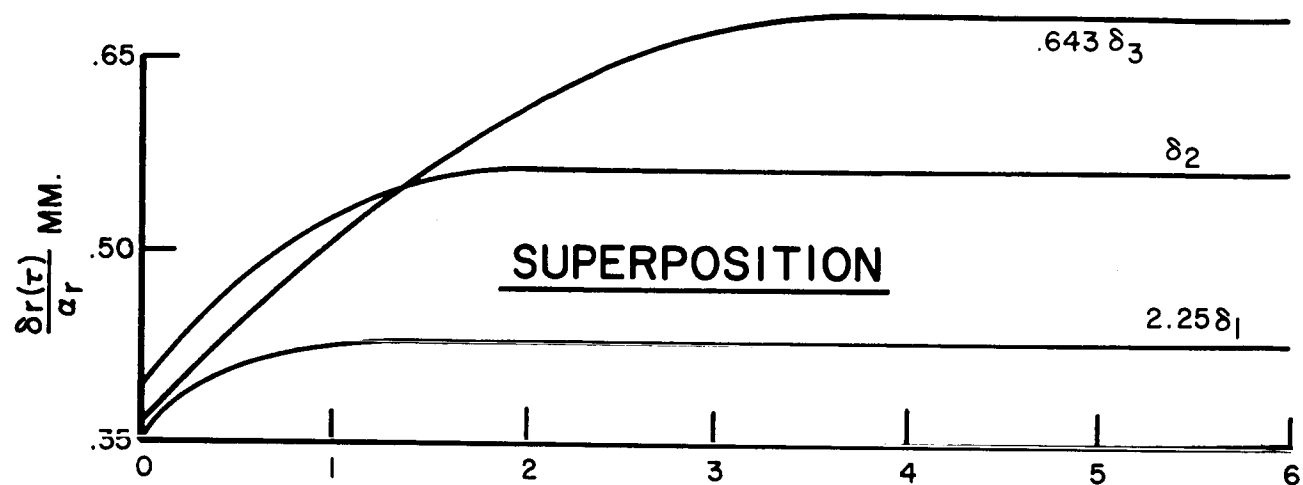
FIGURE 12

ENUCLEATED HOG EYE no.3

TESTED 2 hrs 30 min POST MORTEM
RADIUS 8.9 mm
PRESSURE 40 mm Hg.

SUPERPOSITION

CREEP TEST
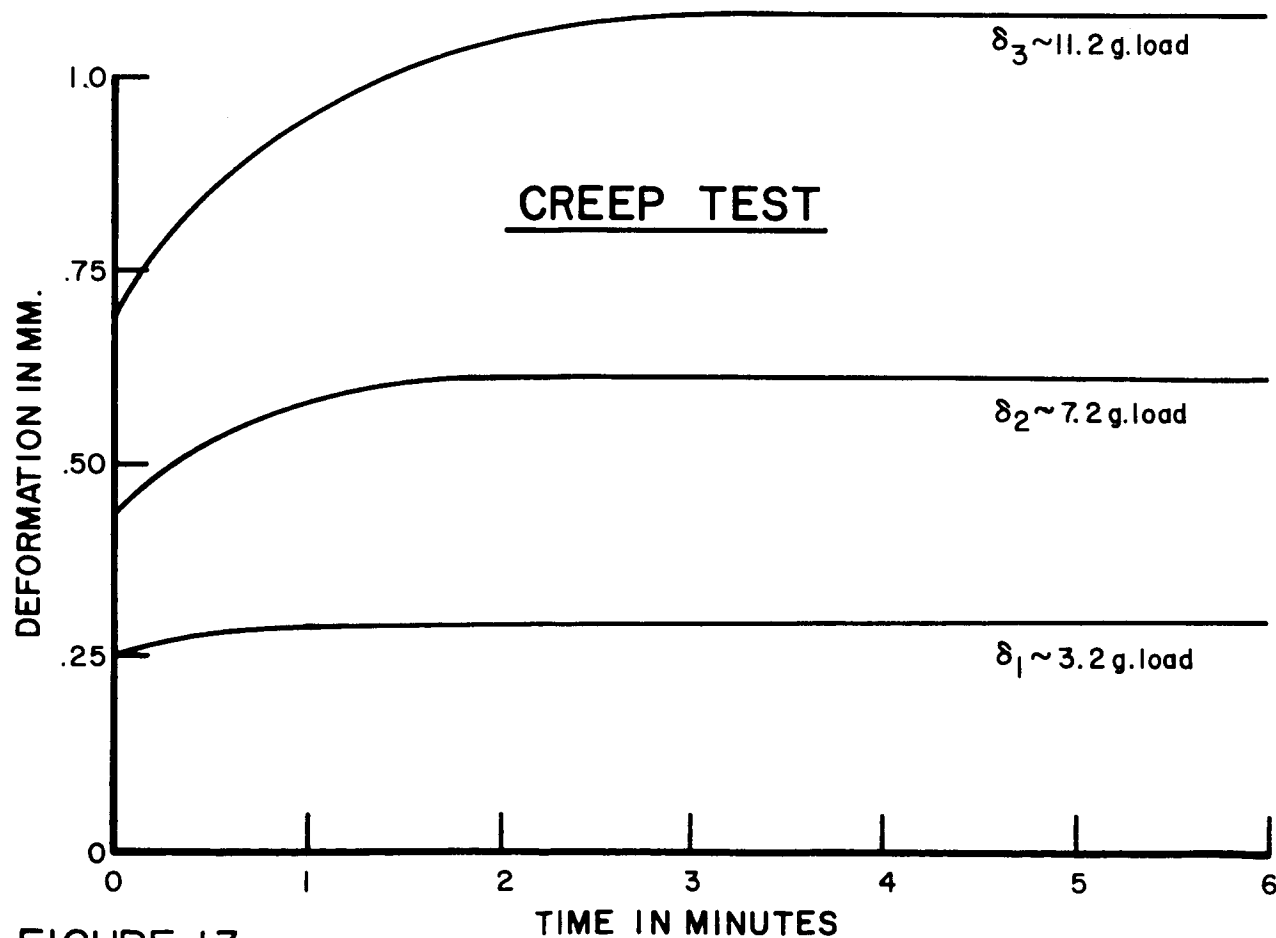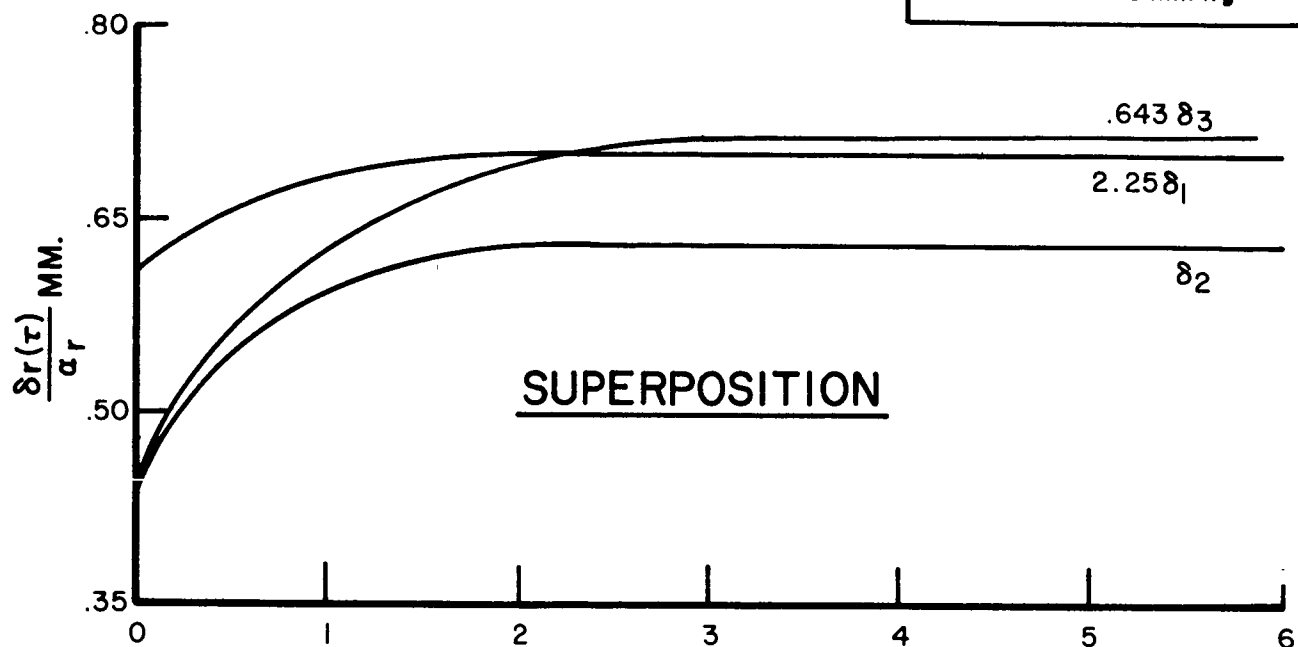
FIGURE 13

HOG EYE no.7
(7.2 GRAM LOAD)
40 mm. Hg. Internal Pressure

CREEP TEST

6 MIN. POST MORTEM
15 MIN. POST MORTEM
MATED, REFRIGERATED
EYE TESTED 1 HOUR
POST MORTEM

FIGURE 14

HOG EYE no.6
(7.2 GRAM LOAD)
40 mm. Hg. Internal Pressure
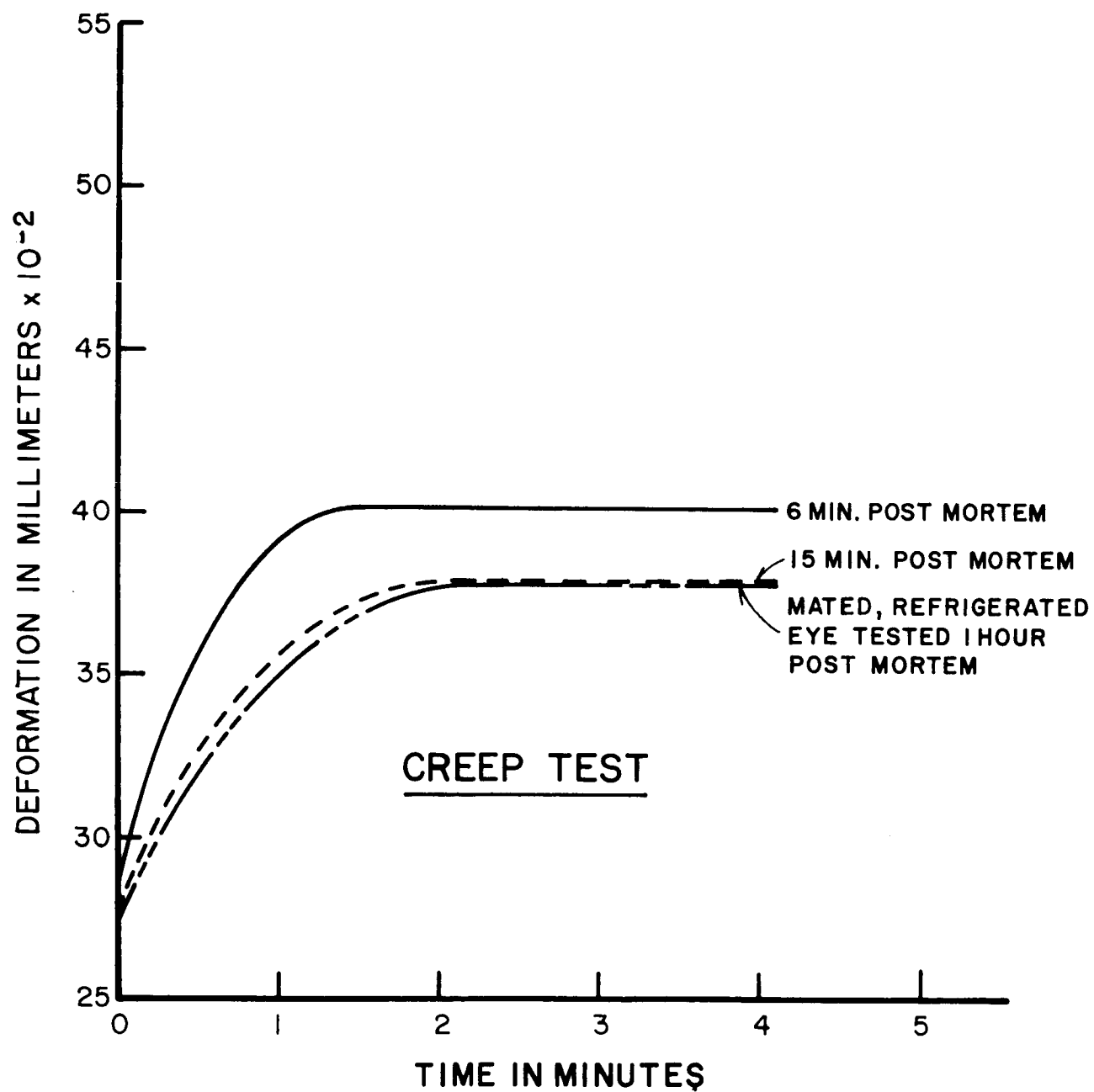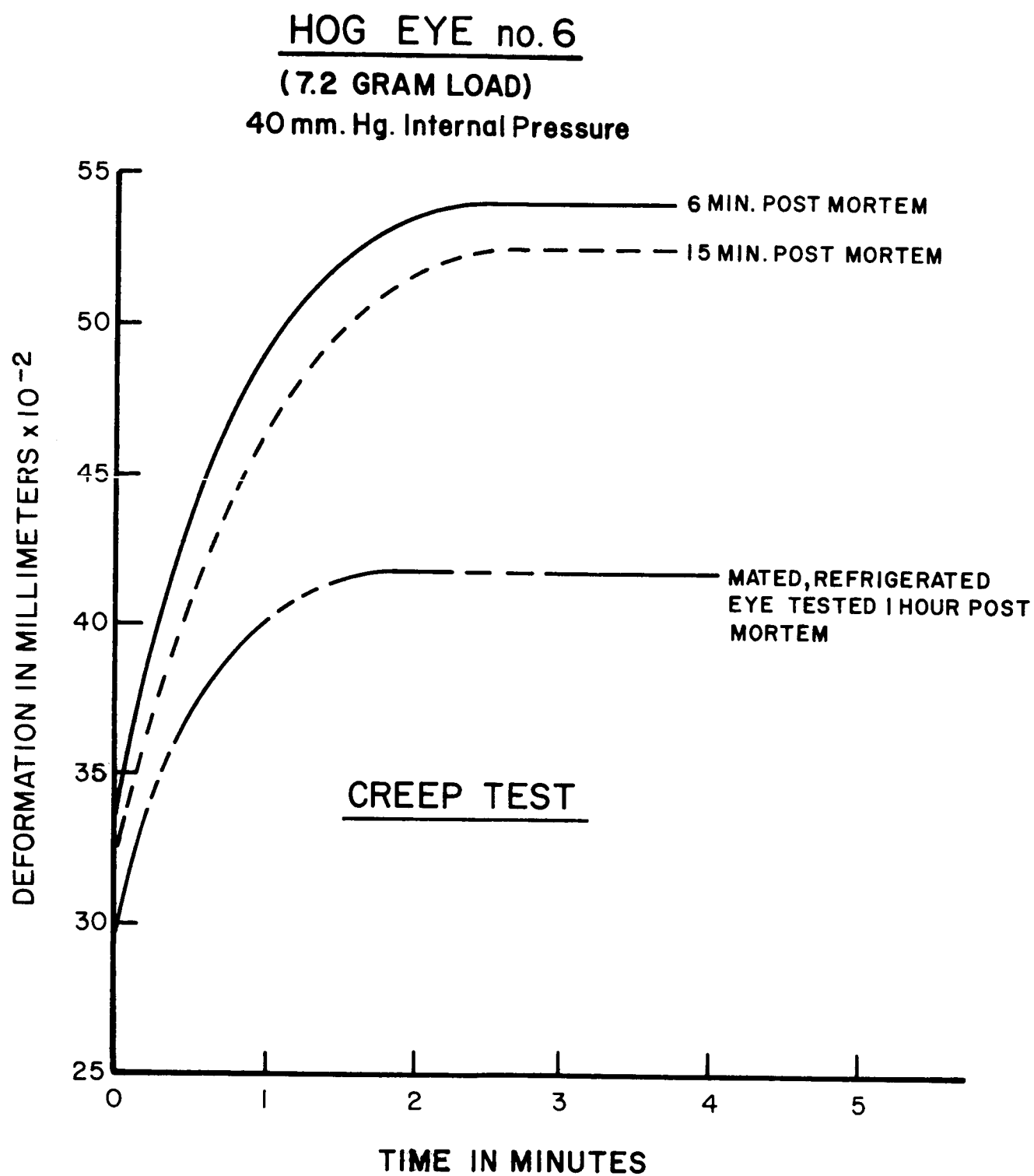
FIGURE 15

ENUCLEATED HOG EYE UNDER INTERNAL PRESSURE
20 mm.Hg.
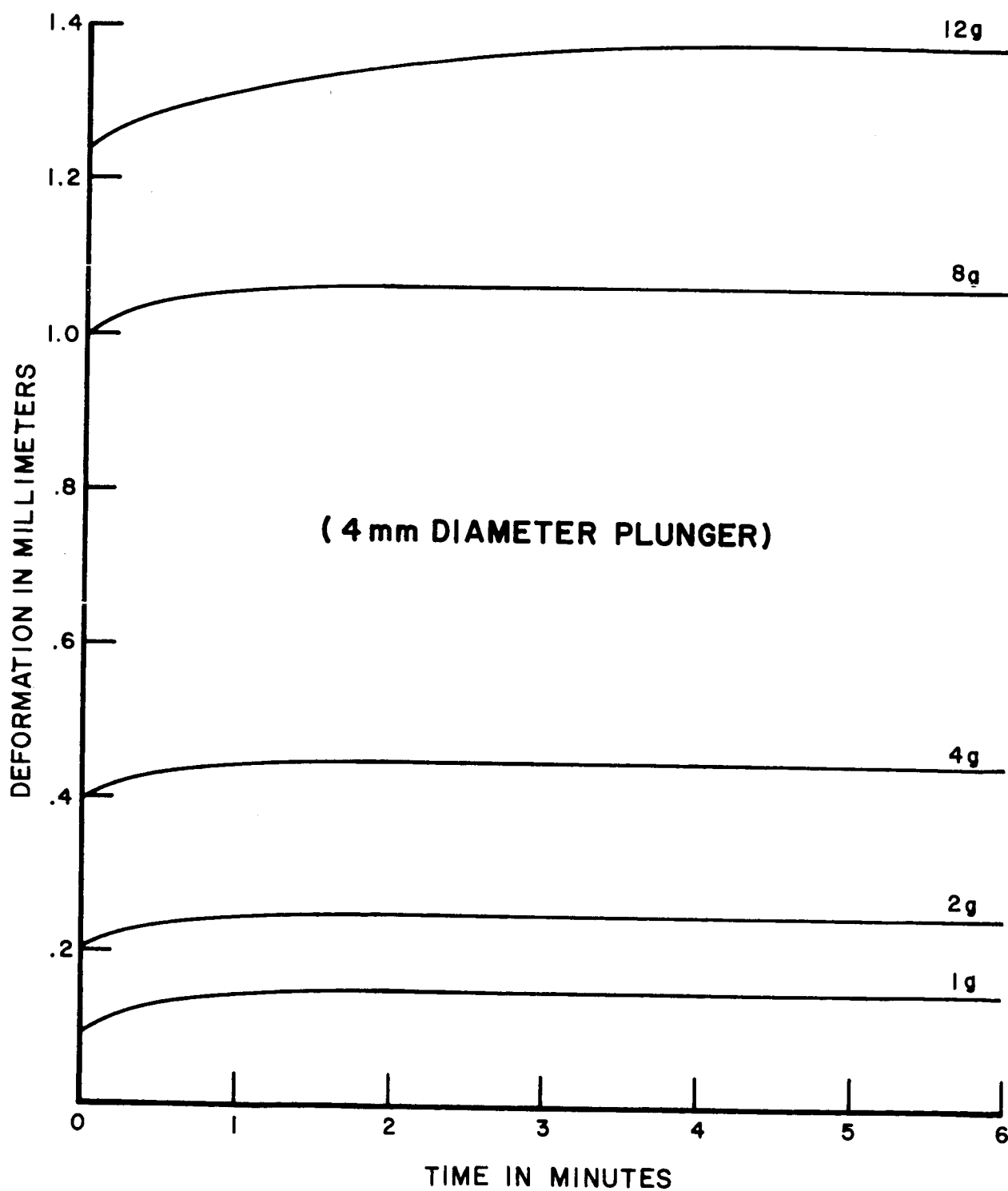
FIGURE 16

ENUCLEATED HOG EYE UNDER INTERNAL PRESSURE

30 mm.Hg.

(4mm DIAMETER PLUNGER)
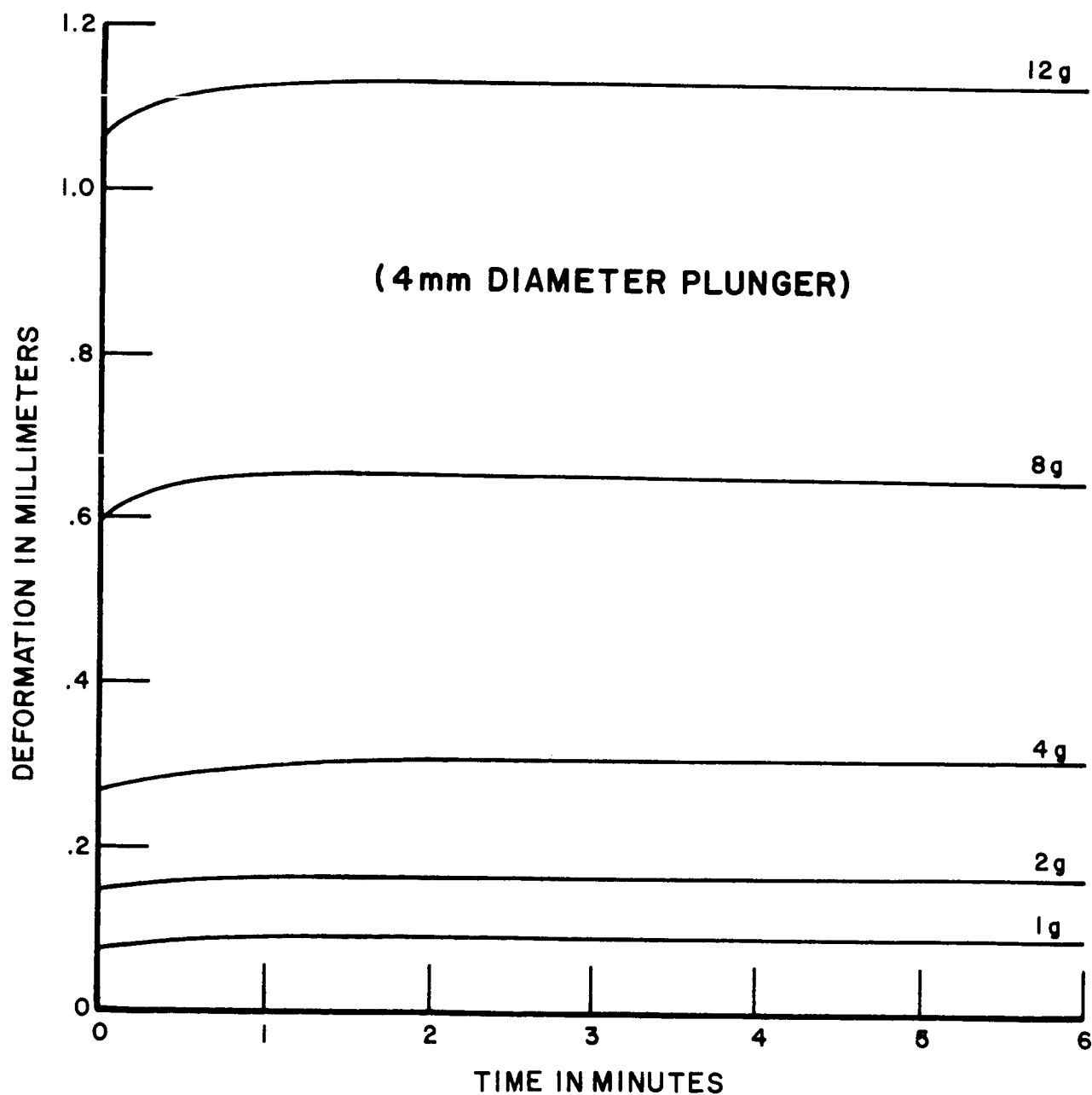
FIGURE 17

ENUCLEATED HOG EYE UNDER INTERNAL PRESSURE

40 mm.Hg.
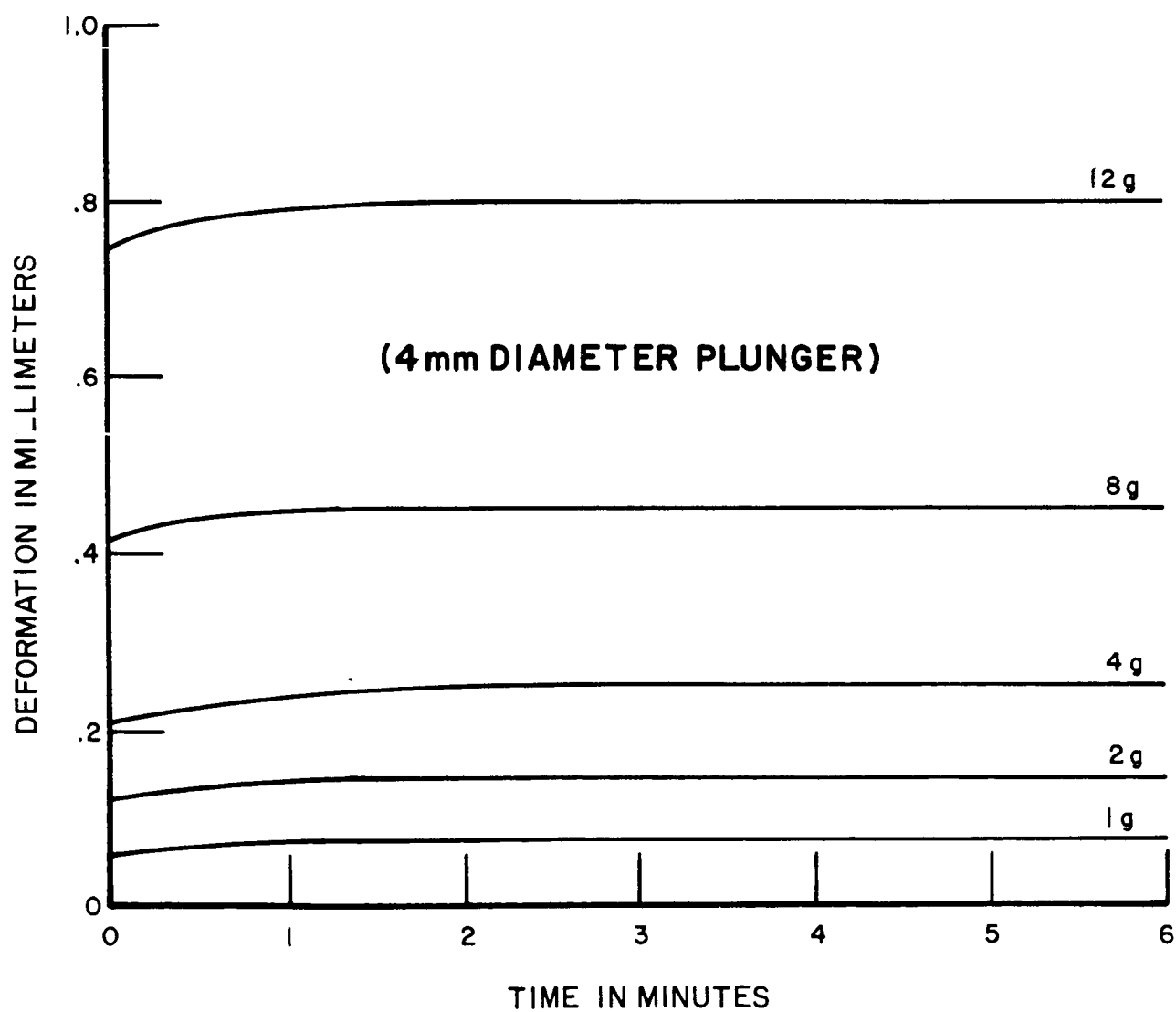
FIGURE 18

ENUCLEATED HOG EYE UNDER INTERNAL PRESSURE
60 mmHg.

(4mm DIAMETER PLUNGER)
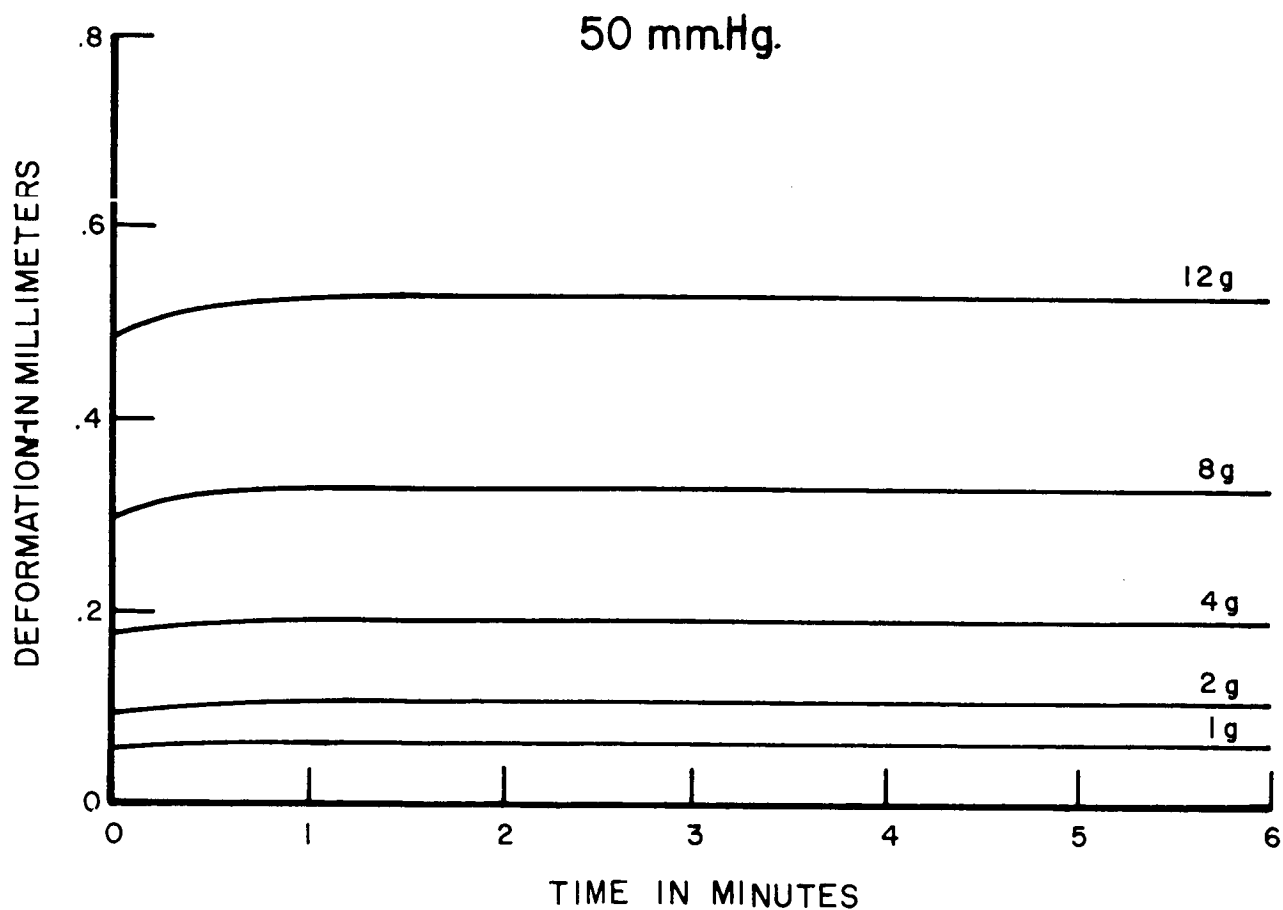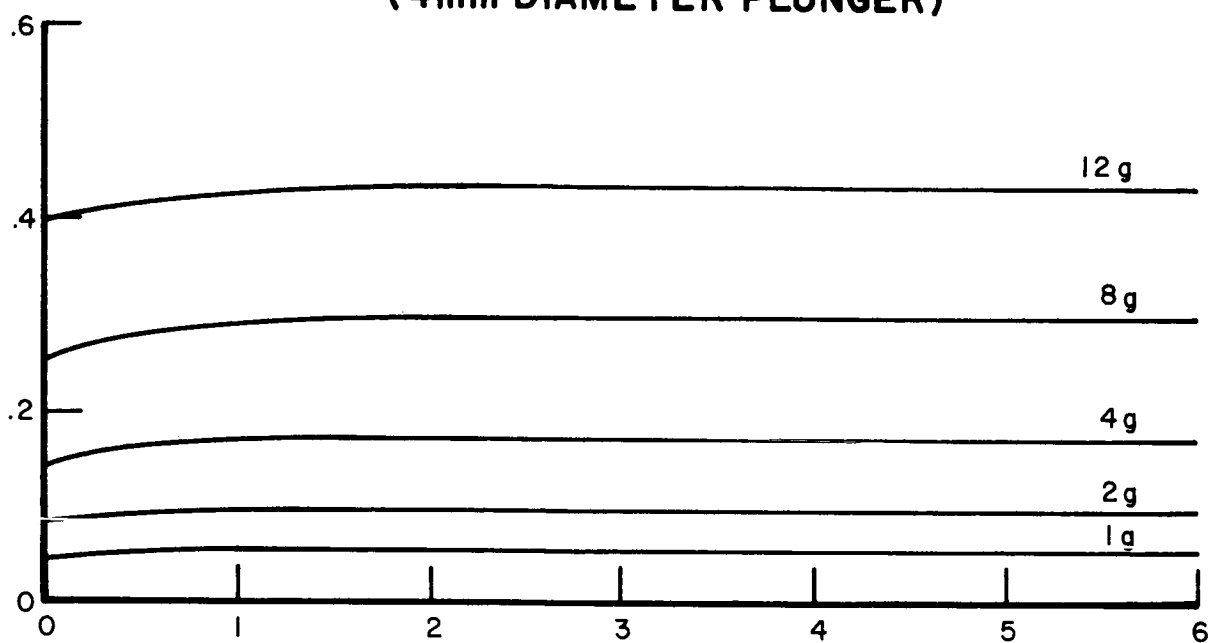
FIGURE 19

DEFORMATION UNDER CONSTANT LOAD, AND DIFFERENT INTERNAL PRESSURES FOR AN ENUCLEATED HOG EYE

(4mm DIAMETER PLUNGER)
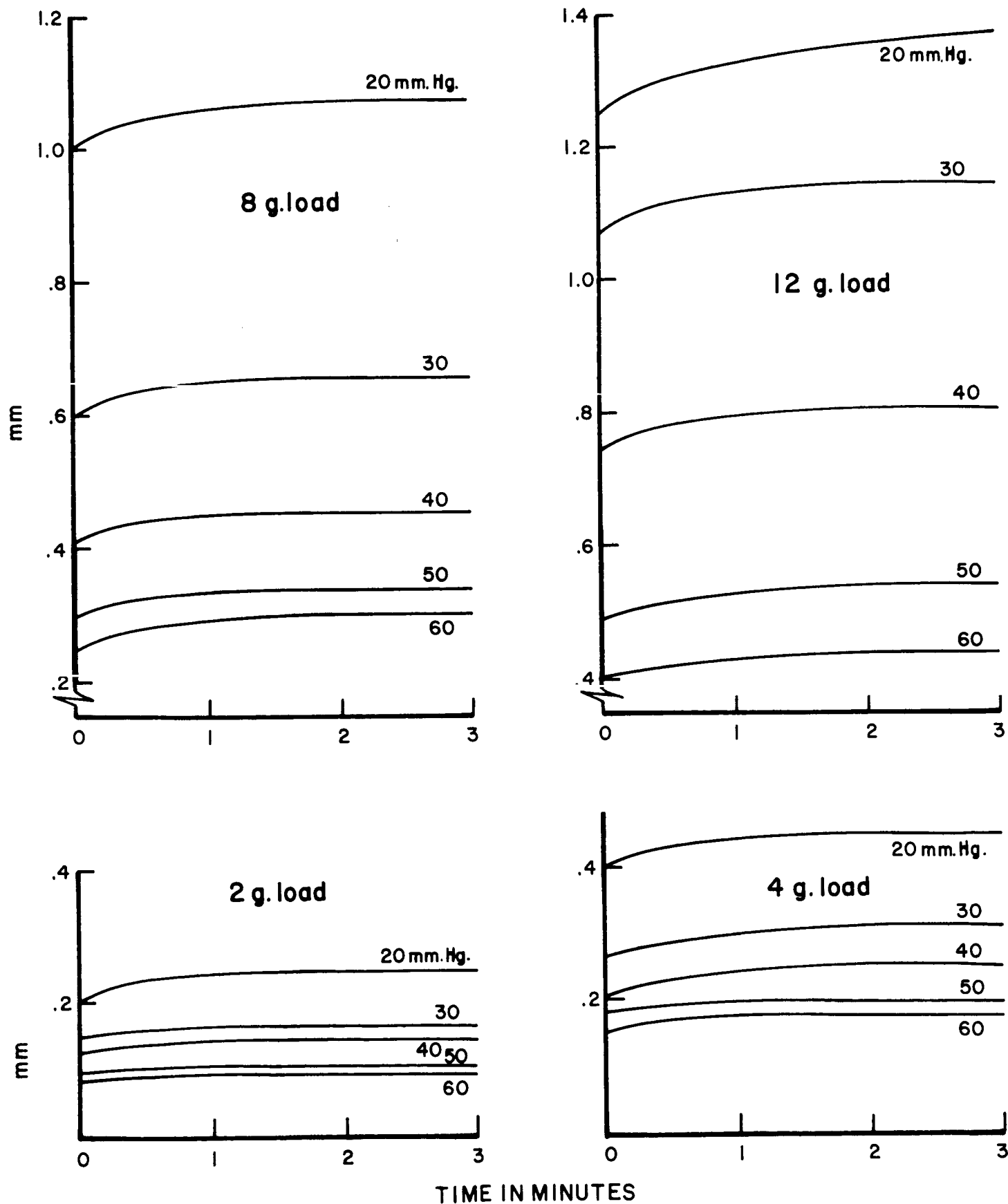
FIGURE 20

CORNEAL COMPRESSION TEST
(4 MM. DIAMETER PLUNGER)
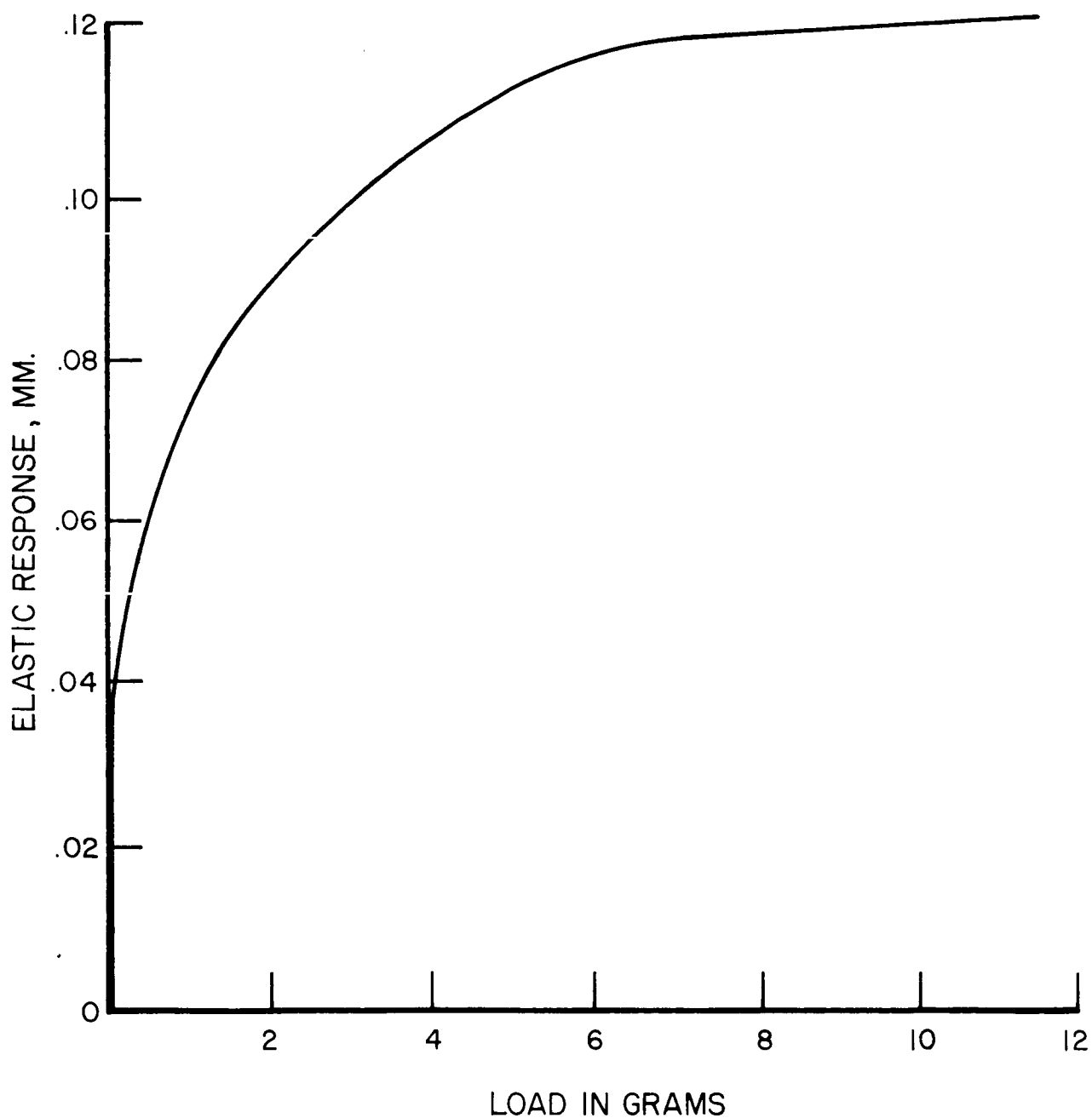
FIGURE 21

VOLUME EXPANSION TESTS
($p_o = 20\,mmHg.$)

SCLERA

$$\Delta W = F\,\log_{10}\left(\frac{\delta p + p_o}{p_o}\right)$$

$$F \doteq .02$$

$$\log_{10} \frac{\delta p + p_o}{p_o}$$

$w(p_o)$

.06 .05 .04 .03 .02 .01

CORNEA

$$\frac{\Delta W}{\Delta P} = .004$$

$p_o + \delta p$

$w(p_o)$

ΔW (mm)

.12 .10 .08 .06 .04 .02

FIGURE 22

Pavement epithelium 5or6 layers thick

Bowman's membrane

Stroma

Descemet's membrane

Endothelium
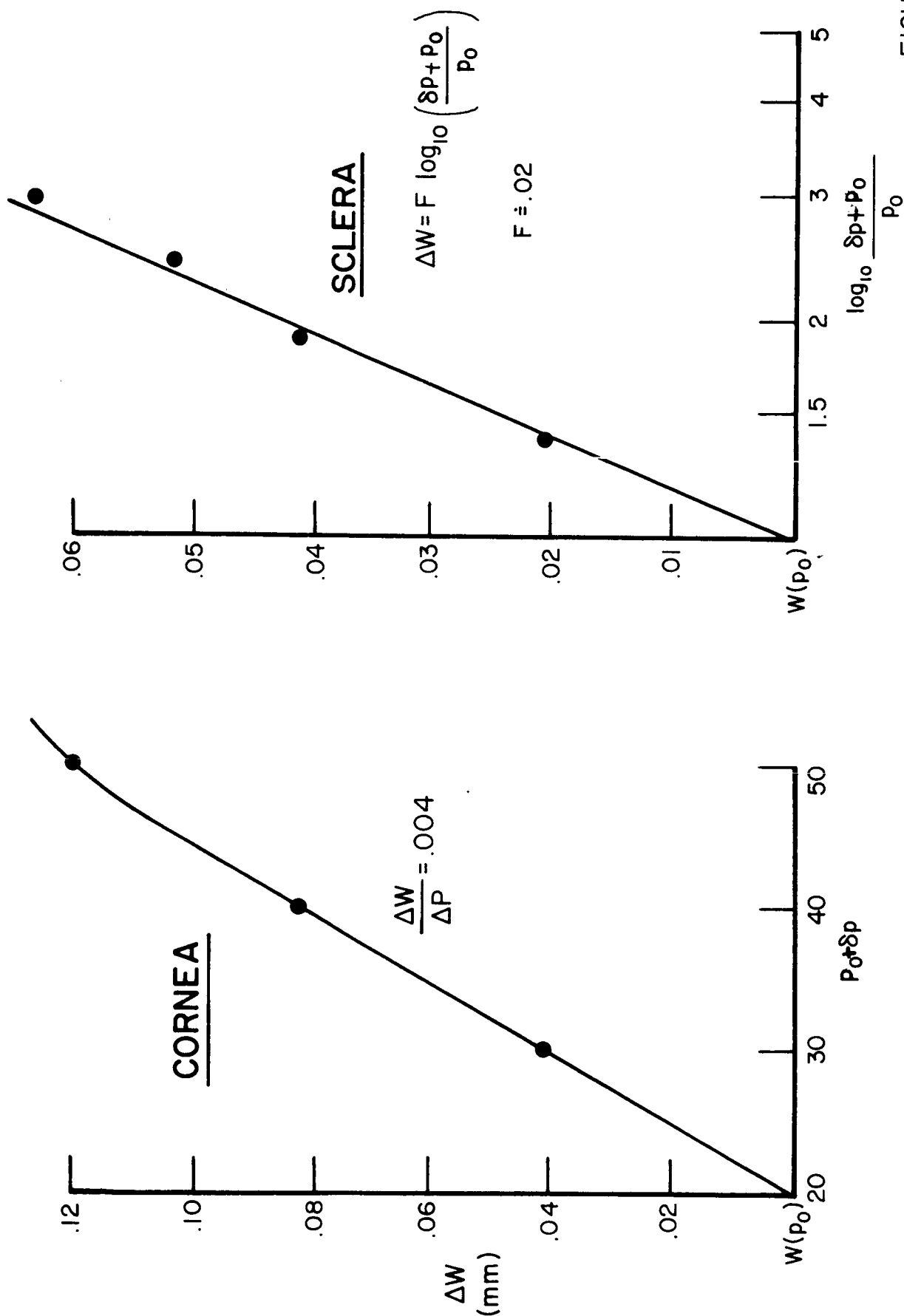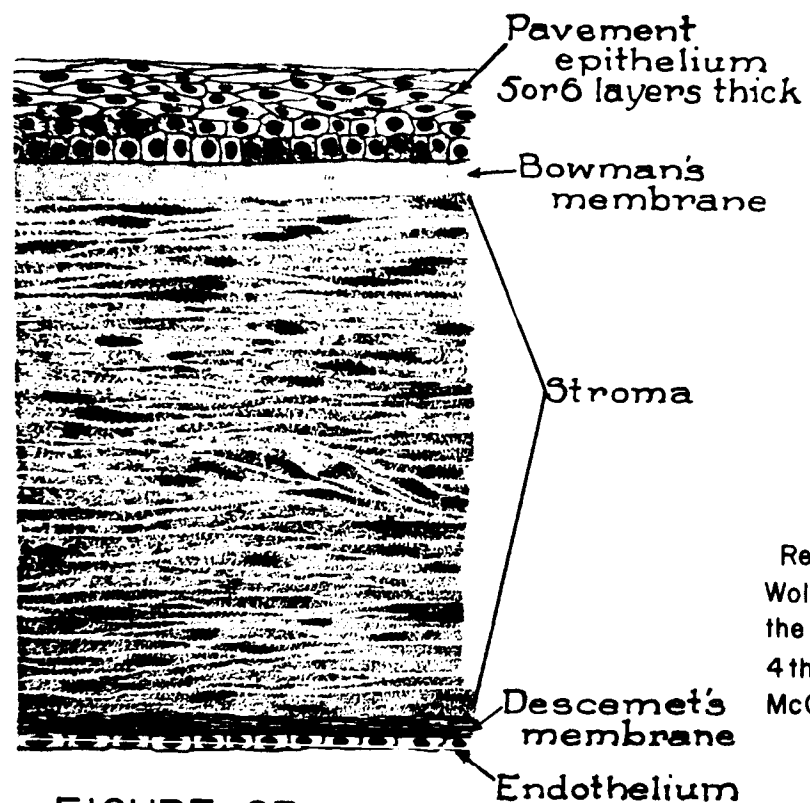
Reproduced from Wolff, Anatomy of the Eye and Orbit, 4th ed, Blakiston-McGraw, 1954

FIGURE 23

Anterior chamber

Pupil

Cornea

Conjunctiva

Iris

Canal of Schlemm

Posterior chamber

Tenon's capsule

Ciliary body

Zonules

Medial rectus muscle

Lateral rectus muscle

Ora serrata

Lens capsule

Lens

Choroid

Retina

Sclera

Retina

Choroid

Vortex vein

Sclera

Branches of ciliary artery and nerve

Vitreous body

Lamina suprachoroidea

Pigment epithelium

Retinal arterioles and veins

Macula lutea

Pia

Lamina cribrosa

Branches of ciliary artery and nerve

Dura

Arachnoid

Medullated nerve fibers

Optic disk

Optic nerve

Central retinal artery and vein

Reproduced from the Anatomy of the Eye, Lederle Laboratories

FIGURE 24

REPRESENTATIVE DIMENSIONS FOR A HUMAN EYE

FIGURE 25

45-60 mm.Hg

ANGLE-CLOSURE GLAUCOMA

FIGURE 27

25-40 mm.Hg

NORMAL TRABECULAR MESHWORK

HYPERSECRETION GLAUCOMA

FIGURE 29

14-20 mm.Hg

TRABECULAR MESHWORK
SCHLEMM'S CANAL
AQUEOUS VEIN
CILIARY BODY
AQUEOUS FLOW

NORMAL FLOW

FIGURE 26

30-45 mm.Hg

INCREASED TRABECULAR POROSITY

OPEN-ANGLE GLAUCOMA
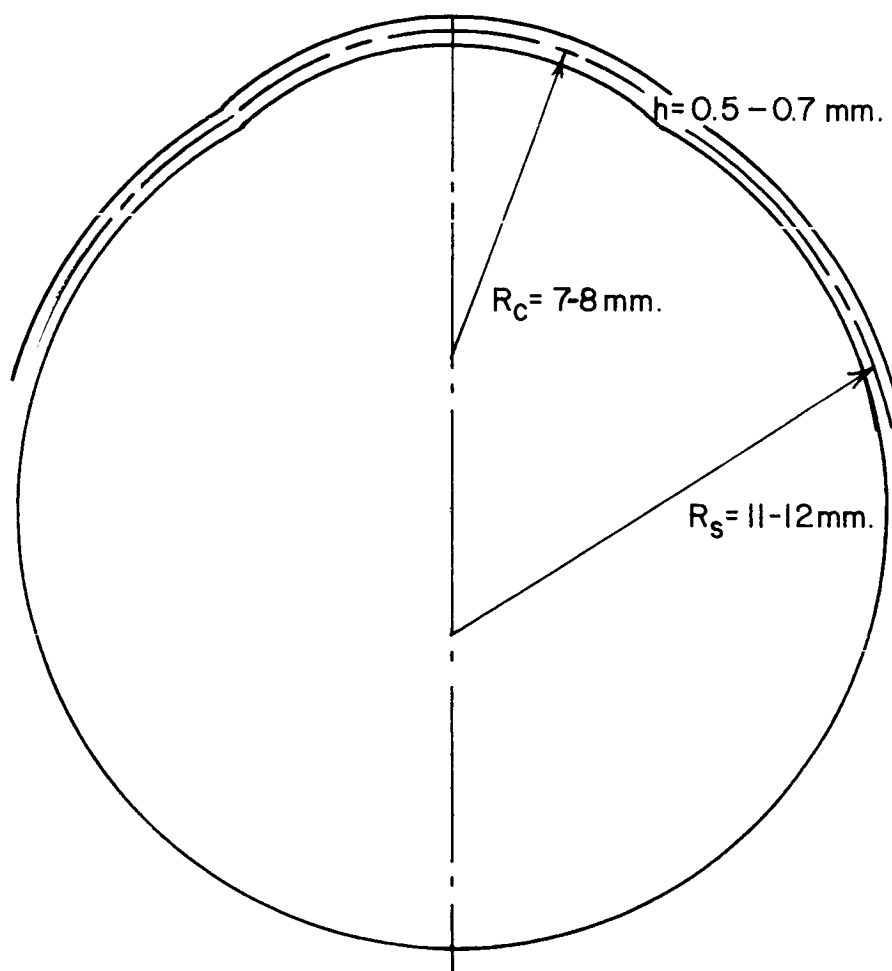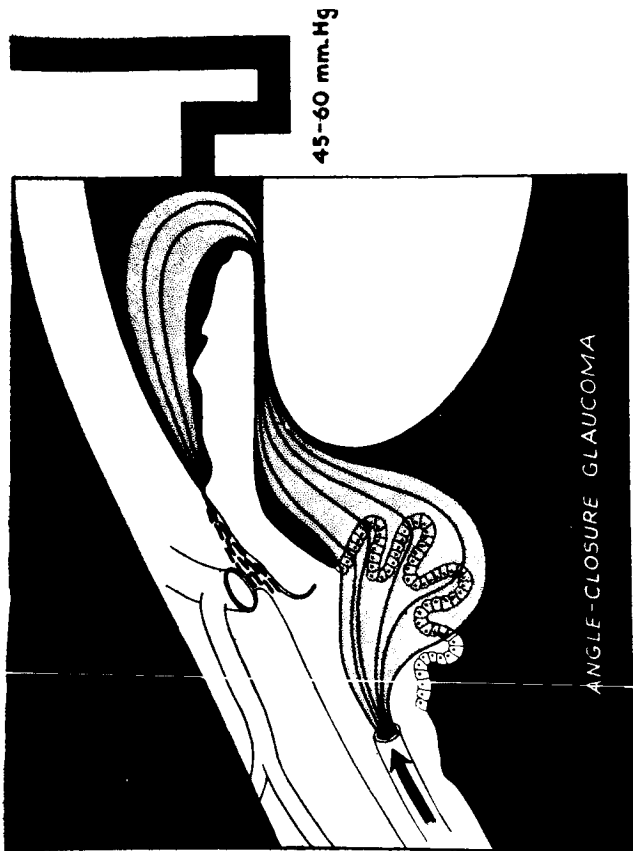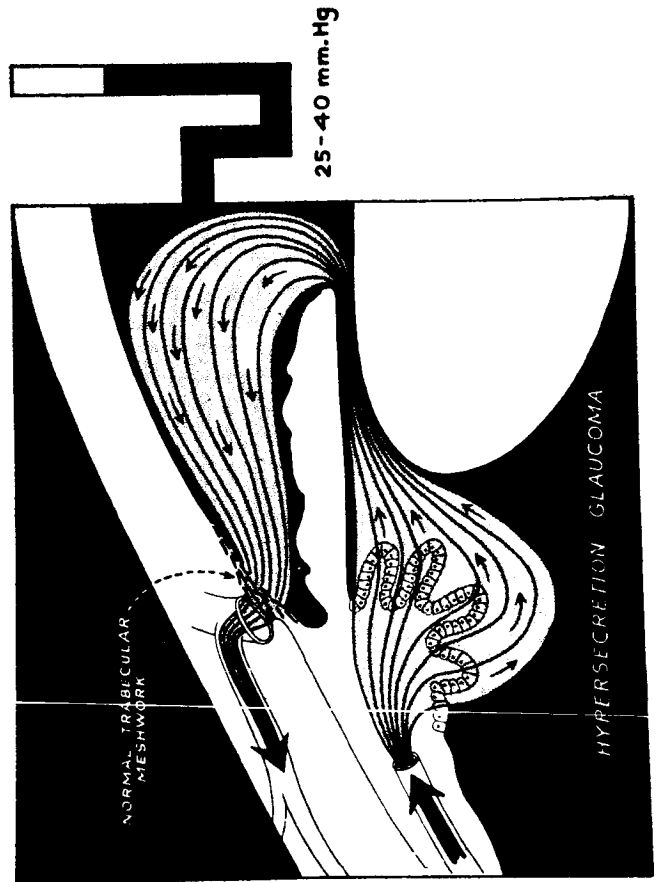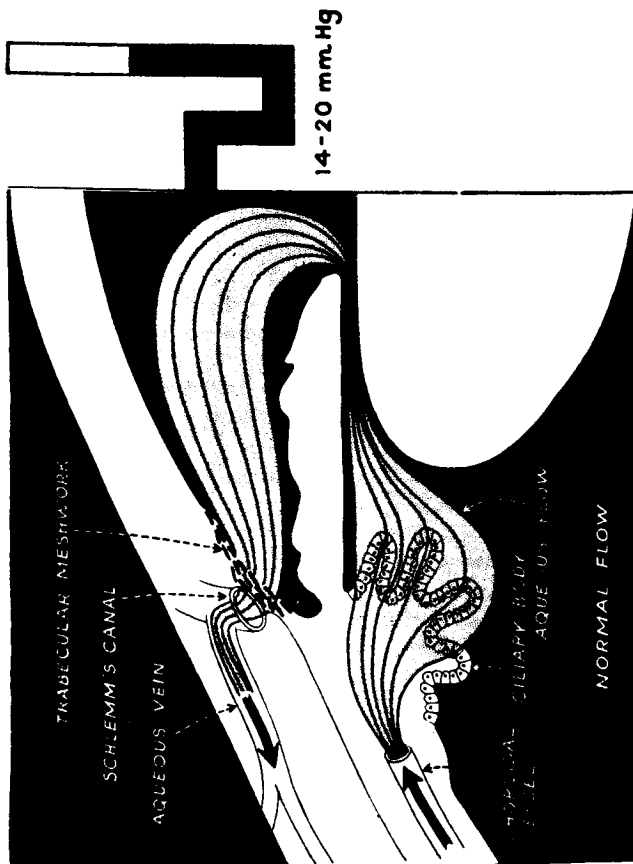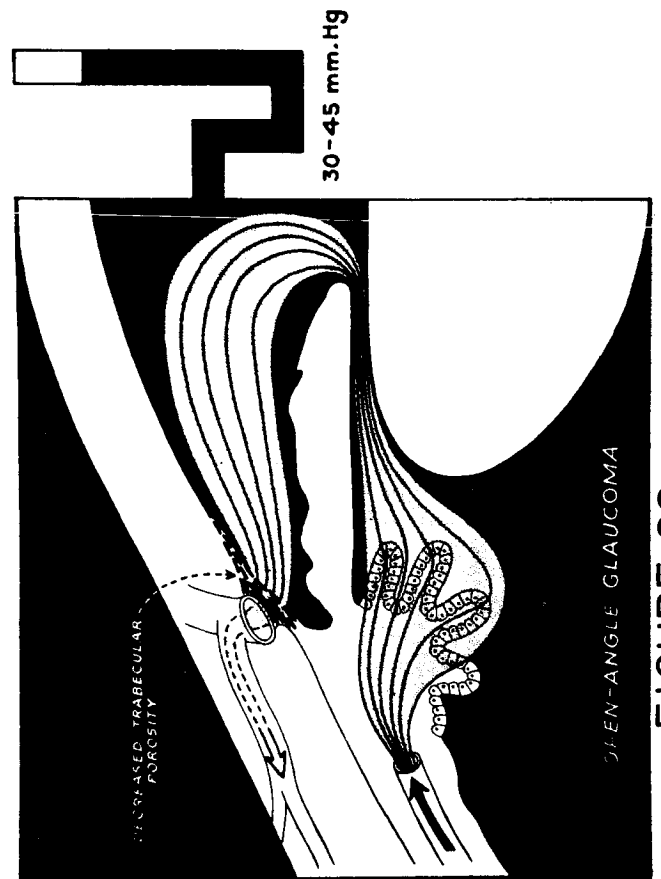
FIGURE 28

TEAR – TONOMETER – CORNEA – INTERFACE
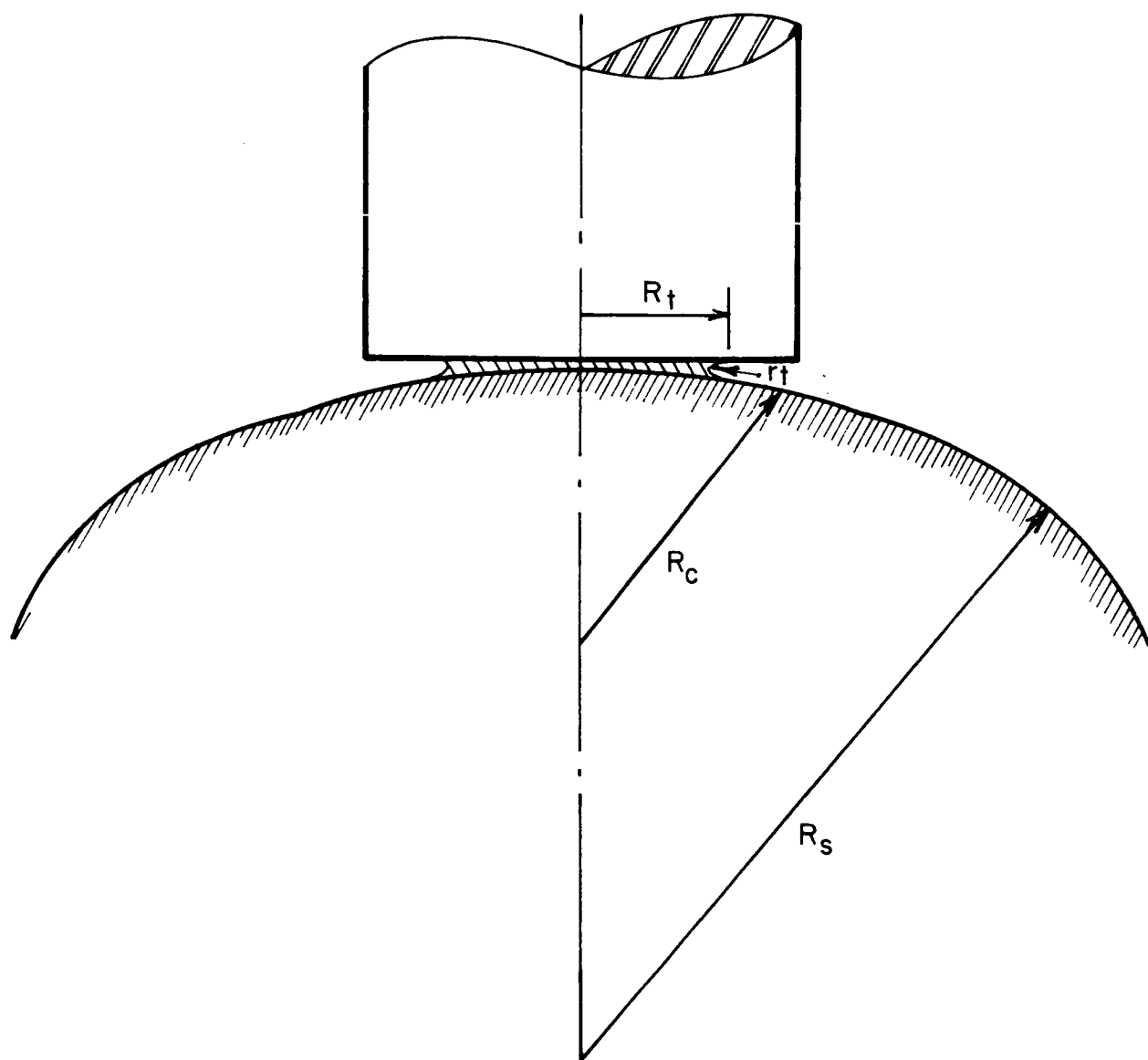
FIGURE 30

RESULTANT FORCE P(r$_0$)
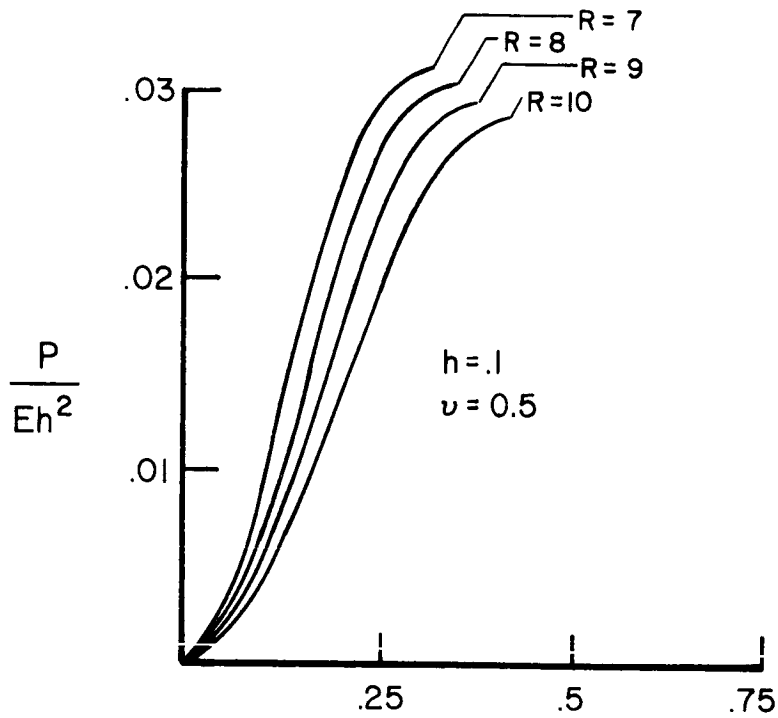
FIGURE 31
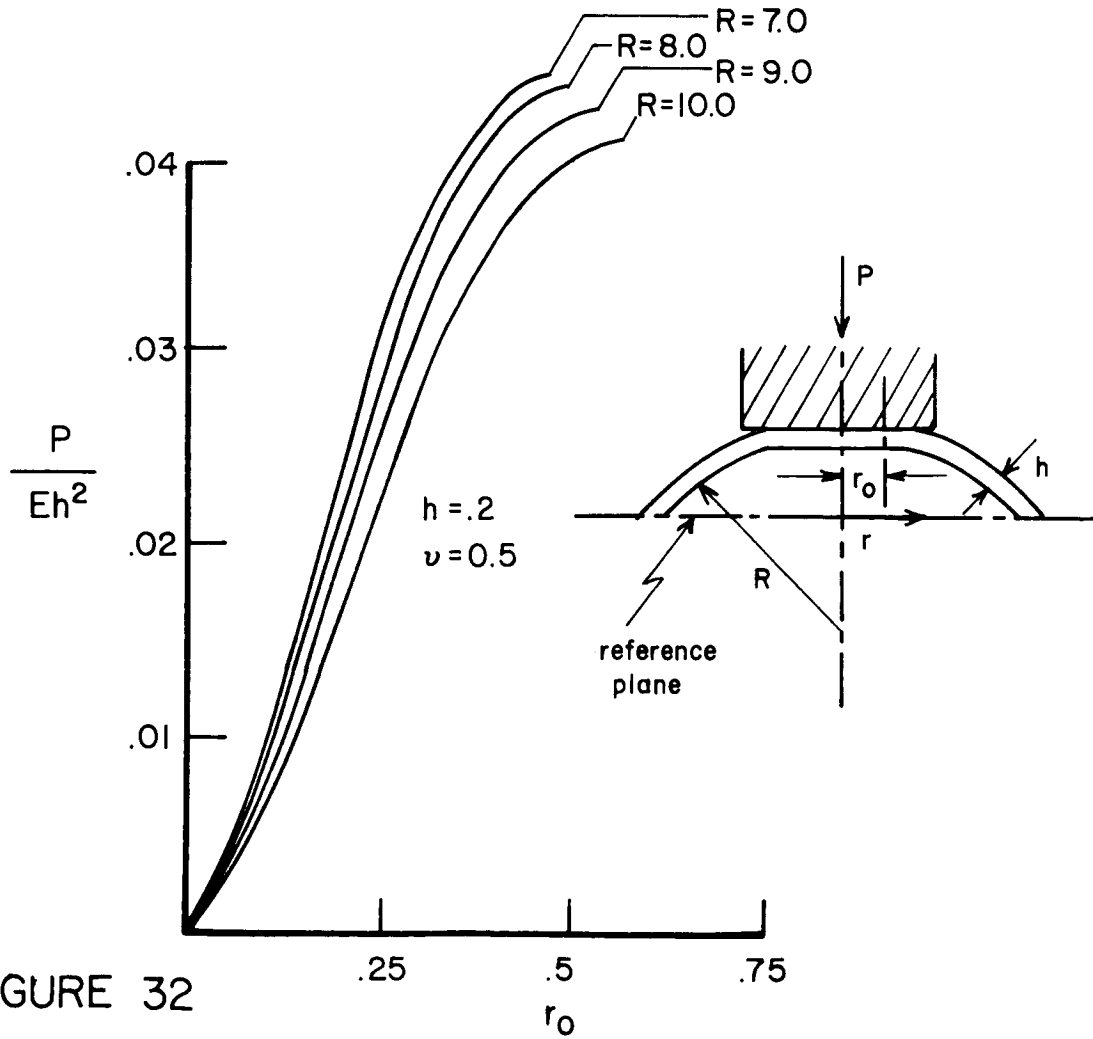
FIGURE 32

RESULTANT FORCE P(r₀)
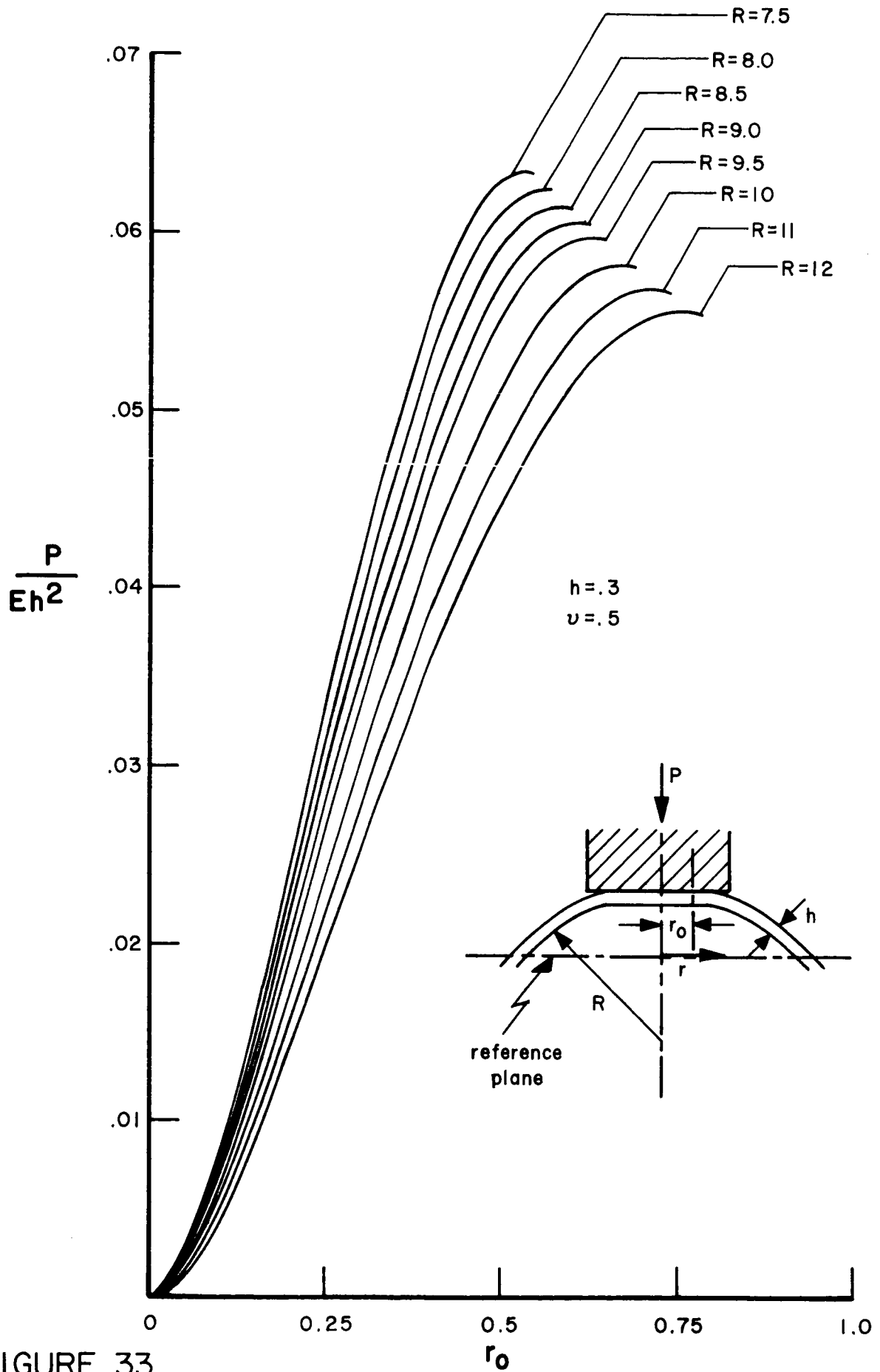
FIGURE 33

RESULTANT FORCE P(r₀)
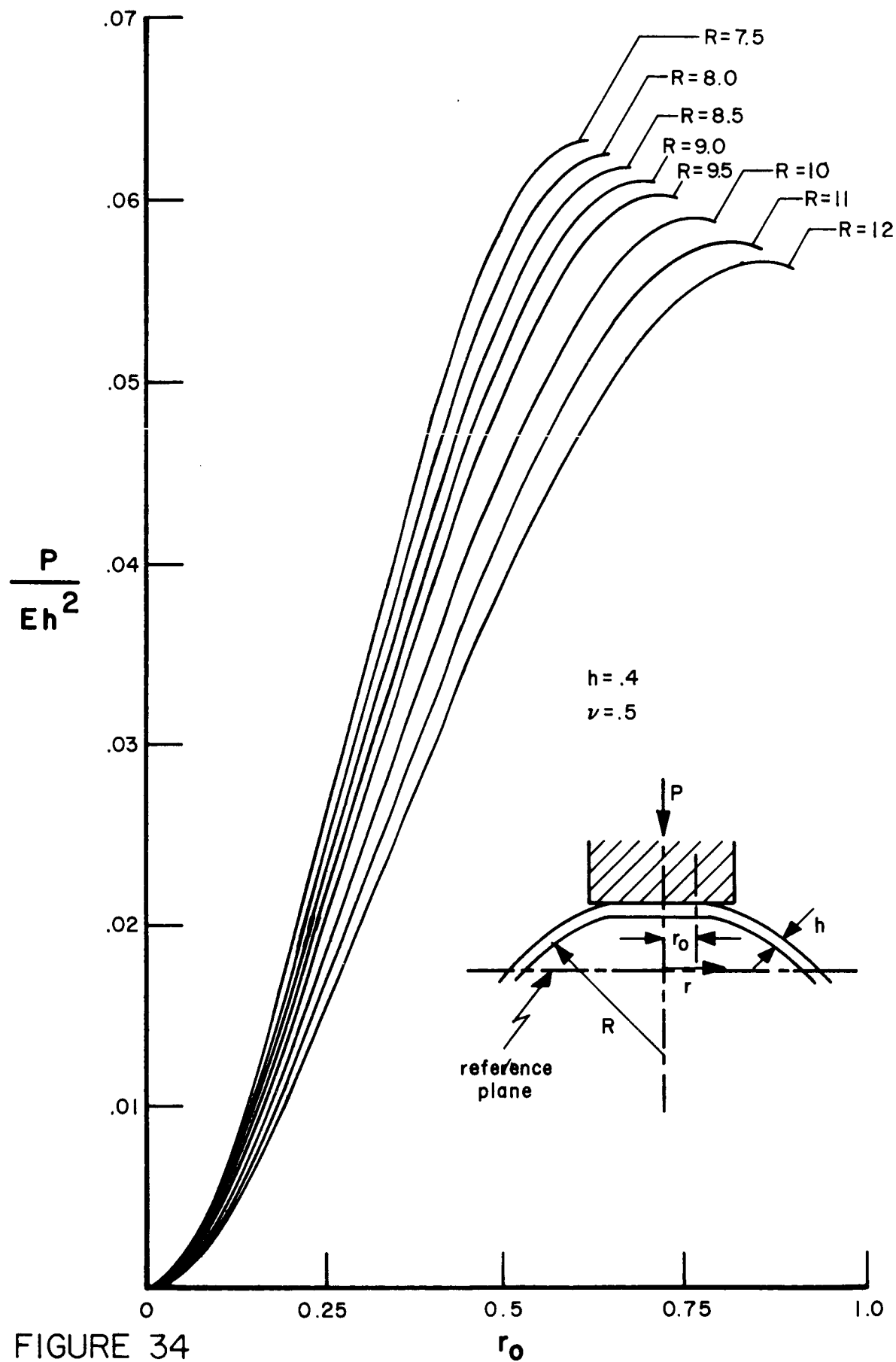
FIGURE 34

RESULTANT FORCE P(r₀)
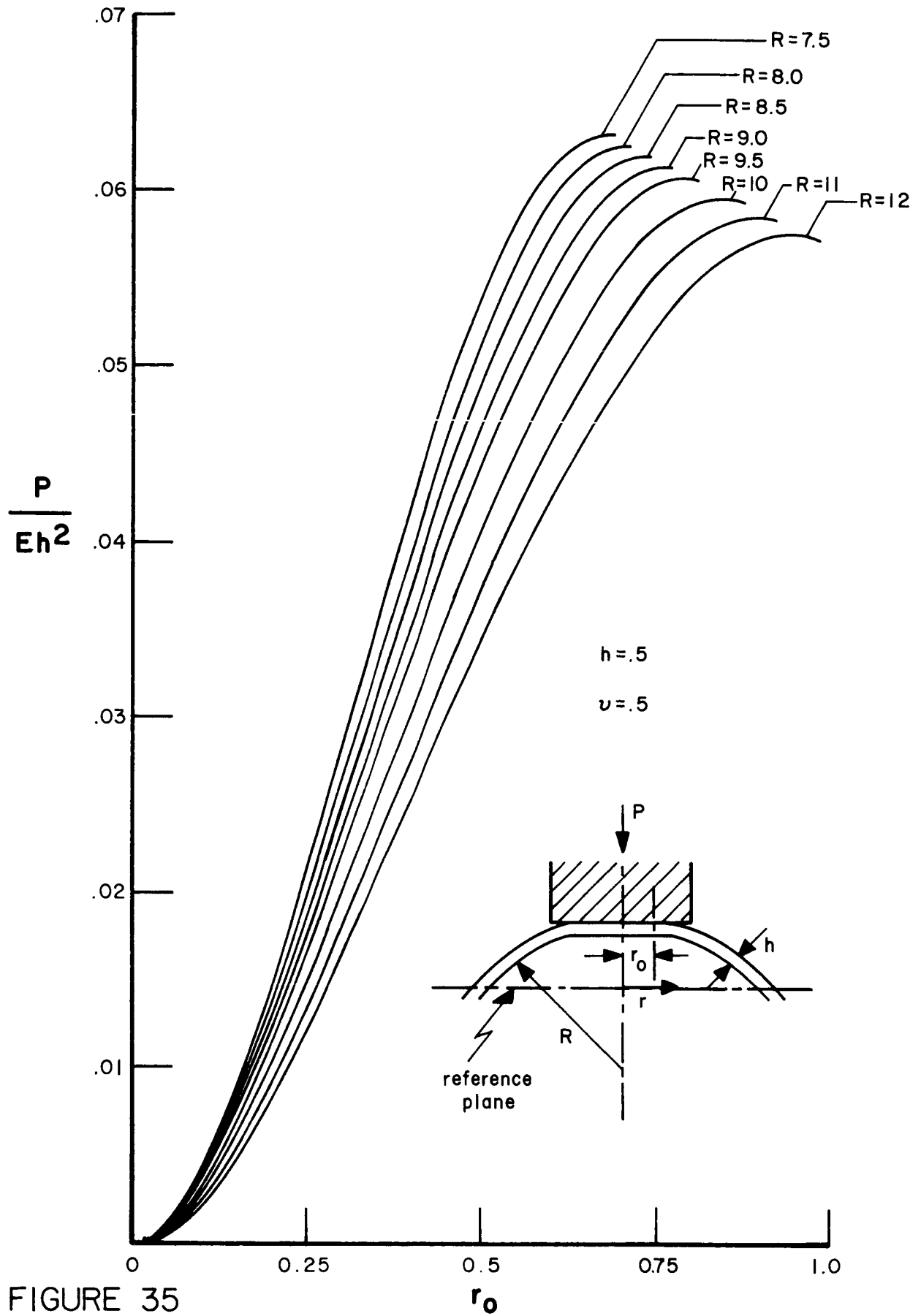
FIGURE 35

RESULTANT FORCE P(r₀)
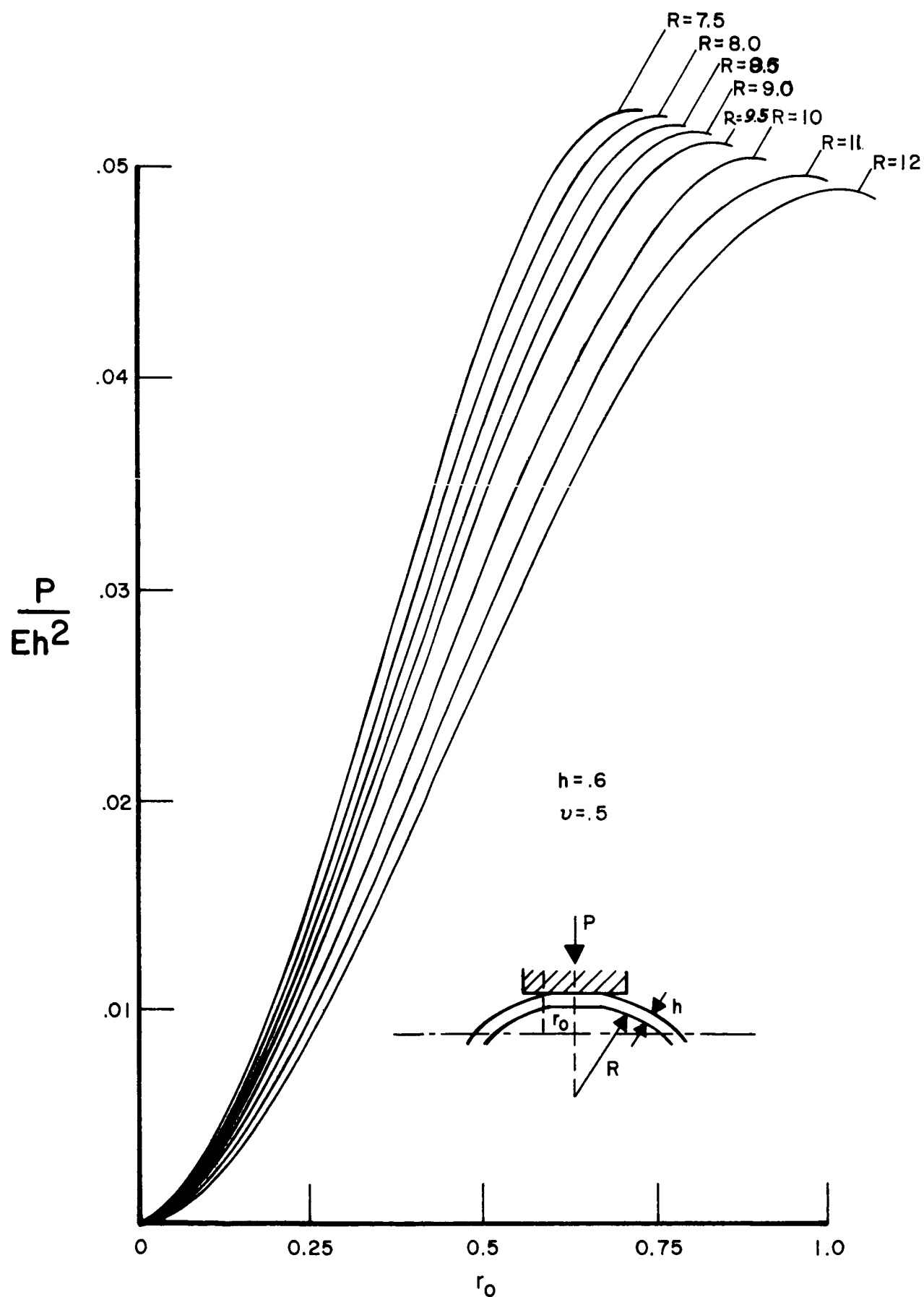
FIGURE 36

CONTRIBUTION OF CORNEAL BENDING RESISTANCE. $r_* = .75$
(MACKAY – MARG TONOMETER)
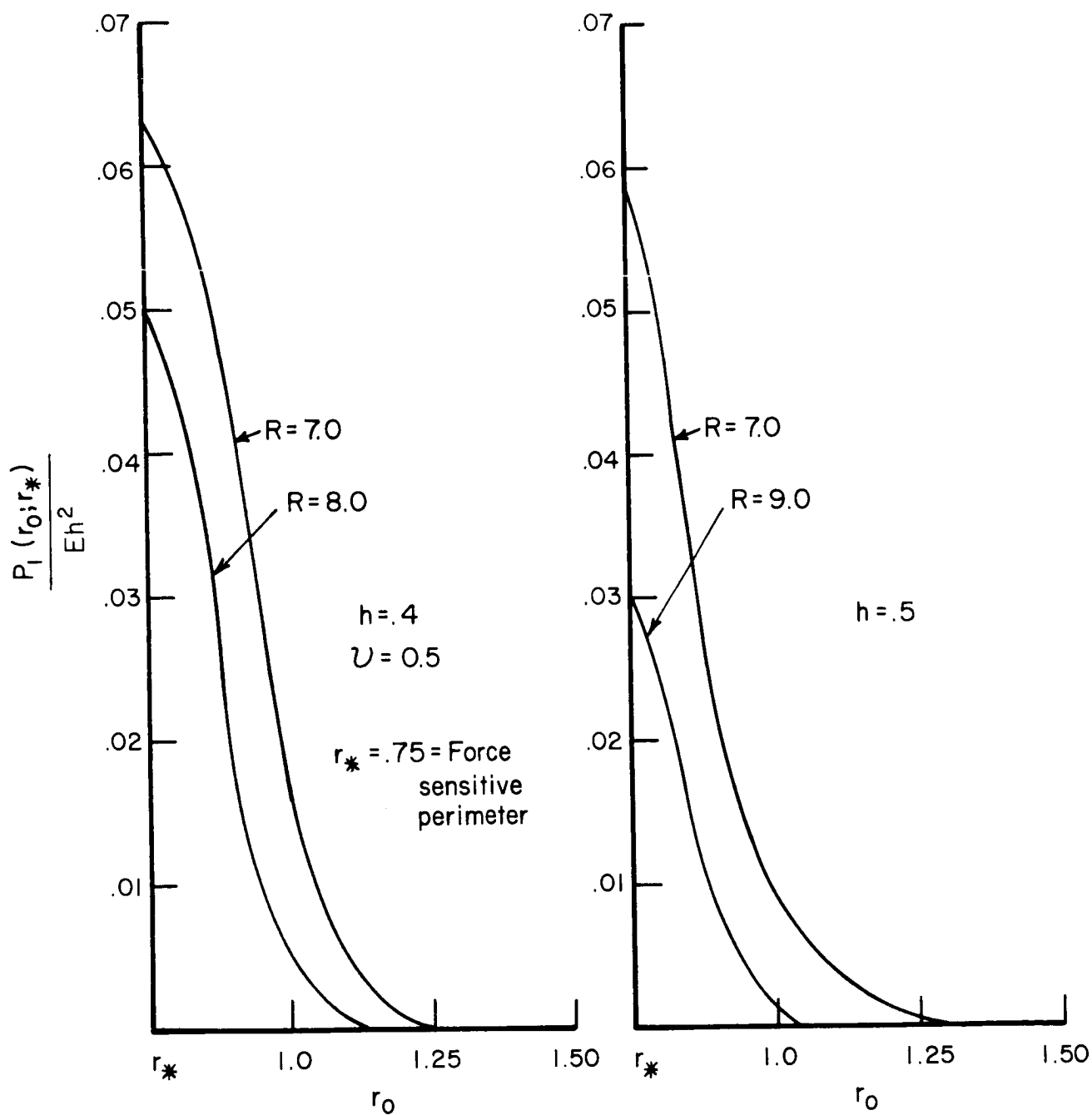
FIGURE 37

SECTION OF THE CORNEA UNDER LOADING
OF A SCHIØTZ TONOMETER

FIGURE 38